

**QUALIFICATION OF JOINT SEALANT EFFECTIVENESS  
REGARDING JOINTED CONCRETE PAVEMENT PERFORMANCE**

Keivan Neshvadian Bakhsh  
Graduate Research Assistant  
Texas A&M Transportation Institute

and

Dan G. Zollinger  
Program Manager  
Texas A&M Transportation Institute

Performed in cooperation with the  
International Grooving and Grinding Association

April 2015  
Revised February 2016

TEXAS A&M  
TRANSPORTATION  
INSTITUTE  
The Texas A&M  
University System  
College Station, Texas  
77843-3135

## **ABSTRACT**

The primary purpose for sealing rigid pavement joints is to prevent or reduce the amount of water infiltrating into pavement structure. It is well accepted that the presence of moisture in a pavement structure is a contributor to a variety of governing distress types that eventually deteriorates the pavement structure and decreases the pavement service life. Effectiveness of joint sealants to protect jointed concrete pavement against water related distresses has been a focus of great interest recently. Over the past 10 to 15 years, both formal and informal studies on the effect of joint sealing funded by State Agencies, the FHWA, and NCHRP have focused on the question of “to seal or not to seal” joints in concrete pavements that involved a variety of performance data, field cores, field observations, personal opinions, drainage modeling, and statistical analysis. The results of these studies have largely pointed to the lack of evidence supporting the use of sealed joints in concrete pavements as being beneficial. To this end, a field testing program was carried out at the Riverside Campus of Texas A&M University, on SR-59 near Joliet, Illinois, and on the SPS-2 site on I-10 in Goodyear, Arizona to study the effectiveness of different sealant types with respect to several years beyond installation after failure conditions begin to manifest to limit surface drainage related infiltration of the joint under different degrees of failure as represented by different joint openings and bonding conditions. Results confirmed that if joint seals are properly installed, they can be very effective in preventing moisture infiltration and thus performance issues related to erosion damage. Unsealed joints had significantly higher flow rates compared to joints with varying degrees of damaged

sealants. The test results in this study have also demonstrated the effect of sealant proper installation on joint seal drainage performance.

A focus of this report is to link joint seal effectiveness at an age beyond the initial performance period (during which the sealant is fully bonded) to when faulting would initiate through the ultimate advancement of a prediction model addressing the potential for erosion as a precursor to faulting and support related issues. The erosion resistance of materials, number of wet days and traffic load were defined and coupled in this model to effectively analyze the potential for faulting and erosion in jointed concrete pavements. The model can be calibrated for local conditions as a function of distinct characteristics of the subbase or subgrade is an important capability in life cycle analysis. The model has been successfully implemented into a spreadsheet format. Results show that the model fits well with the field data and can be implemented for design and maintenance management purposes.

A key outcome of this project is advancement of a tool for the mechanistic analysis of specific combinations of traffic, climate, base materials, and sealant damage or condition to limit water infiltration into the pavement sublayers towards the improvement of concrete pavement performance in terms of erosion. Such a tool should provide a means to strategize the most effective combination of key pavement design features. In this regard, it is clear that the management of a sustainable concrete pavement system requires greater emphasis on performance monitoring rather than performance repair, a concept not widely practiced and certainly challenges traditional repair and rehabilitation philosophies. The insightful prospects offered by the product of

this research certainly would support an examination of the commercial viability of such an approach.

## **NOMENCLATURE**

AASHTO	American Association of State Highway and Transportation Officials
ACI	American Concrete Association
ADOT	Arizona Department of Transportation
ADT	Average daily traffic
ADTT	Average daily truck traffic
ASTM	American Society of Testing Materials
CRC	Continuously reinforced concrete
CRC	Continuously reinforced concrete
DC	Dielectric constant
DOT	Department of Transportation
ESAL	Equivalent single axle load
FHWA	Federal Highway Administration
FWD	Falling weight deflectometer
GPR	Ground penetration radar
HWTD	Hamburg wheel-tracking device
JPCP	Jointed plain concrete pavement
LTE	Load transfer efficiency
LTPP	Long-term pavement performance
MEPDG	Mechanistic-Empirical Pavement Design Guide
NCHRP	National Cooperative Highway Research Program

PCC	Portland cement concrete
SHRP	Strategic Highway Research Program
SPS	Specific Pavement Study
TxDOT	Texas Department of Transportation
WisDOT	Wisconsin Department of Transportation

## TABLE OF CONTENTS

	Page
ABSTRACT .....	II
NOMENCLATURE .....	V
TABLE OF CONTENTS .....	VII
LIST OF FIGURES .....	IX
LIST OF TABLES .....	XII
1. INTRODUCTION .....	1
1.1 Aspects of Sealants Usage in Concrete Pavements .....	1
1.2 Research Approach .....	2
1.3 Report Structure .....	5
2. LITERATURE REVIEW .....	7
2.1 Joints in Concrete Pavements .....	7
2.2 Early Use of Sealant in PCC Pavements .....	7
2.3 Main Sealant Material Types .....	9
2.4 Current Sealant Practice .....	12
2.5 Sealant Adhesive and Cohesive Failure .....	15
2.6 Questioning the Need for Joint Sealing .....	20
3. INFILTRATION TESTING OF JOINT SEALANTS .....	26
3.1 Pavement Test Area at Riverside Campus .....	26
3.1.1 Test Conditions .....	28
3.1.2 Flow Test (Infiltration Test) .....	29
3.1.2.1 Evaluate Infiltration Rates of Sealed Joints .....	31
3.1.3 Flow Test Using a Movable Joint System .....	32
3.1.3.1 Test Results of Movable Joint Systems .....	34
3.1.4 Tests on Joint Sealant Installation .....	39
3.1.5 Radar Scans of Unsealed Joints .....	41
3.2 Tests on SR 59 South Bound .....	43
3.3 Tests on Arizona I-10 SPS-2 Site .....	48

3.3.1 Infiltration Testing.....	49
3.3.3 FWD Testing.....	52
4. EVALUATION OF NUMBER OF WET DAYS FOR DESIGN PURPOSES .....	54
4.1 Pavement Drainage .....	54
4.2 Transmission of water into the pavement sublayer .....	56
4.3 Rainfall Inflow .....	58
4.4 Water Surface Joint Infiltration.....	59
4.5 Infiltration Coefficient Testing.....	63
4.5.1 Sealant Damage Test and Flow Factor .....	65
4.5.2 Sealant Installation Test and Installation Factor .....	69
4.5.3 Model for Condition/Infiltration Coefficient .....	72
4.5.3.1 Permeability based Condition/Infiltration Coefficient .....	73
4.5.3.2 $C_d$ Validation Testing .....	74
4.6 Water Movement in the Subbase .....	75
4.7 Calculation of Number of Wet Days.....	80
5. FAULTING PREDICTION MODEL FOR DESIGN OF CONCRETE PAVEMENT STRUCTURES.....	89
5.1 Introduction .....	89
5.2 Faulting, a Major Distress Type in Concrete Pavements .....	89
5.2.1 Traffic Loads and Pavement Strength .....	90
5.2.2 Existence of Water underneath the Slab.....	91
5.2.3 Erosion Potential of the Subbase.....	92
5.3 Faulting/Erosion Model.....	93
5.3.1 General Form of the Model .....	93
5.3.2 Calculations for Equivalent Traffic Level.....	95
5.3.3 Calculations for Effective ESALs, $N_i$ .....	96
5.4 Demonstration Spreadsheet.....	99
5.5 Sensitivity Analysis.....	100
5.6 Validation Using LTPP Data.....	103
5.7 Conclusions and Discussion.....	106
6. CONCLUSIONS AND DISCUSSIONS.....	107
REFERENCES .....	112



## LIST OF FIGURES

	Page
Figure 1 Overall Failure Rates on Transverse Joints, Arizona Joint Sealant Study [15].	11
Figure 2 Cohesive Failure in Sealants.....	16
Figure 3 Adhesive Failure in Sealants.....	16
Figure 4 Layout of Joint Sealant Test Area.....	26
Figure 5 Joint Sealant Layouts. ....	27
Figure 6 Joint Sealing Process. ....	28
Figure 7 Flow Test on Existing Joint. ....	30
Figure 8 Damaged Sealing Condition. ....	31
Figure 9 Flow Test Results on Damaged Sealants. ....	32
Figure 10 Schematics of Movable Joint System. ....	33
Figure 11 Installation of Movable Joint System. ....	34
Figure 12 Flow Test Results for Various, 100% Debonded Joint Sealant Types. ....	35
Figure 13 Slope of Flow Rate Increase with Joint Opening at 100% Debonding. ....	37
Figure 14 Increasing Rate of Flow with Joint Opening at 100% Debonding. ....	38
Figure 15 Increasing Rate of Flow with Joint Opening for a Silicone Type Sealant at 100% Debonding.....	38
Figure 16 Water Infiltration Rates for Different Joint Dirtiness Levels .....	40
Figure 17 GSSI StructureScan™ Mini HR Radar System.....	41
Figure 18 Schematic of Transmission and Reflection Radar Waves. ....	41
Figure 19 GPR Test Result – Riverside Campus. ....	42

Figure 20 Location Map for SR 59 Test Section. ....	43
Figure 21 R 59 Cells Tested in this Sequence (2009 installation). ....	44
Figure 22 SR 59 Infiltration Testing (2013).....	44
Figure 23 SR 59 FWD Testing.....	47
Figure 24 SR 59 FWD Testing Pattern. ....	47
Figure 25 SR 59 NDT Analysis Results.....	48
Figure 26 I-10 SPS-2 Infiltration Position 1 (interior), 2, and 3 outer edge) Testing. ....	49
Figure 27 I-10 SPS-2 Infiltration Test Results for Section 40215. ....	49
Figure 28 I-10 SPS-2 GPR Test Results for Section 40219.....	51
Figure 29 I-10 SPS-2 Erosion Analysis Results.....	53
Figure 30 Water Related Damages; Potholes, Corner breaking and Wide Cracks. ....	55
Figure 31 Three Stages of Rainfall Transmission into Subbase Layer. ....	57
Figure 32 Maximum 1-hour-duration/1-year-frequency Precipitation in the United States [45]. ....	59
Figure 33 Open Graded Granular Subbase Used for Test Program. ....	63
Figure 34 Fifty Percent Damaged Sealant.....	66
Figure 35 Infiltration Test Results on Damaged Sealants. ....	68
Figure 36 Infiltrations for Different Damage Levels Compared to 100% Damaged.....	68
Figure 37 Water Infiltration Rates for Different Joint Dirtiness Levels. ....	70
Figure 38 Average Infiltration Rates for Different Dirtiness Levels. ....	71
Figure 39 Variation of the flow factor ( $F_c$ ) with the installation factor ( $F_I$ ). ....	72
Figure 40 Sample Flow Net And Flow and Equipotential Lines [36]. ....	77

Figure 41 Flow Net for Water Seepage from the Concrete Joints into the Subbase.....	79
Figure 42 Regression to Fit the Ratio of Flow Net Lines to Base Thickness. ....	80
Figure 43 Algorithm to Calculate the Number of Wet Days. ....	82
Figure 44 Example of Subbase Seepage Distribution. ....	84
Figure 45 Computer Spreadsheet Program that Calculates the Number of Wet Days.....	85
Figure 46 $P_2$ Distribution for the Example Analysis. ....	87
Figure 47 $P_2$ Cumulative Distribution for the Example Analysis. ....	87
Figure 48 $P_{sb}$ Distribution for the Example Analysis.....	88
Figure 49 $P_{sb}$ Cumulative Distribution for the Example Analysis. ....	88
Figure 50 Three Main Elements Contributing in Subbase Erosion and PCC Faulting...	90
Figure 51 Sample Gumbel S-Shaped Distribution. ....	94
Figure 52 Shear Strength and Angle of Friction Determinations.....	98
Figure 53 Sensitivity Analysis on Base Curve.....	102
Figure 54 Changes of Load Transfer Efficiency with and Without Dowel Bars. ....	103
Figure 55 Calibration of the Model Using the Field Data.....	104
Figure 56 Modeled versus Measured Faulting of LTPP Data.....	105

## LIST OF TABLES

	Page
Table 1 Factors and Causes of Sealant Failure.....	18
Table 2 Test Controlling Factors.....	29
Table 3 Flow Test Results for Various Joint Sealant Types. ....	35
Table 4 Infiltration Test Results from SR 59. ....	44
Table 5 GPR Permeability Test Results from SR 59. ....	46
Table 6 GPR Test Results from SR 59.....	46
Table 7 SPS-2 Pavement Section Details.....	48
Table 8 Summary of Sectional Infiltration and GPR Test Data.....	50
Table 9 FWD Tested Sections.....	52
Table 10 $C_d$ Model Coefficients.....	65
Table 11 Infiltration Test Results on Damaged Sealants. ....	66
Table 12 Condition/Infiltration Coefficient ( $F_c$ ) for Different Sealant Conditions.....	69
Table 13 Dirtiness levels, Installation Qualities and Calculated Installation Factor.....	71
Table 14 Installation Factor ( $F_I$ ) for Different Installation Qualities. ....	72
Table 15 Effective $w$ based on New Infiltration Model.....	75
Table 16 Number of Flow Lines and Equipotential Lines for Different Base Thicknesses. .....	79
Table 17 Input Values for the Example Pavement.....	84
Table 18 Output Values for the Example Pavement. ....	86
Table 19 Input Parameters for the Base Analysis. ....	101



# **1. INTRODUCTION**

## **1.1 Aspects of Sealants Usage in Concrete Pavements**

Joints in concrete pavements are intended to provide freedom of movement of the slab relative to concrete volume changes due to drying shrinkage, temperature changes and moisture differences. The primary purpose for sealing rigid pavement joints is to prevent or reduce the amount of water infiltrating into pavement structure, which results in slab erosion, loss of support and other water related distresses.

It is well accepted that the presence of moisture in a pavement structure is a contributor to a variety of governing distress types that eventually deteriorates a pavement structure and decreases service life. Effectiveness of sealants to protect jointed concrete pavement against water related distresses has been a focus of great interest recently. There have been numbers of studies, field observations, and testing programs that have been performed on joint sealants in concrete pavements. State and other DOT's have adopted a wide variety of joint sealing practices and policies for jointed pavements, derived from local experience, climate, and traffic conditions. In response to an NCHRP survey, "nine state highway agencies reported that they seal joints, but do not provide positive subsurface drainage in every instance. Thirty states reported that they sealed joints but also use a permeable base layer, a subsurface drainage system, or both. The remaining eleven states reported that they took the position that water will inevitably enter the pavement system and sought only to control it through use of a drainage layer or other subsurface drainage, or both rather than relying on the capability of joint sealant. And one of the eleven states, Wisconsin, reported that it had dispensed with joint sealing entirely" [1].

The research presented in this report is focused in the evaluation of sealant effectiveness on jointed concrete pavement performance. The outcome of this study should be useful to state DOT's, contractors, maintenance agencies and pavement designers in making critical design related decisions on using sealants in respect to long term performance. Such decisions that strike a balance between traffic, climate, and base erodibility can save costs, maintenance, and improve performance and pavement serviceability.

## **1.2 Research Approach**

A testing program was carried out at three different field locations to study the effectiveness of different sealant types in limiting drainage related infiltration at a joint under different joint openings. A portion of the program included testing on three sealant types; silicone based sealants, hot pour asphalt based sealants, and compression sealants with different sealant debonding conditions and joint reservoir geometries. This testing included a movable joint system to simulate joint widening in order to address the importance of installation on joint sealants effectiveness. A flow test was conducted as an easy, quick and reliable in situ test to evaluate the amount of water infiltration into a joint and therefore to evaluate the effectiveness of a sealant to keep the water from entering a pavements sublayers.

The aim of the test program was:

- To evaluate how effectual is a joint sealant to prevent water from the sublayer
- To evaluate the difference of unsealed joint versus the sealed joint in terms amount of water infiltration
- To assess the sealant bond quality in different joint openings (a movable joint system was used as a simulation of joint sealant's behavior during hot and cold seasons when joint width changes)

- To compare different types of sealants in different joint opening and debonding conditions in respect to water infiltration
- To determine the importance of installation quality and joint reservoir's cleanness prior to sealing the joints
- To develop an approach to assess the number of wets days a pavement may be subjected to annually

The test program led to fruitful results and key conclusions on sealants effectiveness in respect to water infiltration.

Furthermore, the sealant effectiveness in terms of concrete pavement long term performance was analyzed. Beside the importance of sealant capability to keep the water away from the sublayers, it is of a great interest of project owners, designers, contractors and maintenance agencies to determine how sealing or not sealing may affect concrete pavement sustainability. Sealant effectiveness was included in a concrete pavement performance model so the effect of sealing or no sealing could be determined for any particular pavement structure in terms of erosion related damage and distress development over its service life.

An inevitable consequence of water infiltration through joints in concrete pavement is the erosion at the interface of the subbase. Subbase erosion directly contributes to the process of joint faulting which can involve several factors. Faulting as a major distress type in jointed concrete pavements is a key item for designing concrete pavements. The effects of faulting have implications on a pavement both structurally and in terms of serviceability. Faulting, if not maintained in a timely manner, can also lead to other distresses that may result in considerable repair costs.



A mechanistic-empirical faulting prediction model was improved as part of this research. The effect of joint seal effectiveness was directly employed within a faulting prediction model. The three main elements of erosion, the rate of erosion of the base/subbase, existence of moisture under the slab (as reflected by the number of wet days), and traffic were included. The model was calibrated with lab and field data and is useful for design and maintenance purposes.

Using this model, sealant effectiveness in respect to concrete pavement long term performance and sustainability can be evaluated. This makes agencies and designers capable of deciding if sealing is necessary for a given project.

There have been two other studies to support this modeling to connect the sealant influence into erosion related distresses. One important factor that was addressed in the model was a means to evaluate the number of wet days. Number of wet days is the actual number of days per year that water exists underneath the slab at the slab/subbase interface. This number is not only a function of annual rainfall but also a function of surface inflow, sealants effectiveness and subbase drainability. The number of wet days was determined with respect to probability functions that can be used for each site to evaluate the number of days that water exist underneath a slab.

Finally this process can be included within a computer program that would analyze a concrete pavement structurally towards the prediction of erosion and faulting with respect to a sealants effect. This program would be capable of calibration to field performance or laboratory erosion data. Results thus far show that the model fits well with the field data and can ultimately be implemented for design and maintenance management purposes.

### **1.3 Report Structure**

This report consists of six chapters, each with specific objectives. Chapter one is the introduction and brief review of the approach. Chapter two includes a review of the literature where background information, history of joints and sealing, different agencies approach and policies regarding sealing, brief overview of sealant failure modes and causes and other issues related to the seal or no seal discussion.

Field testing on joint sealant performance in regards to infiltration is discussed in chapter three. This chapter includes a thorough explanation of the test methods and test variants. Flow test is introduced as a very effective field test method. Moreover test results are shown in figures and tables along with discussion and analysis.

An important design factor, number of wet days, is defined and analyzed in chapter four. This chapter includes discussions on how water transmits into the sublayers. Infiltration coefficient is defined and determined using results from test program in Chapter three. Water seepage into subbase has been calculated. The number of wet days is presented as a probability function that counts for annual rainfalls, surface inflow, sealants effectiveness and subgrade permeability.

A mechanistic-empirical faulting model that was developed is explained in chapter five in a step by step format. Three major factors contributing to the erosion/faulting process are considered in this model. Passing traffic, existence of water in the subbase/slab interface and erodibility of the base material are the three major factors. Sensitivity analysis on the model and calibration of the model using field data is presented to demonstrate the sensitivity and accuracy of the model.

Finally, a summary of the major findings and conclusions are summarized in chapter six. In the appendices, details of erosion testing are provided along with a description of material samples, test results, and the test procedure for erosion are explained.

## **2. LITERATURE REVIEW**

### **2.1 Joints in Concrete Pavements**

Joints in concrete pavements are primarily intended to provide freedom of movement of a slab relative to volume changes in the concrete due to drying shrinkage, temperature changes and moisture differences. Functionally speaking, joints are designed to control cracking, minimize stresses in the pavement caused by volume change as well as prevent damage to immovable structures.

Joints have always played an integral part in concrete pavement construction where joint geometry and design has been improved over the years [2]. Joints were typically placed at regular intervals that have been validated by experience. The first specifications regarding the placement of joints in concrete pavements was included in guidelines for transverse joint spacing by the American Concrete Institute (ACI) in 1914 [1]. Discontinuities in portland cement concrete (PCC) pavements such as joints have been a major performance concern since they tend to create planes of weakness in the slab; in many instances, distresses often initiate and propagate at or near joint locations. Therefore, attempts have been made to reduce the number of joints by extending joint spacing. Use of customized curing techniques and construction methods has yielded PCC pavements with longer joint spacing. Nonetheless, field observations that have been suggested related to improved joint patterns to help avoid early distresses at the joint. Other improvements have affected the use of joint sealants [3].

### **2.2 Early Use of Sealant in PCC Pavements**

Sealing joints is widely believed to be beneficial to concrete pavement performance in two ways [4]; first by minimizing water infiltration into the pavement structure. This effects the presence of moisture in the pavement and the occurrence of moisture-related distress since moisture can

cause support issues that may decrease pavement service life. Secondly, sealed joints reduce the infiltration of incompressibles (i.e., sand and small stones, debris) into the joints, therefore reducing the possibility of joint distresses such as spalling due to the pressure in the joint reservoir under the load. Incompressible materials are thought to create point loading within the sawcut notches as slabs expand due to temperature changes possibly leading to spall damage but this type of distress is more likely load rather than temperature related [4].

As alluded to; infiltration into the pavement structure could result in slab erosion, loss of support and loss of joint stiffness [5]. Faulting for instance, considered as a major failure in jointed concrete pavement is directly associated with the presence of water. Accumulation of water under the slab combined with traffic loading can initiate erosion along the interface between the base and the slab particularly where they are separated along the edges and corners. Corner breaks and freeze-thaw damage (D cracking) are other examples of distress related to moisture trapped in the pavement joints.

In 1871, a U.S. patent represented the use of gum, tar or rubber materials as joint filler in concrete joints [2]. Later and in the early 1900s, it was common construction practice to use bituminous materials in order to fill the joints. Bituminous materials were relatively inexpensive and easy to produce and place. In 1912, the first reinforced concrete pavement in Port Huron, Michigan was constructed. Expansion joints in this project extended through the entire slab thickness. Asphalt cement was used to fill the joints and to prevent infiltration of water [1]. Sealing the cracks as a part of maintenance program was also considered in the early 1910s; the material was mostly a mixture of sand and tar [1].

In the early 1920s, many states studied various tar and asphaltic filler materials in repairing cracks in concrete pavements. One of these studies was sponsored by the Iowa State

Highway Commission in 1923 to identify grades of tars and asphalts suitable for use in crack maintenance. The experimental sections were located outside of Des Moines, Iowa. Different materials were tested, including three tars, nine asphalts and blown oils, an emulsified bitumen and a single light-colored material [1]. The cracks were pressure-cleaned and dried before installation of the filler material. After the final inspection, all three grades of tar were nearly 100 percent intact, adhering well to the concrete joint wall. These were the only materials exhibiting excellent performance.

### **2.3 Main Sealant Material Types**

There are mainly three kinds of sealant materials used for rigid pavement applications currently; asphalt based sealants, silicone based sealants and compression sealants. Historically, the hot-applied asphalt based materials have been the most commonly used sealant materials for concrete pavement joints. However, silicone based sealants (ASTM D5893) and preformed compression seal materials (ASTM D2628) have gained increased acceptance for use in rigid pavements and have become the preferred choice of a significant number of state DOTs [6] [7] [8] [9].

Hot pour rubberized asphalt materials typically possess good sealing characteristics and flexibility at a relatively low cost, however; as they age over time the possibility of water infiltration increases due to reduction of flexibility and bond along the seal/joint wall interface [10]. Hot pour rubberized joint sealants if installed properly may provide long term service. A study by Federal Highway Administration (FHWA) showed that hot pour sealants last over 110 months (about 9 years) with overall 75% effectiveness [11]. This study also showed that service life of sealants varies and might not always be as long. Several factors such as installation practice, climatic condition, traffic level, etc. play role in joint sealant's serviceability. The study

includes the Strategic Highway Research Program (SHRP) H-106 maintenance experiment and the FHWA Long-Term Monitoring (LTM) of Pavement Test Sites [11]. Another sealant study by California Department of Transportation (Caltrans), in their Caltrans/ industry joint sealing field review, stated that rubber joint seals with 10 years of service were still in good condition [12].

Silicone based materials developed much later provide better bonding and expansion characteristics. The application of this type of sealants is easier and safer than the asphalt based sealants. Silicone sealants typically have excellent adhesive characteristics as well as having less sensitivity to changes in flexibility due to aging and temperature effects [13, 14]. Cost is higher than hot pour rubberized asphalt while expected service life is longer. A study conducted on silicone based joints in Arizona showed an excellent performance of joint seal system in a very long period of time (about 20 years) [15]. The Arizona Special Pavement Studies (SPS - 2) jointed concrete pavement test site, was constructed in 1993 with 12 LTPP and 9 ADOT test sections. Each test section includes about 33 transverse joints which were reportedly sealed using Crafcro 34902 non-sag RoadSaver Silicone sealant. Various combinations of base type, concrete strength, slab width, and slab thickness were designed to allow statistical analysis of the contributions of each factor. A March 2013 evaluation of the condition of the joints and seals indicated that overall performance of the SPS-2 joint seal systems was extraordinarily good, considering the seals have been in place for 20 years and the truck lane has carried about 31 million Equivalent Single Axle Loads (ESALs). Figure 1 shows the percent of sealant failure for each section which shows no section exhibits more than 35 percent overall failure [15]. Further performance data obtained from this section of pavement under this study is presented and discussed in Chapter 3.

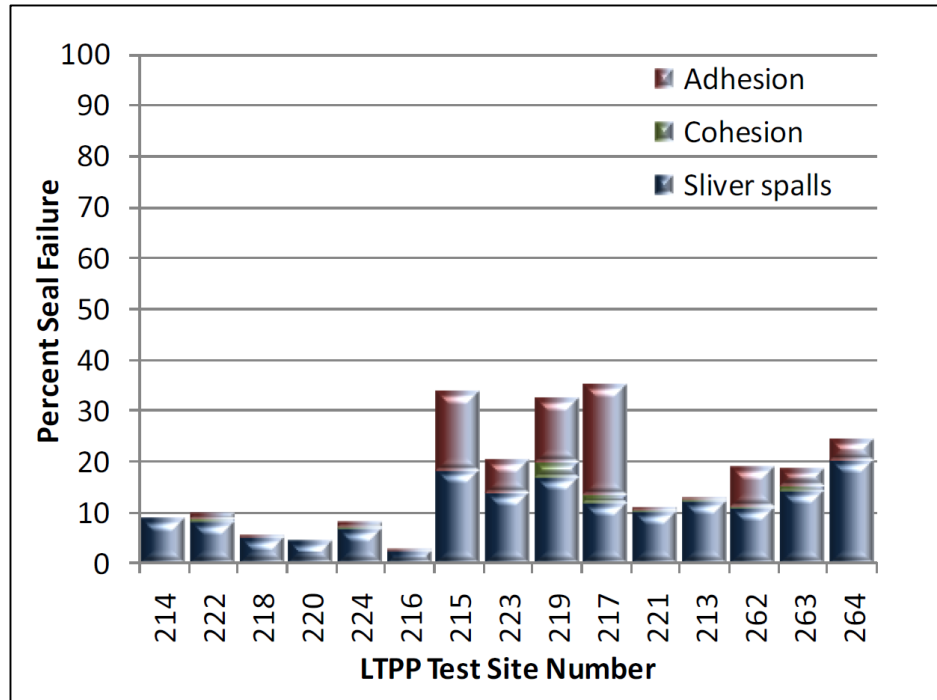


**Figure 1** Overall Failure Rates on Transverse Joints, Arizona Joint Sealant Study [15].

The third major category of sealants along with asphaltic base and silicone base materials is the compression sealant, also called preformed sealants. The compression sealants are designed to remain tight in the joint well when the joint is at its maximum opening and are able to bear the compressive force when the opening are at the smallest as would occur in the summer time. The important consideration when using compression sealants is they should remain in compression. Compression sealants are probably more resistant than other sealant types to deterioration from exposure to weather, sunlight, oils, chemicals, heat, abrasion and impact and hydrostatic pressure. Preformed compression seals normally provide a long service life if the sealant remains in compression (in the appropriate range between 20 to 50 percent of its original width); therefore, these types of sealants must be sized based on expected joint movements in order to function properly. From the economical perspective, the compressed sealants are the most



expensive choice and the asphalt base sealants are comparatively cheap. A study by Michigan Department of Transportation on various concrete pavement joint sealants concluded that preformed compression sealant performed better than other sealant types [16].

Even though some field investigations reported that sealants may not provide a long service life, results from two recent unique studies confirm that sealants if installed properly can achieve service life of 20 years. One of the two studies was at the Federal Highway Administration's Long-Term Pavement Performance (LTPP) SPS-2 Experiment in Phoenix, Arizona as mentioned previously [15]. The other study was coordinated by pavement preservation product manufacturer Crafc0, and took place at Fairchild Air Force Base in Spokane, Wash [17]. In 1989, the U.S. Army Corp of Engineers Construction Productivity Advanced Research (CPAR) conducted a sealant performance study consisting of both laboratory and field evaluations. The study evaluated both hot-pour and silicone sealants. A silicone sealant installed in a conventional manner and a low-modulus, hot-applied asphalt sealant installed using flush-fill geometry. Sealants exhibited a performance period of more than 21 years [17].

Findings of these two studies indicate that properly installed sealants can provide at least a 20 year service life. Previously, there has not been any factual evidence to prove the long-term effectiveness of sealant's serviceability but these findings confirm and document that sealants can last a long time.

## **2.4 Current Sealant Practice**

In recent years, states have adopted a wide variety of joint sealing practices for jointed pavements, based on local experience, climate, and traffic conditions. The purpose of these guides is to have better quality control and assurance and to decrease inspection and

rehabilitation costs. Generally, where there is naturally positive drainage in the sub layers or where climates are very hot and dry, joints experience minimal distress and likely hold less moisture. This may allow agencies to think they could get by with narrower saw cuts without sealing, while in wet climates and less drainable subgrade materials, agencies prefer to have sealed joints [4]. Transverse contraction joints in PCC pavements are traditionally constructed in the following sequence of steps:

- Making an initial saw cut to control cracking.
- Making a second saw cut to create a reservoir for joint sealant.
- Cleaning and preparing the reservoir faces.
- Placing a backer rod in the reservoir, to keep the sealant from adhering to the bottom of the reservoir and to create a curved bottom surface for the sealant.
- Placing sealant material in the reservoir (which may include tooling the sealant into place).

It was reported that saw and sealing operations are estimated to be between 2 and 7 percent of the initial construction cost [1]. A study on relative cost of concrete highway features by American Concrete Pavement Association, ACPA, indicated the relative cost of the unsealed joint is approximately seven percent less than the silicone sealed joint [18]. According to the study this cost is even higher if more expensive sealant materials are used (the most expensive sealant option found to be ½ inch compression sealant) [18].

This is one reason that several State Departments of Transportation (DOTs) have been suggesting alternative methods; the most prevalent alternative is to cut the joints narrowly with the single saw cut and leave them unsealed. This approach is used by the State of Wisconsin DOT where they avoid having wide saw cuts and sealants. In 1990, WisDOT adopted a policy eliminating all PCC joint sealing, in new construction and maintenance. According to the report by Shoher, 1997, this “no-seal” policy has saved Wisconsin \$6,000,000 annually with the claim

of no loss in pavement performance while achieving increased customer safety and convenience [19].

A second alternative is to use narrow joints but to fill them with sealant. In this configuration, the sealant attempts to adhere to the sides as well as the bottom of the saw cut; saving the expense of the second wider saw cut but this places the sealant in a high state of debonding stress. In recent years construction of narrower joints become more common. A Caltrans joint and sealant evaluation showed that joints with the narrowest width (1/8 inch) had least distresses. Also these joints have functioned well even in areas of high temperature variations like in the Central Valley (80 degree temperature swing) [12].

A third alternative is to have the narrow sealed joints, consisting of single saw cuts with a narrow backer rod and sealant installed. Backer rod helps the sealant to have a better support and lay with a structurally better shape which can distribute the stresses more effectively.

These alternatives are intended to reduce the initial cost not necessarily to enhance the performance. All three alternatives (mentioned in order of increasing cost) eliminate the second sawing operation needed to form a joint sealant reservoir, and the additional joint sealant material that would be required to fill the reservoir. This also makes the procedure faster and could save the time [4].

Resealing operations tend to be costly, due to the expenses of the material, labor, construction, joint widening, and lane closures. Lane closure costs depend on both time and traffic level. Shober stated that the cost for maintaining a sealed pavement for 10 years (sawing a joint reservoir and sealing it to resealing the joint whenever it was needed) amounted to as much as 45 percent more than the cost for a similar unsealed pavement [19]. Of course there is a

cost associated with base erosion that should be considered when comparing sealed and unsealed pavements.

## **2.5 Sealant Adhesive and Cohesive Failure**

This section briefly discusses the sealant failure causes and mechanism. In order to evaluate sealant effectiveness during the service life, there is a need to identify and evaluate the effects of different factors on sealants failure mechanism. As discussed previously there are mainly three different sealant types currently used; asphalt based sealants, silicone based sealants and preformed compression sealants. With respect to the sealant, are basically two types of mechanism for failure - cohesive failure and adhesive failure. Other mechanisms pertain the concrete such as swallow spalling or chipping.

Cohesive failure is defined as the failure of the sealant material itself when stresses within the sealant exceed the sealant's strength. Stresses within sealants caused by several factors such as joint movements, traffic load, etc. Over the time, combination of horizontal and vertical stresses coupled with the aging of the sealant may cause internal micro-cracking. Once micro cracking has begun, the problem often grows in scale. Smaller micro cracks lead to larger and larger micro cracks and so on until eventually macro cracks develop. Consequently, such a macro crack may form along the entire sealant depth until the sealant fails [20-22].

Adhesive failure is defined as a failure at the sealant-concrete interface. Adhesive failure in joint sealants is more common than the cohesive failure. Adhesive failure should take some time to develop in properly installed sealants. Aging of the sealant material can make the sealant stiffer and less flexible. Therefore sealants receive higher stresses at the interface that leads to debonding and failure [23]. Another type of adhesive failure may occur when joint reservoir walls are not properly cleaned and dried prior to installation. If there is debris or moisture at the

interface, sealant will adhere to the debris instead of the concrete slab, thereby decreasing the amount of contact area between slab and sealant. This makes the initial bond between sealant and joint wall weak that leads to debonding. This type of adhesive failure happens in early ages therefore it is called premature failure [20, 21]. Figure 2 and Figure 3 show the cohesive and adhesive failures in sealants. Table 1 shows common factors and causes of sealant failure.



**Figure 2** Cohesive Failure in Sealants.

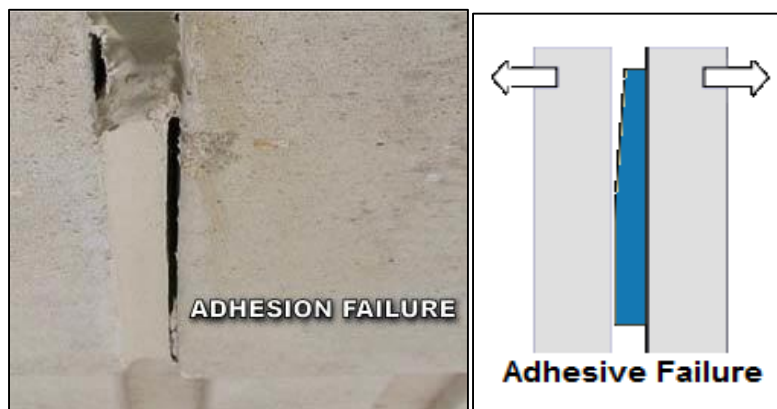


**Figure 3** Adhesive Failure in Sealants.

Sealant installation is a critical factor as many researcher have shown that if sealants installed properly can provide a long service life [3, 17]. Improperly installed sealants are often subjected

to premature deterioration from weather and traffic [21, 24]. The sealant must be installed under suitable weather conditions, with virtually no moisture present in any form. Excessive humidity causes a problem in achieving the full adhesion potential. Moisture present between the substrate and sealant will result in a poor wetting surface for sealant and lowers the adhesion [23]. Given the stringency of cleaning and installation procedures, these operations should be inspected as they proceed. Without such inspection, a great deal of effort and money could be wasted on ineffective seals. Before the installation the joint seal, joint well walls should be cleaned to prevent contamination of the sealant materials affecting the bond to the joint wall [4].

There are many popular techniques for surface preparation and to achieve better installation that are used to clean and prepare the concrete substrate for sealing purposes. These pretreatments of the substrate generally include one or more techniques such as water-blasting, sand-blasting, air-blasting, etc. [23, 25].

Moreover, if sealants are installed too far below the pavement surface, incompressible materials are likely to enter the joints. Conversely, sealants installed at or slightly above the pavement surface are likely to be damaged or destroyed by vehicle tires.

**Table 1** Factors and Causes of Sealant Failure.

Factor	Cause	Failure Type
Factors related to sealant material properties	Low bond strength between sealant material and joint reservoir	Adhesive Failure
	Low cohesiveness quality	Cohesive Failure
	Lack of sealant material's extension capacity	Adhesive/Cohesive Failure
Climatic factors (Solar radiation, temperature changes, etc.)	Weathering and aging (Stiffening and losing flexibility)	Crack initiation in the middle of the sealant - Cohesive Failure
Factors related to construction/installation	Existence of moisture at the joint wall prior to installation	Premature Failure (Adhesive)
	Joint wall dirtiness prior to installation	Premature Failure (Adhesive)
Pavement/Joint and sealant design related factors	Sealant size and geometry (depth to width ratio)	Affects stress distributions, lead to fatigue - Cohesive Failure
	Joint width too wide; compression sealant not in compression	Sealant displacement
	Joint width too narrow during summer; Sealant in excessive compression	Sealant press/damage
Traffic/Load related factors	Slabs vertical displacements while traffic passes (Particularly in case of joints with faulting) - sealants elongation cycles	Adhesive /cohesive Failure
Joint distresses	Spalling, corner breaks, etc. directly make damages to the sealant	Sealant damages and failures
Sealants chemical reactions	Destructive chemical reactions between sealant materials and fuel/engine oils particularly the jet fuels in airfields	Stiffening - Cohesive Failure

As it shown in Table 1, although the sealant material plays an important role, the failure of the sealant is not always related to sealant material properties. Sometimes failure occurs due to the poor design of the slab and joint system or due to poor quality curing. Researchers found that sealant failures could often be attributed to under estimating the characteristics of a joint rather than to deficiencies of the sealant material itself [26]. This might happen when the joint opening is wider than the sealant extension properties (during winters), or when the joint becomes too narrow causing the sealant material to be over compressed (during summers). The design of a joint should ensure the joint movement without failure of the joint sealant. The main failure mechanism in compressed sealants occurs when the joint opens too wide. Sealant geometry and size also influence the sealants performance. A 1992 study based on finite element analyses showed the advantage of using seals with low depth to width ratios. Sealants with better geometry distribute the stresses and may last longer. The researchers also found that for seals with higher depth-to-width ratios, adhesion failure is likely to originate at the center of the contact region between the seal and joint wall, rendering the failure undetectable [26-29].

Although not all may agree, a study involving measurements taken on more than 100 expansion joints in concrete pavements in Massachusetts, concluded that although the effect of vertical movements on joint seal performance may be negligible, the effect of horizontal displacements was not. Three distinct stress or strain states were recognized in sealants:

- Stress reversals: sealant alternating between tension and compression,



- Sealant always in compression, and
- Sealant always in tension.

The stress reversal case was cited as the most detrimental condition to joint seal performance. The author stated that “many joints sealed in the past with the sealants alternating through compressive and tensile stress-strain cycles have shown adhesion failure and distortion in the sealant shape”. Apparently a sealant in a continuous state of compression was desirable, since this produced no adverse stresses at the bond interface between the sealant and joint wall [30].

Joint sealant failure cause could be construction related. A common joint distress is spalling which accelerates joint sealant’s failure. Another construction related factor is the uniform distribution of broken saw cut joints. Inconsistent, jointing often leads to irregular joint movement causing some joints to open more than others. In Pennsylvania, for example, some projects experience only every third joint at 6-m (20-ft) cracking full-depth. The detrimental result of this phenomenon is that the joints that do crack are not contracting according to the theoretical joint movement calculated for the designed joint spacing. So the adjacent joints experience wider movements than can be sustained by the sealant. Problems experienced by many joint-seal designs result from inadequate construction quality control [4].

## **2.6 Questioning the Need for Joint Sealing**

At the 16th World Congress of the Permanent International Association of Road Congresses (PIARC), the Technical Committee on Concrete Roads presented a report concluding that for joint spacing of 4 to 6 m there was no disadvantage in leaving

narrow transverse joints unsealed when: (a) traffic is light, (b) traffic is heavy but the climate is dry, or (c) traffic is heavy and the climate is wet, but the pavement is doweled [24]. Earlier published literature from Europe had suggested similar conclusions [19, 31].

As early as 1967, S. E. Hicks addressed the Highway Research Board concerning 20 years of observations that illustrated the lack of benefits from joint sealing [19]. After that in 1987, another study by Karl Dunn of the Wisconsin DOT indicated the same results [32]. Followed by two test programs, one in the period of 1958-1966, in the southbound lanes of US-41 in Washington County Wisconsin and the other one which was larger experiments project between 1966 and 1977 in Columbia County Wisconsin, researchers found that there is no difference in measurable pavement performance between the sealed and unsealed sections. A paper by Shober from the Wisconsin DOT stated that regular joint resealing was judged to have no benefit to overall pavement performance compared to not resealing [19]. Shober also reported the performance of sealed and unsealed sections that were 8 to 22 years old. In order to measure distresses, Wisconsin uses the pavement distress index (PDI), which measures all distresses (extent and severity) and combines them into one index. Each distress is weighted to account for its significance on pavement performance. The PDI scale ranges from 0 to 100; with 100 the worst score. The report indicates that almost in all cases the performance of the unsealed sections is better than the performance of the sealed sections. A statistical analysis of pavement ride (in terms of IRI), concluded that joint sealing has no significant effect on pavement ride qualities.

While Wisconsin state officially has passed the policy not to seal the joints, researchers from other states criticized the Wisconsin's findings. In 1996 two independent teams visited Wisconsin's field sections and tried to verify the WisDOT's findings. They noted that the sealed sections had not been maintained properly during the experiment and did not reflect a sealed condition. Obviously if the joint seals were not maintained properly then the comparison between sealed and unsealed conditions would not be differentiable.

Later in 2002, Burke et al. in response to Wisconsin research findings stated that valid generalized conclusions about the suitability of unsealed pavements cannot be made based on extrapolations of short-term visual performance observations. This study also reported that pavement specialists of transportation agencies with the most long-term unsealed pavement experience (California and most Western European countries), have concluded that well-maintained pavement with doweled and sealed joints, and stabilized well-drained bases provide the most functional, durable and cost-effective pavement applications [33].

Morian and Stoffels 1998, observed one reason that joint sealing isn't as effective as expected is because of poor design or installation; they also stated that some factors such as climate conditions were limited in unsealed experiments. Arizona's drying climate, or Wisconsin's drainable base makes comparison difficult. No comprehensive field tests thoroughly evaluating joint seals and pavement performance in an appropriate manner over a significant period of time were unavailable at that time [4].

An analysis on LTPP Database in 2000 on relative performance of sealed and unsealed joints concluded that despite the conventional wisdom concerning the need to keep concrete pavement joints well sealed, studies on the subject have not demonstrated that JPCP with sealed joints and JPCP with unsealed joints perform differently in terms of spalling, faulting, IRI, or deflections” [34].

A joint seal study was funded by the U.S Department of Transportation, August 2008, in which data were collected from a total of 117 test sections in 11 states (Arizona, Colorado, Florida, Georgia, Illinois, Indiana, Iowa, Minnesota, New York, Ohio, and Wisconsin). Statistical analyses of the collected distress data detected no significant difference between average pavement performance in the unsealed-joint test sections and the silicone-sealed, hot-pour-sealed, or preformed-sealant test sections at the same site [1].

An evaluation report in 2009 by North Dakota Department of Transportation on unsealed joint performance showed the sealed joints would reduce the amount of water intrusion into the pavement and base section. This study did not recommend leaving the concrete joints unsealed [35].

As it has been discussed, research over the past decade on the efficiency of the sealing has involved field studies. The main problem with all these studies is the limited number of variables involved, making extension of results to other situations a challenge. Most of the studies considered 4 types of sealing (3 main sealant types; hot pour, silicone and preformed plus unsealed joints) but for each single study other variables such as traffic, climate, base type, joint geometry and opening etc were not

changed. Additionally, these studies have only reported performance over a short period of time limiting application of the results.

Despite all the shortcomings of these experiments, they are helpful to answer some of the questions in the debates of seal no seal. Research shows that for some situations there is no need to seal the joint, particularly in dry areas or those that have drainable structures. Some studies show that considering a particular base material, traffic and climate there is no difference between the performance of the sealed and unsealed PCC pavement. Faulting, spalling and cracking are the main criteria's that has been considered in these studies. So the general question of "seal no seal" is better to be asked as "where or in what conditions warrant sealing?"

The major factor in this debate has been the cost; if the elimination of the seal and reseal process is really a cost-wise benefit, then the cost saving of not having them sealed will be higher than the costs associated with consequential resulting pavement repair and maintenance. "If joint sealing does enhance pavement performance, it is necessary to determine if the enhancement is cost-effective. Cost effectiveness must include costs of second saw cuts, all sealing costs and all resealing costs for the life of the pavement, and user delay and safety costs caused by resealing. Thus, it is not enough just to prove an enhancement in performance; the enhancement must equal the costs" [19].

From a risk perspective, the consequences of not sealing may be too high because the expenses of reconstruction are too high. Thus, sealing is only economical if it can be shown to be necessary. Therefore, the key to answering the seal-no seal

question in most cases is determining the probability that the cost and risk are both reasonable. Like many other engineering decisions there is little interest in wasting money on low risk situations while on the other hand, there is also little interest in saving a little money by ignoring a huge risk. By changing the combination of influential factors such as base type, climate, traffic, etc. the different combinations and pavement configuration would yield a different probability or need for sealing. Hence, the general question of “seal-no seal” would perhaps be better phrased if it were asked in terms of where or in what condition should sealing be done? When and where does joint sealing achieve a cost-effective improvement in pavement performance?

### 3. INFILTRATION TESTING OF JOINT SEALANTS

#### 3.1 Pavement Test Area at Riverside Campus

The Riverside Campus pavement test area consists of a concrete segment that is 38 ft long and 12 feet wide, with four existing transverse joints spaced at 15 foot intervals. The 12 foot wide lane includes a curb on one side. The concrete slab is 6 inches thick with an open graded high permeable subbase beneath. The test area was divided into four test areas as shown in Figure 4.

In addition to the four existing transverse joints, four additional full-depth sawn joints were made on 2 ft intervals in each test area as shown in Figure 5. Each full depth cut was 1/8 inch wide with wells cut 1/4 inch wide and 1.5 inch deep. After sawing the joint wells, washing operations were conducted to clean the joint reservoir.

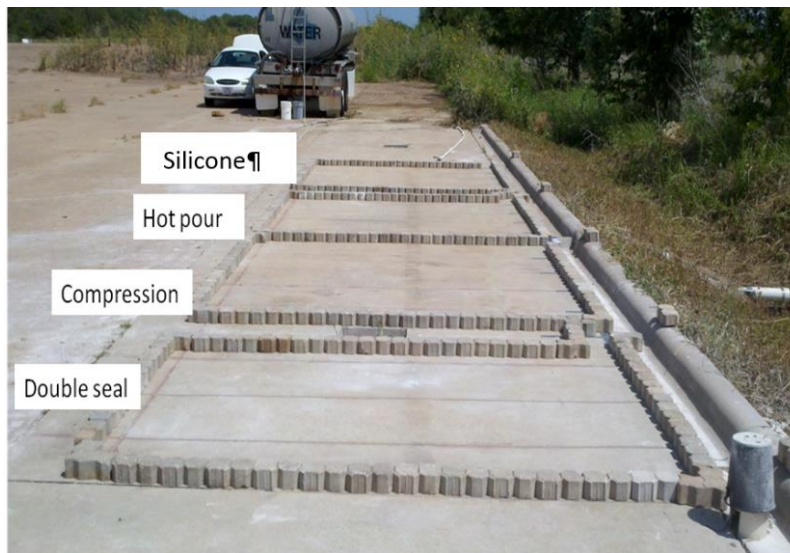


**Figure 4** Layout of Joint Sealant Test Area.

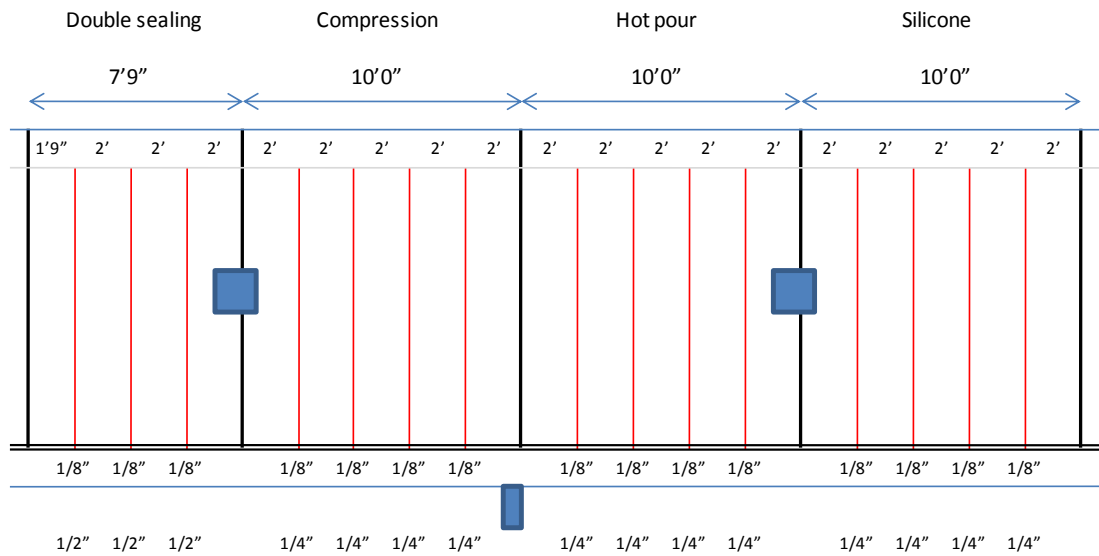


**Figure 5** Joint Sealant Layouts.

Figure 6 shows the process of joint sealing. Joints walls were cleaned and completely dried before placing the sealants. Sufficient time (at least one day) was provided to ensure that adequate drying of the joint walls took place. The sides of the new joints were sandblasted and then air blasted before sealing (Figure 6-a). Preformed compression sealant were placed using an adhesive and an installation machine (Figure 6-b). For the liquid type sealants, backer rods were used to shape sealant reservoirs.





a) Sand and Air Blasting

b) Compression Seal Placement



c) Backer Rod Placing

d) Silicone and Hot-pour Seal Placement

**Figure 6** Joint Sealing Process.

They were placed to a depth of 3/4 inch using a wheeled roller (Figure 6-c). Both, hot pour rubberized asphalt materials and silicone sealants were placed with backer rods and were placed with care to avoid trapping air bubbles (Figure 6-d).

### 3.1.1 Test Conditions

The project work at the Riverside Campus focused on advancing the understanding of the sealant effectiveness related to moisture infiltration. Many factors influence the performance of a joint sealant where the ones that were included in the experimental design for examination in this project are shown in Table 2. The three most popular types of joint sealants were tested under the following sealing conditions. Generally, joints that are well sealed as a result of the installation and are highly effective in limiting the infiltration of water. Joint seal materials generally deteriorate over time either cracking or separating from the joint wall which accordingly leads to a possibility of moisture infiltrating the pavement substructure.

**Table 2** Test Controlling Factors.

Sealant Type	Hot pour rubberized asphalt
	Silicone self-leveling
	Preformed compression
Sealant Condition	100% sealed (No debonding)
	75% sealed (25% debonding)
	50% sealed (50% debonding)
	25% sealed (75% debonding)
	0% sealed (No bonding)
Joint Configuration	1/4" (6mm) wide by 1-1/4" deep
	3/8" (6mm) wide by 1-1/4" deep
	1/2" (6mm) wide by 1-1/4" deep

The rate of surface water infiltration is thought to be governed by the degree of degradation that has taken place in the joint sealant. The seal condition in this study was represented in part by the amount of debonding present. Sealants were carefully debonded along the joints prior to the tests at different levels; 100%, 75%, 50%, 25% and 0%. 100% debonding represents a condition in which sealant is not bonded to at least one side of the joint well; as such one side of the sealant to varying degrees (as noted) was carefully cut along the joint wall.

### **3.1.2 Flow Test (Infiltration Test)**

Infiltration or flow testing was performed using a falling head permeameter. The edge of the permeameter was sealed prior to filling the device with the water and recording the time for water head drop to occur. This test method is relatively quick, cheap and

sufficiently adaptable to allow measurements to be made at multiple locations along the sealed joint under field conditions.

Figure 7 shows an infiltration test on an existing joint. The original saw cut width was 1/8 inch and the crack widths were approximately 0.04 inch. Since the pavement was constructed over 15 years ago, saw cut joints and cracks were clogged with debris and dust resulting in a low infiltration rate of 0.11 gal/hr/ft. After pressure washing the joint, the infiltration rate increased to 0.14 gal/hr/ft. Cleaning through the full depth of the existing joint (to the extent that was accomplished) resulted in an increase in the infiltration rate.



**Figure 7** Flow Test on Existing Joint.

### 3.1.2.1 Evaluate Infiltration Rates of Sealed Joints

After 3 weeks of cure time, a series of infiltration tests were conducted for each of the three joint sealant types. It was immediately observed that no infiltration occurred for any of the three types of seals and all joints were sealed completely without any defects.

In order to better represent the type of deterioration that occurs under normal wear due to weathering and traffic, as a second series of testing, thin slots were cut along the interface between the joint sealant and the joint well wall to create varying degrees of debonding. Sealants were carefully cut along the joint wall to make different debonding levels. Figure 8 shows 25% and 50% debonding for silicone joint sealants.

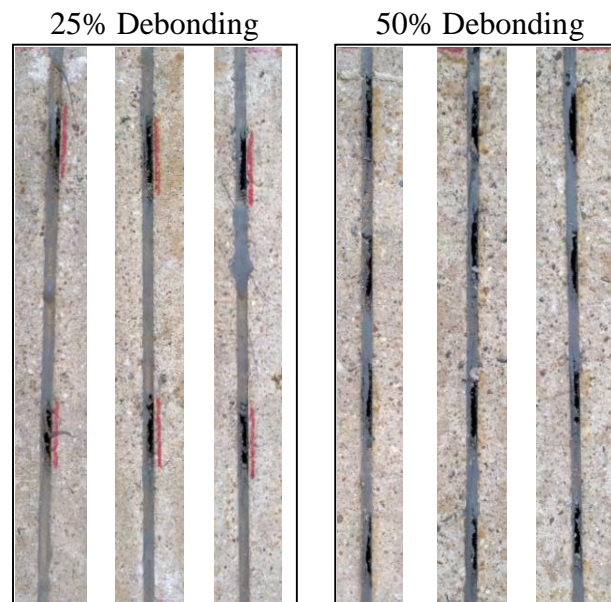


**Figure 8** Damaged Sealing Condition.

Flow test results on damaged sealants are shown in Figure 9. The measured flow rates were higher due to the increased amount of sealant damage. The hot pour sealants showed the highest flow rate while the silicone sealants showed the lowest flow rate.

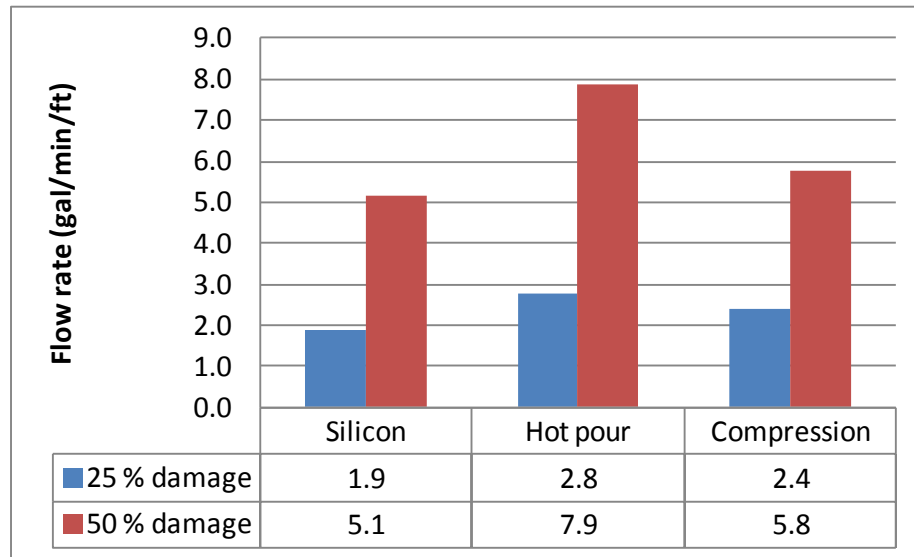


**Figure 9** Flow Test Results on Damaged Sealants.

### 3.1.3 Flow Test Using a Movable Joint System

With the original test setup, the feasibility of representing the effects of realistic joint movements under field conditions was limited; therefore a movable joint system was installed. Joint seals under a specified amount of debonding while subjected to tensile strains (as would occur under widening conditions) most likely will yield larger amounts of flow over the debonding length, similar as what would occur under temperature contraction after a certain amount of debonding has occurred (several years into the performance cycle), causing the joint to be subjected to greater moisture infiltration. To consider joint movement and debonding effects on subsequent moisture penetration, the field experiments considered variable joint openings for different joint widths and

degrees of debonding. Such a system is helpful to simulate different joint opening widths due to temperature changes that occur during a given time period of a sealant that is beginning to experience failure. Figure 10 and Figure 11 show the schematic view and the picture of the installed movable joint system. Using this system, the opening of the joint reservoir was controlled for different joint widths to cause different amounts of flow to take place.

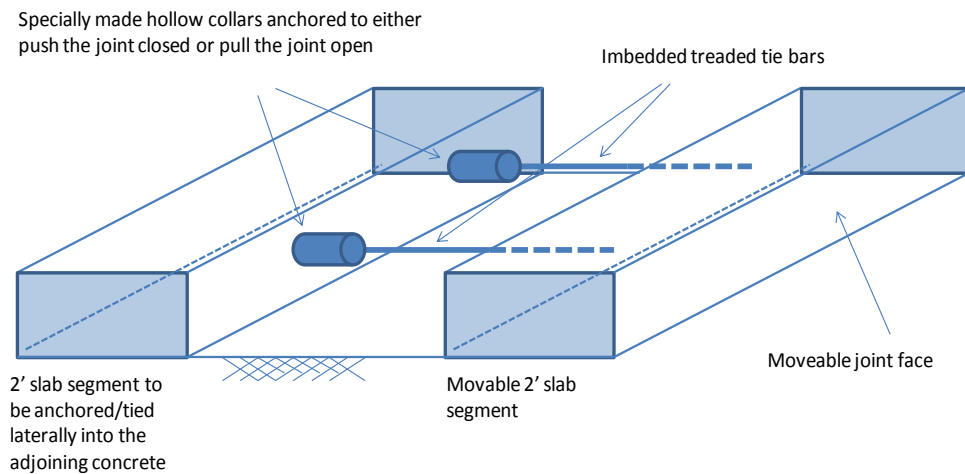


**Figure 10** Schematics of Movable Joint System.





**Figure 11** Installation of Movable Joint System.

### **3.1.3.1 Test Results of Movable Joint Systems**

Test results from joints with 1/4 inch wide joint reservoirs using the three types of sealants (hot pour, silicone, and preformed compression) as well as an existing unsealed joint that was 1/8 inch wide are reported here in. Sealants were debonded from the joint wall using a sharp knife with minimum disturbance of the original shape and opened gradually under controlled testing to measure the water infiltration rate. The gap width was increased at 1/128 inch (0.008 inch, 0.2 mm) increments.

Table 3 and Figure 12 show the infiltration rates versus joint openings for three sealant types at 100% debonding and an unsealed joint (the zero opening represents the

original joint width which is 1/4 inch for the sealed joints and 1/8 inch for the unsealed joint).

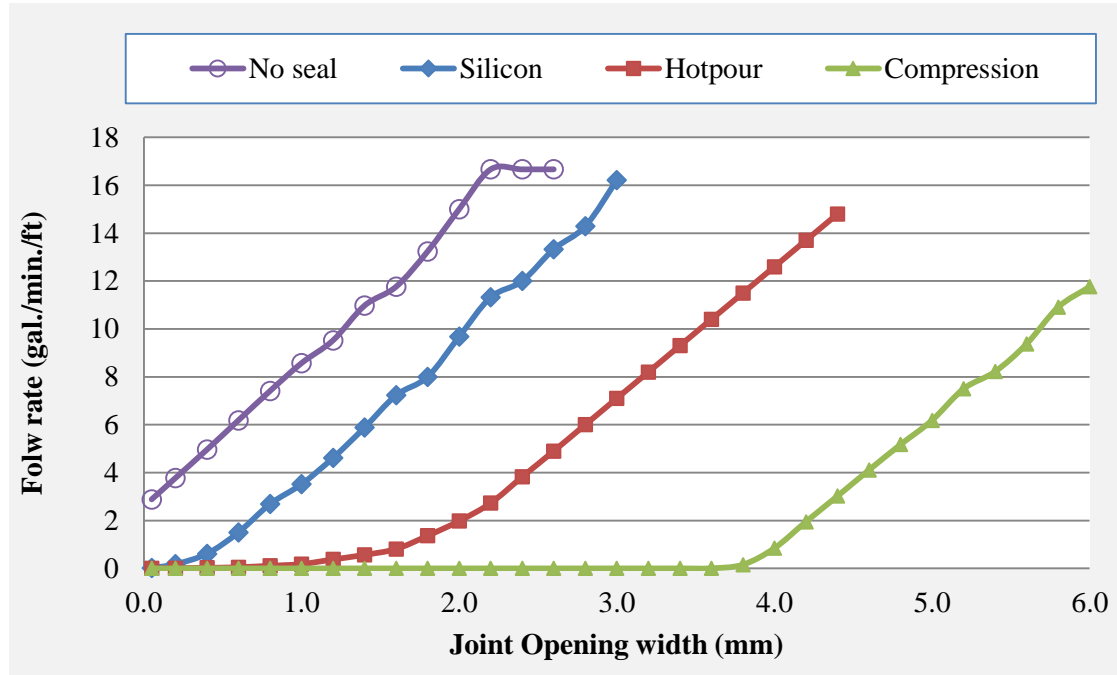


**Figure 12** Flow Test Results for Various, 100% Debonded Joint Sealant Types.

**Table 3** Flow Test Results for Various 100% Debonded Joint Sealant Types.

Joint opening width (inch)	Joint opening width (mm)	Flow rate (gallon/min./ft)			
		No seal	Silicone	Hot pour	Compression
0.002	0.1	2.88	0.020	0.001	0
0.008	0.2	3.77	0.18	0.010	0
0.016	0.4	4.96	0.61	0.025	0
0.024	0.6	6.19	1.50	0.050	0
0.031	0.8	7.41	2.69	0.11	0
0.039	1.0	8.57	3.52	0.18	0
0.047	1.2	9.52	4.62	0.38	0
0.055	1.4	10.98	5.88	0.57	0
0.063	1.6	11.76	7.23	0.81	0



Joint opening width (inch)	Joint opening width (mm)	Flow rate (gallon/min./ft)			
		No seal	Silicone	Hot pour	Compression
0.071	1.8	13.24	8.00	1.36	0
0.079	2.0	15.00	9.68	1.98	0
0.087	2.2	16.67	11.32	2.73	0
0.094	2.4	16.67	12.00	3.82	0
0.102	2.6		13.33	4.90	0
0.110	2.8		14.29	6.00	0
0.118	3.0		16.22	7.10	0.000
0.126	3.2			8.20	0.001
0.134	3.4			9.30	0.002
0.142	3.6			10.40	0.005
0.150	3.8			11.50	0.16
0.157	4.0			12.60	0.85
0.165	4.2			13.70	1.95
0.173	4.4			14.80	3.02
0.181	4.6				4.11
0.189	4.8				5.17
0.197	5.0				6.19

The unsealed joint showed the highest infiltration rate. Infiltration of the joint with the silicone sealant initiated flow at a threshold joint opening less than 0.04 inch (1 mm) while the threshold flows for the joint with hot pour sealant occurred with an opening greater than 0.04 inch (1 mm) joint opening; the threshold with preformed compression sealant occurred at the flow when the openings were greater than 1/8 an inch (3 mm) as shown in Figure 12.

Even though the threshold opening for the different sealant types were different, the flows beyond the threshold are not for 100% debonding. The increasing rate of water infiltration with the increase of joint opening shows the lowest infiltration occurs

with the hot pour sealant and highest for the unsealed joint (as shown in Figure 13 and Figure 14). For all the sealants as joint width increases greater flows occur, but since the flows in question here occur along the unsealed length of the joint, the rates are similar (the rate in the case of the hot pour sealant although lower appears to approach the rate of the other sealants). At 100% debonding, it is difficult to discern any real differences among sealant types and, as noted later, any differences across similar lengths of debonding notwithstanding differences in the threshold flow levels or recommended extension limits. Characteristics of preformed compression sealants was their tendency to recover to their original shape over time; thus, infiltration initiated only when the opening width exceeded its recoverable range (recoverable range was also gradually reduced with time due to creep recovery under continuous compressed conditions).

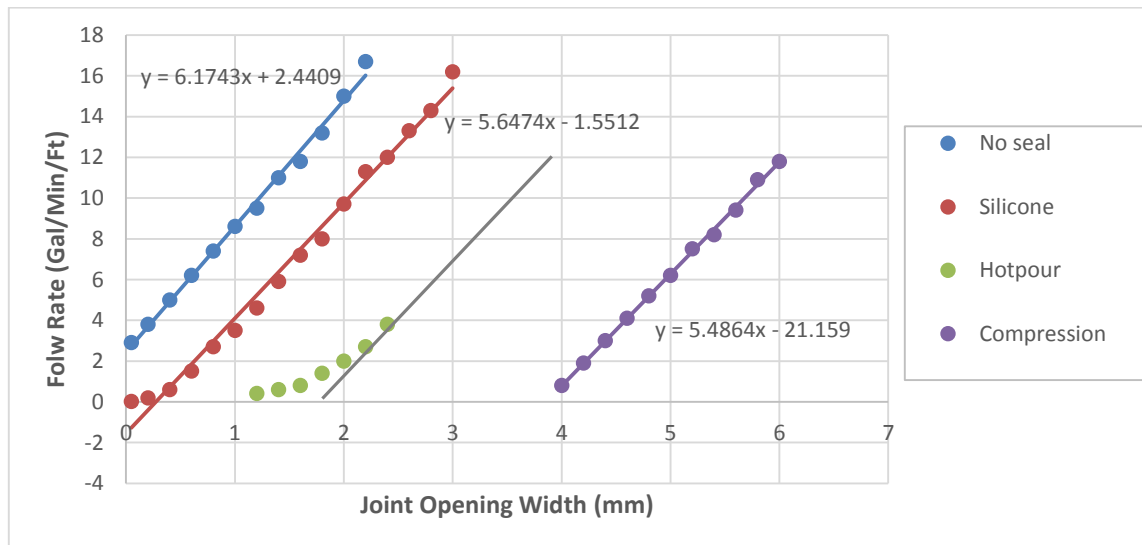


**Figure 13** Slope of Flow Rate Increase with Joint Opening at 100% Debonding.

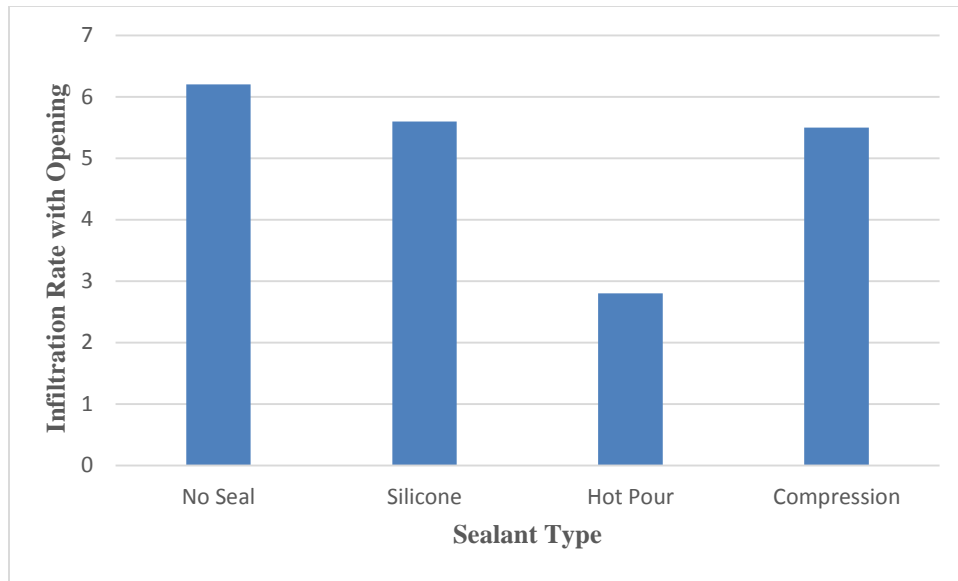


**Figure 14** Increasing Rate of Flow with Joint Opening at 100% Debonding.

Another perhaps more important factor besides the type of joint sealant affecting flow is the pressure head shown in Figure 15 shown for a silicone type sealant.

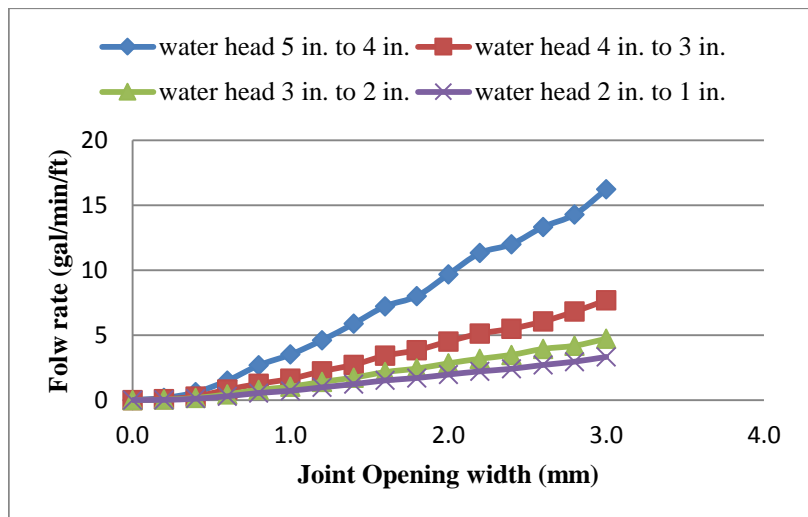


**Figure 15** Increasing Rate of Flow with Joint Opening for a Silicone Type Sealant at 100% Debonding.

Figure 15 results are different for the other types

of joint sealants included in the test program but it is clear that important factors are joint sealant type, joint opening, and pressure head in the computation of infiltration rate.

### **3.1.4 Tests on Joint Sealant Installation**

The most common form of failure in a joint seal is the adhesive type of failure where the seal debonds from the joint wall; this is principally thought to be a premature type of failure that is mainly due to installation factors.

The procedure of sealing or resealing involves sawing, and refacing the sides of joint reservoir. The cutting blade is cooled with water which forms a watery mix with the saw cuttings which when dried can leave a heavy residue on the face of the joint. This residue must be thoroughly removed in order for a sealant to have proper bond to the joint wall. Any residue can significantly decrease the bond strength between the sealant material and the joint. Even though water blasting or sandblasting is done in order to clean the joint prior to sealing, these procedures may not be carried out well enough in the field as effectively as needed. It should be mentioned that water blasting or sandblasting may contribute to the dirtiness of the joint wall if they are not done correctly. Field observations and investigations from contractors and others indicate that the installation process has a major impact on bond capacity of the joint [10].

The testing program addressed the importance of installation quality associated with joint sealing. As previously noted, a main element of joint preparation is cleaning of the joint side walls prior to placing the joint seal. Tests were conducted using a slurry of saw dust with density of 68041.5 grain per gallon (1164.74 kg/m<sup>3</sup>) varied to make three different concentration levels (Slurry to water ratios of 1:1, 1:1/5 and 1:2). Results were then analyzed with respect to dirtiness or the degree of contamination and sealant

performance. After cleaning the joints, joints were prepared with four different dirtiness levels:

1. Clean joints, no dirt (0% slurry),
2. Dusty joints (33% concentration of slurry),
3. Dirty joints (40% concentration of slurry), and
4. Very dirty joints (50% concentration of slurry)

Slurry mixes were brushed on the joint reservoir walls. Application of the slurry in this manner allowed for the needed accuracy and consistency of the contamination and distributed the dirtiness equally along the joints. Sealants were placed and later the joints were moved to various openings to perform flow testing. The results for the silicone sealants are shown in Figure 16.

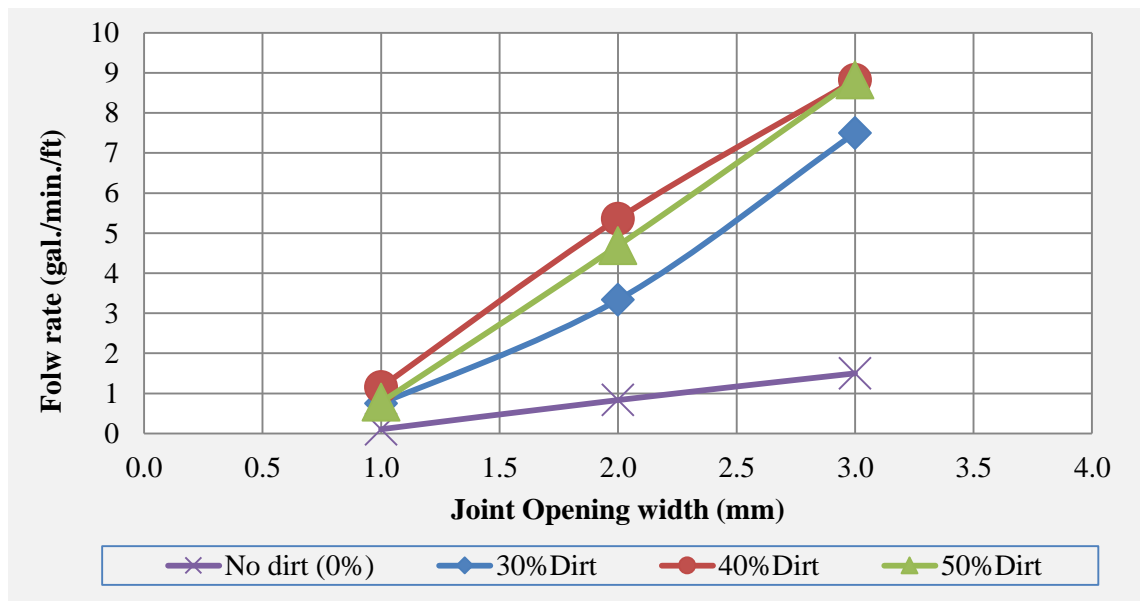


**Figure 16** Water Infiltration Rates for Different Joint Dirtiness Levels

There is a significant difference when the dirtiness level was close to zero. Results also show that after a certain level of dirtiness or debonding, the joint sealant allowed a greater amount of water into it but at levels much lower than 100% debonding which is the case with either hot poured or silicone sealants since they restrict flow due to the bonding they do have to the edges of the joint.

### 3.1.5 Radar Scans of Unsealed Joints

Several radar scans using GPR technology were made over unsealed joints as part of a special study to compare dry versus wet conditions. The type of radar used to make the scans was the 2.6 GHz ground-coupled GSSI StructureScan™ Mini HR radar system shown in Figure 17. This radar system measures the reflection amplitude and the time of travel of a micro wave it sends through the concrete floor slab and layers immediately below. This information is used to calculate the dielectric constant as well as

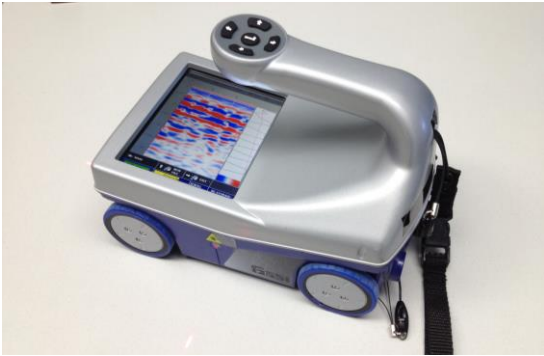


**Figure 17** GSSI StructureScan™ Mini HR Radar System.

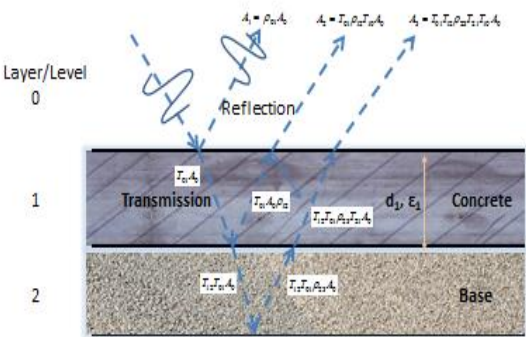


**Figure 18** Schematic of Transmission and Reflection Radar Waves.

the reflection and transmission coefficients. Figure 18 schematically illustrates a radar

wave travelling through a concrete medium with a pavement structure along with mathematical relationships useful to account for the speed of travel of light in a vacuum (c) and signal attenuation effects.

$$\text{Wave Velocity} = \frac{2d_1}{\Delta t} = \frac{c}{\sqrt{\epsilon_1}}; d = \frac{c}{\sqrt{\epsilon_1}} \frac{\Delta t}{2}; \epsilon_1 = \frac{c\Delta t}{2d_1}$$

where

$d_1$  = slab thickness (L)  
 $\Delta t$  = time of travel (t)  
 $c$  = velocity of light in a vacuum  
 $\epsilon$  = dielectric constant

Also,

$$\text{Reflection Coefficient } (\rho_{01}) = \frac{A_1}{A_0} = \frac{\sqrt{\epsilon_1} - \sqrt{\epsilon_0}}{\sqrt{\epsilon_1} + \sqrt{\epsilon_0}}$$

$$\text{Transmission Coefficient } (T_{01}) = \frac{2\sqrt{\epsilon_1}}{\sqrt{\epsilon_1} + \sqrt{\epsilon_0}}$$

The reflection coefficient is a function of the wave amplitude before and after passing through any layer interface

while the transmission

coefficient is a function of

the material dielectric

constant above and below a

layer interface. As shown in

the figure, the amplitude of

the various returning waves

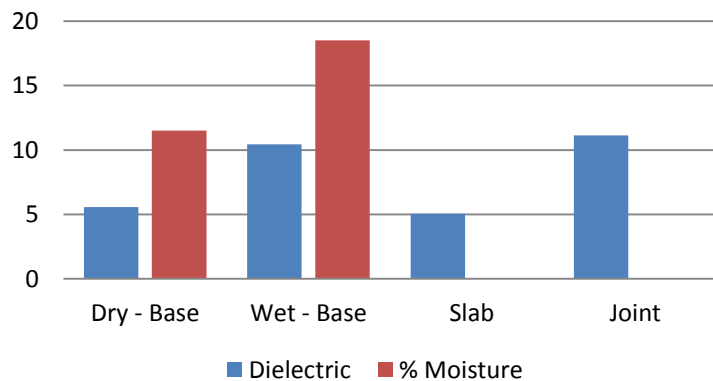


**Figure 19** GPR Test Result – Riverside Campus.

to the slab surface carry with them the reflectance and transmissibility of each layer they travel through. Results of testing at the Riverside Campus site are summarized in Figure 19. Since the Riverside test slabs had a 6 permeable base, the joints did not hold water (unless it was retained in a plastic bag). As a consequence the base dielectric and % moisture were determined from the test data using the approach described in Appendix A. Slab and joint dielectric data is also shown in the figure indicating the difference in dielectric when water is held within the joint.

### 3.2 Tests on SR 59 South Bound

Joint seal testing was carried out on a special experimental joint sealant section located near Joliet, Il (see Figure 20) constructed in November 2009. The test section consisted

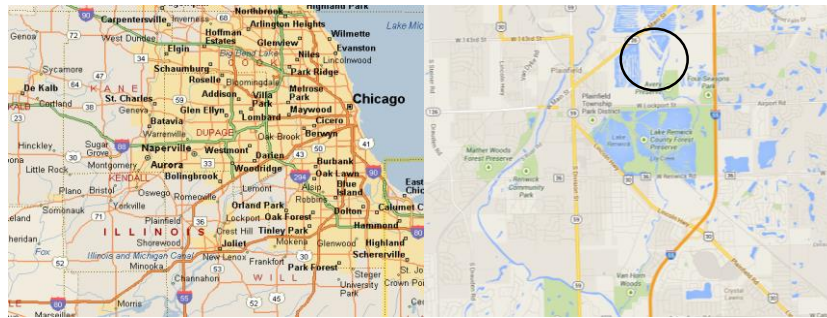


**Figure 20** Location Map for SR 59 Test Section.

of a dowelled 9 3/4 inch jointed concrete pavement at 15 foot joint spacing with a variety of joint seal configurations constructed to demonstrate the long term effectiveness of sealants on overall pavement performance. The test section consisted of ten different test cells that had combinations of hot pour, silicone, and unsealed joints each on an open graded, recycled RAP base. The testing reported here included only three of the cells



shown in Figure 21. TS-3 is a control section for the entire experiment and TS-2 was constructed using a single saw cut design.

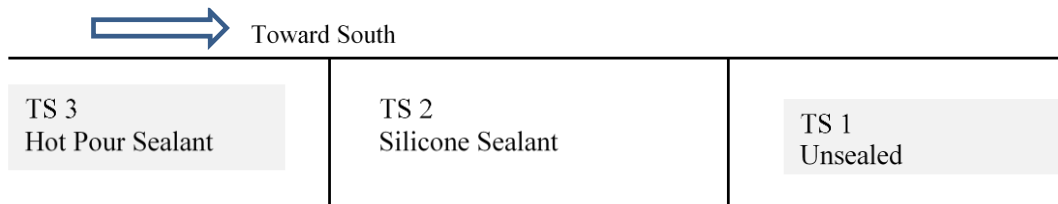


Figure 21 R 59 Cells Tested in this Sequence (2009 installation).

The testing mainly focused on section TS-3 and TS-1 and consisted of the following:

- Flow Tests (Infiltration Test)
- Ground Penetration Radar (GPR)
- Falling Weight Deflectometer (FWD)
- Core Samples
- Flooding the pavement to consider test results in both dry and wet conditions

Results of the infiltration testing in the form of a measured flow rate, (Figure 22) as previously described, are shown in Table 4 where a comparison between sealed and unsealed joints can be made. Clearly, unsealed joints transmit water at a much higher



Figure 22 SR 59 Infiltration Testing (2013).

**Table 4** Infiltration Test Results from SR 59.

Test No.	Section	Sealant Type	Flow Rate (gal/min)	Comment
6	TS 1	No Seal	3.94	Two Locations

Test No.	Section	Sealant Type	Flow Rate (gal/min)	Comment
7	TS 1	No Seal	4.04	along Same Joint
8	TS 1	No Seal	11.30	Two Locations along Same Joint
9	TS 1	No Seal	11.13	
10	TS 1	No Seal	11.30	After Flood
11	TS 1	No Seal	9.70	Longitudinal Joint
1	TS 3	Hot Pour	1.75	Same Joint- Sealant Removed
2	TS 3	No Seal	10.13	
3	TS 3	Hot Pour	1.68	
4	TS 3	Hot Pour	0.51	After the Artificial Flood*
5	TS 3	Hot Pour	0.17	

rate of flow. The flow data was also used with the follow expression for hydraulic conductivity or permeability (K):

$$K = 2.303 \left( \frac{L}{t} \right) \log \left( \frac{h_1}{h_2} \right)$$

Where

- L = Flow length (L)
- t = Infiltration time (t)
- h<sub>1</sub> = Initial hydraulic head (L)
- h<sub>2</sub> = Final hydraulic head (L)

As shown in Table 5 there was approximately a 6 fold increase without the sealant in place. It is speculated that this value of permeability (k) effectively measures the hydraulic conductivity of the base layer or the cavity between the slab and the base at the joint.

**Table 5** GPR Permeability Test Results from SR 59.

Section	Sealant Type	Permeability (ft/day)	Comment
TS3	Hot Pour	116	Average Permeability with Sealant (Before Flood)
TS3	Hot Pour	682	Average Permeability without Sealant

## Results from GPR

testing carried out on the test sites are summarized in Table 6. The analysis of the data was as previously described

**Table 6** GPR Test Results from SR 59.

Section	PCC	Composite	$\epsilon$	% $\Theta_w$
<i>TS3 – Hot Pour</i>				
Dry	6.10	11.04	9.96	0
Wet		8.58	17.19	29
<i>TS1 - Unsealed</i>				
Dry	7.32	8.44	17.18	0
Wet		9.05	16.04	22

led to the dielectric values listed in the table which involved the separation of the joint seal from the GPR measurements (which effects were included in the composite readings). Further analysis based on the discussion provided in Appendix A utilizes the dielectric data for the water, air, and concrete to delineate volumetric proportions (% $\theta$ ) of each component referred to as the volumetric concentration. The % $\theta$  parameter can be used to assess the number of wets days for a pavement section.

NDT was also conducted using the FWD set up for testing highway pavements (Figure 23). The testing was carried out on sections TS3, TS2, and TS1 according to the pattern shown in Figure 24 testing along the three positions shown along the pavement center and the longitudinal edge. The effective thickness and percent erosion (%E) results are shown in Figure 25. Section TS2 was observed to consist of partially sealed

silicone joints. The method of analysis for the determination of this type of data is discussed in Appendix

B. The effective thickness ( $h_e$ ) represents the stiffness between the slab and the base layer as well as the stiffness between adjacent slabs

depending upon where the FWD loading was applied to the slab.

Clearly, the stiffness of



**Figure 23** SR 59 FWD Testing.

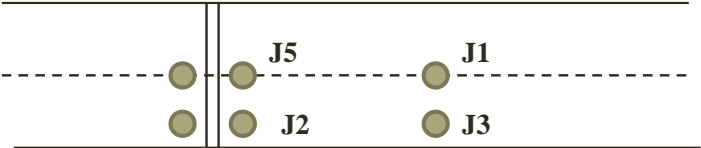


**Figure 24** SR 59 FWD Testing Pattern.

the pavement at the slab center (J1) is very good; this area of the slab rarely experiences erosion damage while in comparison to other location such as the slab corner, the stiffness is much less. These areas often experience erosion damage depending on the presence of water and the frequency of loading. The data also indicates that a joint that is partially sealed may trap water over time and increase the potential for erosion damage to occur. HWDT erosion testing of the SR-59 base materials carried out in the laboratory was reported and analyzed in Appendix D. The results in the laboratory tend to explain the high level of erosion noted in Figure 25.

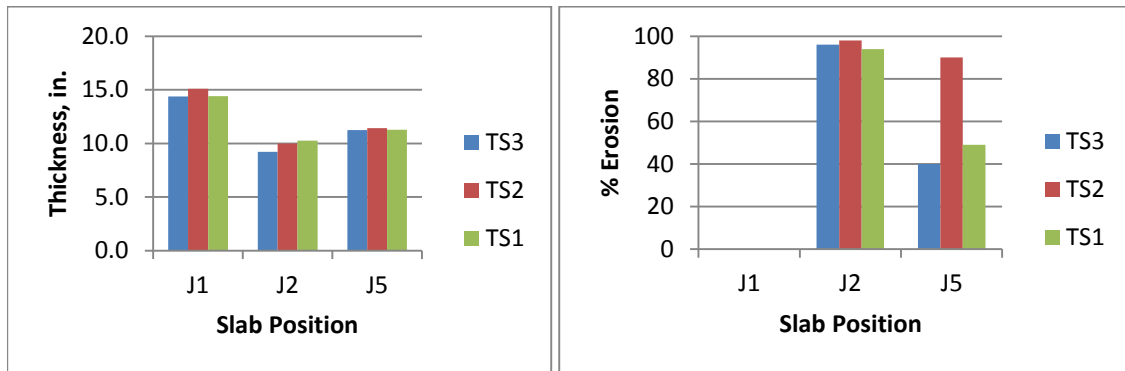


**Figure 25** SR 59 NDT Analysis Results.

### 3.3 Tests on Arizona I-10 SPS-2 Site

The SPS-2 site sections shown in Table on I-10 near Goodyear, AZ were tested during our site visit:

**Table 7** SPS-2 Pavement Section Details.

Section	Slab Thickness (in)	Base Thickness (in)	Base Type	Comments
40215	11	6	AB	
40223	11	4/4	PBTB/AB	
40219	11	6	LCB	
40221	8	4	PBTB	
40262	8	6	AB	Widened lane; skewed joints
40263	8	4/4	PBTB/AB	Widened lane; skewed joints

The test program carried out on the consisted of the following:

- Infiltration testing,
- FWD testing (carried out by Nichols Consulting), and
- GPR scanning

The results of each will be discussed in order.

### 3.3.1 Infiltration Testing

Infiltration testing, previously described but further characterized in terms of permeability, was carried out on each section listed in Table 7 at three positions within the traveled lane as shown in Figure 26. Testing in this manner indicated that the joint sealant effectiveness varied widely across the lane (Figure 27). The joint sealing



**Figure 26** I-10 SPS-2 Infiltration Position 1 (interior), 2, and 3 outer edge Testing.

showed reasonably good effectiveness the interior portions of the slab even after it had been in place for over 20 years but much lower effectiveness (almost none) towards the pavement edges – especially along the outside edge of the lane where deflections are likely the highest and at the greatest frequency. Again, the effectiveness of the joint sealant is measured in terms of its

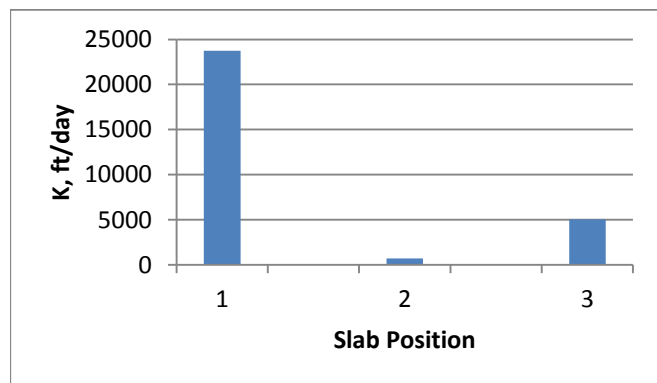


**Figure 27** I-10 SPS-2 Infiltration Test Results for Section 40215.

permeability (K -ft/day) but it is noteworthy what portions of the joint may require

maintenance at greater frequency. Table 8 lists average K values (typically for the central portions of the lane) for the joint sealant in each section. K values for the base layer are also shown in Table 8.

**Table 8** Summary of Sectional Infiltration and GPR Test Data.

<b>Section</b>	<b>Joint K* (ft/day)</b>	<b>Base K** (ft/day)</b>	<b><math>\epsilon_{\text{joint}}</math></b>	<b><math>\theta_{\text{w int}}</math></b>	<b><math>\epsilon_{\text{joint}}</math></b>	<b><math>\theta_{\text{w edge}}</math></b>
40215	9831	281	14.0	0.20		
40223	44	204	6.8	Dry		
40219	686	9983	26.5	0.38		
40221	3196	132	8.1	0.08	15.65	0.25
40262	13	664	10.0	0.14		Dry
40263	25	2	10.0	Dry		

Note: \*Sealed permeability; \*\*Unsealed permeability

Again, a series of infiltration tests and K values were determined after a portion of the joint sealant was removed from the joint allowing for the water to penetrate the base layer (or the cavity between the slab and the base layer) towards an effective permeability of the base layer to be measured. It is interesting to note that the section with the LCB layer had the greatest effective K value suggesting that slab warping was likely playing a role in the flow characteristics displayed by the joint tests.

During the infiltration testing, sections of the joint sealing were removed to facilitate the infiltration testing of the joint and base layer (represented in Table 8 by the data listed in the base K column. The removed sections were retained and tested by Crafcro Inc. for deformation characteristics described in detail in Appendix C with typical results shown. Rough calculations indicate that the modulus after 20 years of

service life was approximately 100 psi which is again is approximately 3 times the original modulus of the silicone.

### 3.3.2 GPR Testing

A series of testing was also conducted on the same sections using the mini-HR GPR system. Radar traces similar to the one shown in Figure 28 were obtained for the same joints tested for infiltration. From the trace, both depth and time of wave travel data can be obtained and used to determine the dielectric of the joint area. The presence of water in this case is only on the leave side of the joint as noted by a slight downward shift in the wave pattern associated with the bottom of the slab while the presence of a dowel is much more prevalent in the trace. Results of the analysis of the data are listed in Table 8. Table 8 also lists the calculated volumetric concentrations of the water ( $\% \theta_w$ ) in the joint based on the dielectric determinations. The dielectric of the joint is actually a composite measure of the sealant, air, and moisture in the joint and the effects of each

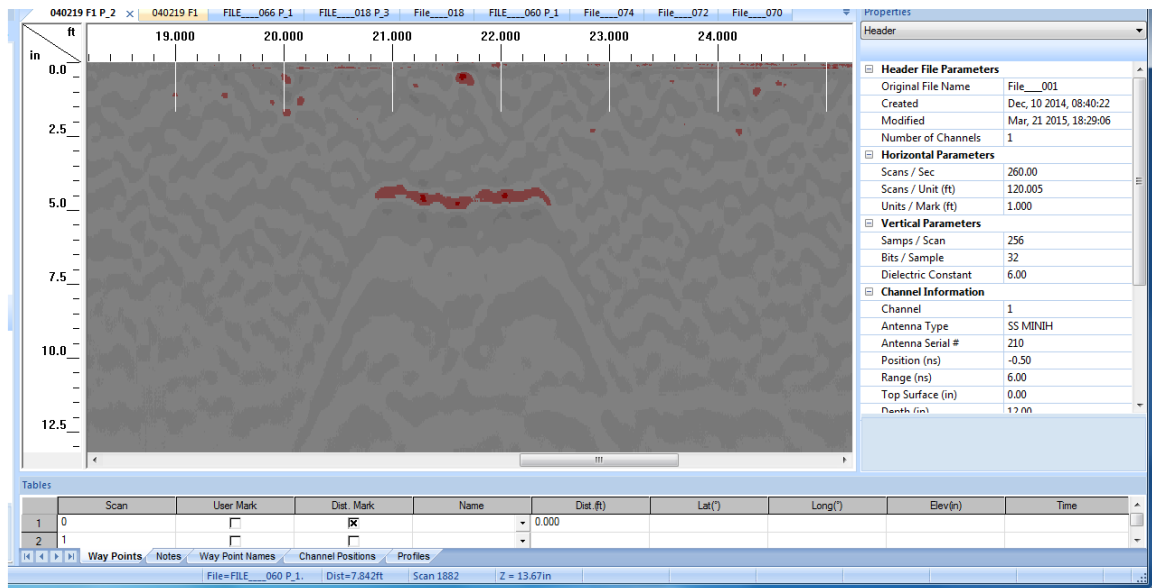


**Figure 28** I-10 SPS-2 GPR Test Results for Section 40219.



must be separated to determine the amount of moisture in the vicinity of the joint.

Again, it is interesting to note that the section with the highest % $\theta$  is the one with a lean concrete base (the GPR scan indicated water trapped on the leave side of the joint) while the permeable or of the unbound bases shown good propensity to drain and to minimize the presence of moisture in the joint.

### 3.3.3 FWD Testing

FWD testing was carried out by the regional LTPP contractor following the typical testing pattern on the sections listed in Table 9 below.

**Table 9** FWD Tested Sections.

Position	J1		J2		J3		J4		J5	
Section	$h_e$	$\mu_e$	$h_e$	$\mu_e$	$h_e$	$\mu_e$	$h_e$	$\mu_e$	$LTE_{app}$	$LTE_{leave}$
40219	13.4	49.4	6.2	0.0	12.7	39.3	6.8	2.0	47.1%	48.7%
40262	9.4	66.7	4.7	0.0	9.3	66.6	2.8	0.0	19.1%	25.0%
40263	11.1	124.9	6.1	0.0	10.5	106.4	4.5	0.0	33.0%	34.8%

The deflection bowl data was analyzed according to the discussion in Appendix B and used to determine the parameters shown in Table 9 and in Figure 29; namely effective slab thickness ( $h_e$ ), effective coefficient of friction ( $\mu_e$ ), and the percent of erosion (%E).

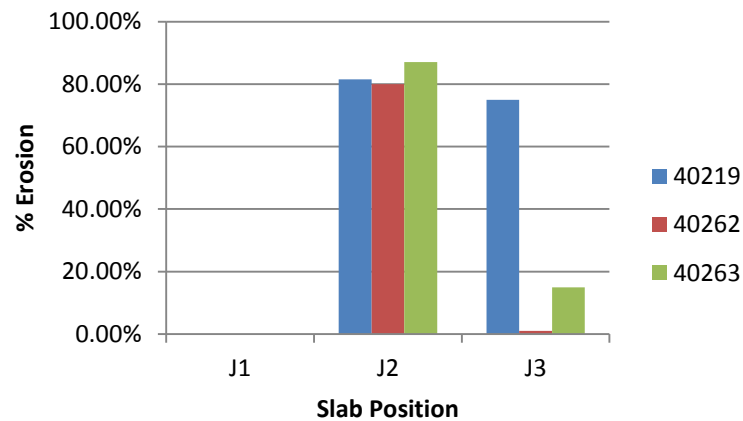


**Figure 29** I-10 SPS-2 Erosion Analysis Results.

As expected, the corner region of the SPS-2 slabs showed the most erosion damage, but some of it may have been due to a gap between the slab and the base layer caused by warping effects particularly in the case of Section 40219 where the LCB layer was in place. Structurally speaking, very little support is provided in that part of the slab when erosion percentages are that high but the results the erosion levels at the corner are basically equivalent among all the sections illustrated in Figure 28; results of erosion testing in the lab appears to be a function of the base shear strength as reflected in cohesion and friction parameters. However, since LCB sections displayed the highest slab stiffness and thus the lowest % erosion at least along the slab edge in spite of the fact that the shear of permeable base may be greater than that of the LCB. Clearly, structural stiffness is dominant with regard to erosion damage.

## **4. EVALUATION OF NUMBER OF WET DAYS FOR DESIGN PURPOSES**

### **4.1 Pavement Drainage**

Drainage an important factor in concrete pavement design that is not well accounted for. Water contributes to several major distresses in jointed concrete pavements and can significantly affect concrete pavement's longevity. There has for several years been mounting evidence that good drainage will provide better, longer lasting pavements [36]. Forsyth stated that if the excess infiltrated water can be drained quickly, the life of a concrete pavement can be extended by 50 percent [37]. Some of the major detrimental consequences of trapped water under a concrete slab can be summarized as follows [38]:

1. Reduces the shear strength of the sub layer,
2. Reduces the bond at the slab/subbase interface,
3. Causes pumping leading to subsequent faulting, cracking and corner breaks, and
4. Reduces the sustainability of a concrete pavement.

Figure 30 shows how water can accelerate distresses in Jointed Concrete Pavement, JCP. Consequences of inadequate control water within a pavement section can be major source of failure ultimately risking the sustainability of the pavement. The development of realistic practices to protect pavements from the damaging action of water is one of the key drainage challenges facing engineers [36]. Therefore drainage considerations should be a part of the pavement design process. The importance of designing an effective drainage system in a pavement was acknowledged by AASHTO guide for design of pavement structure by incorporating the drainage factors in their design [40].



**Figure 30** Water Related Damages; Potholes, Corner breaking and Wide Cracks.

The presence of the moisture underneath the slab is one of the main elements of erosion process. Passing traffic may pump moisture along the base/slab interface and create voids that lead to the development of joint faulting. Most recent erosion/faulting models address the moisture under the slab in terms of the number of wet days [10, 41, 42]. Since this factor represents existence of water in pavement sublayers, it plays an important role in pavement design and analysis.

The effect of moisture in this regard has not received the attention it merits in concrete pavement design. Most definitions relate the number of wet days only to climatic factors such as rainfall. But the actual number of days that water exists underneath the slab is one of other factors that should be considers. Factors such as surface and subsurface drainage, joint sealants or subbase permeability should also be

taken into consideration as part of determining the number of wet days. As an example, the Mechanistic-Empirical Pavement Design Guide (MEPDG) defines wet days as number of days with rainfall greater than 0.1 inch without any consideration of joint sealants effects or different base materials drainage capacity [41].

Major factors regarding the existence of water within pavement sublayers are further discussed towards a better definition of the number of wet days that can be used for concrete pavement design and analysis.

#### **4.2 Transmission of water into the pavement sublayer**

Water primarily enters the concrete pavement by penetrating through the joints, surface cracks or shoulders. Transmission of water into the pavement sublayer happens in three steps:

1. Rainfall as the main source of the water
2. Water flow on pavement surface and infiltration into the joint wells
3. Water infiltration or seepage in to the subbase.

Accordingly there is a possibility to avoid the water and overcome the water being trapped underneath the slab by using proper drainage systems. In order to define the number of wet days, each of the three steps needs to be studied. In other words, the number of wet days for a particular pavement section relates to the local precipitation and how effective is the pavement drainage system in respect to surface drainage, joint and sealant's effectiveness and subbase layer permeability.

$$\text{Number of Wet Days} = f(\text{Rainfall, Joints and Surface Inflow, Subbase Drainage})$$

Rainfall is assumed to be the main source of water. Once the rain water drops on the surface of jointed concrete pavements, a portion of water flows away from the joints

due to the impermeability of concrete slabs, cross sectional slope or surface drainage. The other parameter to consider when defining the number of wet days is the joint capacity and joint sealants effectiveness. Once the water has filled the joint well, the third and last parameter is the subbase layer drainage capability. Figure 31 schematically shows the three stages of water transmission into subbase layer.

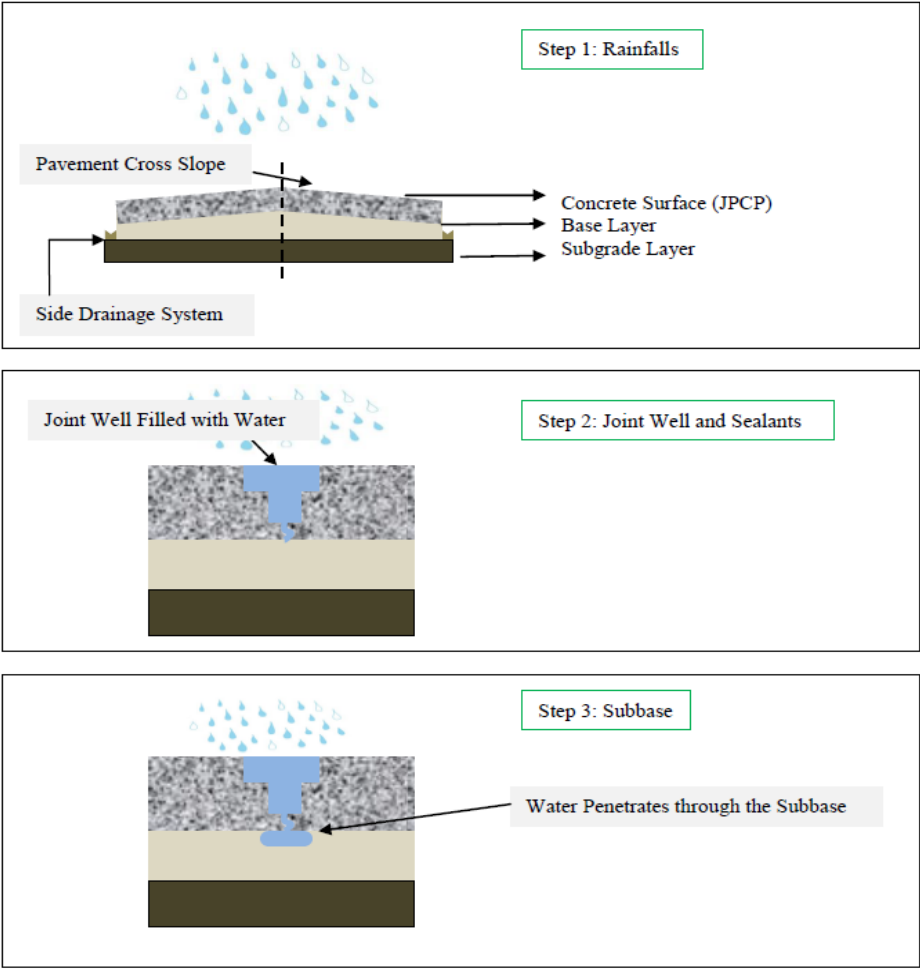


**Figure 31** Three Stages of Rainfall Transmission into Subbase Layer.

### **4.3 Rainfall Inflow**

The source of water contributing to inflow into the pavement systems is mainly due to rainfalls. With a simple calculation assuming a typical joint geometry, it can be shown that on the average, around 0.02 inch of rainfall is needed to completely fill a joint well cavity assuming that joints are unsealed. Therefore the amount of precipitation to be considered for wet day's calculation must be significantly higher knowing the surface drainage potential, effects of the sealant, and the constant water head needed to penetrate into the sublayer. Which are generally ignored in the Mechanistic-Empirical Pavement Design Guide, MEPDG, since it defines wet days as number of days with rainfalls greater than 0.1 inch [41]. As a climatic factor, rainfall intensity serves as a key inflow input to account for the amount of rainfall to be considered in erosion analysis. But on the other hand, rainfall less than 0.1 inch (2.5 mm) is barely enough to inundate the surface of the pavement or create sufficient head to cause infiltration into the pavement sublayers. Similar findings on inflow were obtained using the computer program DRIP. DRIP is a design program that was developed by the United States Department of Transportation and Federal Highway Administration (FHWA) for the design and analysis of pavement subsurface drainage [43]. Therefore in calculation of the number of wet days, the number of days with rainfalls greater than 0.1 was considered as the input that may need adjustments regarding the pavement joint capacity and sublayer conditions.

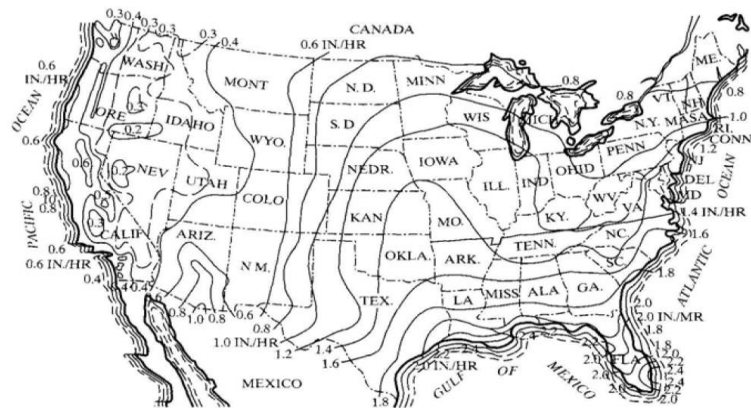
#### 4.4 Water Surface Joint Infiltration

Runoff that infiltrates into a pavement is the net difference between precipitation and that removed via surface drainage. Surface drainage is mainly due to cross sectional slope, shoulders, longitudinal edge drainage, side ditches and culverts. In designing surface drainage systems, the primary objective is to properly accommodate surface runoff along and across highway through the application of hydraulic principles.

According to TxDOT, the recommended pavement cross slope for typical conditions is 2 percent. In areas of high rainfall, or based on geometry steeper cross slopes may be used. Shoulders should be sloped sufficiently to drain surface water but not to the extent that causes safety concerns. The algebraic difference in cross slope between the traveled way and the shoulder should not exceed 6 to 7 percent. Maximum shoulder slope should not exceed 10 percent [44].

Surface drainage can prevent 35 to 50 percent of the total rainfall water from infiltrating the pavement

structure. Figure 32 shows the expected 1-hour-duration/1-year-frequency precipitation rate in the United States. Cedergren recommended that the design infiltration rate to be determined by





multiplying the expected precipitation by a coefficient varying from 0.5 to 0.67 for concrete pavements for surface drainage design calculations [38, 45, 46]. Hence to estimate the surface inflow Cedergren et al. [45] recommended the design infiltration to be determined by multiplying the 1-hour-duration/1-year-frequency precipitation rate by a coefficient varying from 0.50 to 0.67 for jointed concrete pavements.

Given the results of infiltration tests in Connecticut, Ridgeway suggested that the duration of rainfall is a more critical factor than the intensity. He found that the amount of infiltration can be calculated by the following equation [47];

$$q_i = I_c \left( \frac{N_c}{W_p} + \frac{W_c}{W_p C_s} \right) + K_p \quad (4-1)$$

where

- $q_i$  = Infiltration rate per unit area, ft<sup>3</sup>/day/ft<sup>2</sup>
- $I_c$  = Joint infiltration rate (ft<sup>3</sup>/day/ft)
- $N_c$  = Number of longitudinal joints
- $W_p$  = Width of pavement lane subjected to infiltration
- $W_c$  = Length of transverse joints
- $C_s$  = Joint spacing
- $K_p$  = Concrete infiltration rate

This is also the equation used by United States Department of Transportation and Federal Highway Administration (FHWA) in DRIP program.

Although Ridgeway concluded that rainfall duration was far more important than rainfall intensity, Equation 4-1 may not directly consider rainfall duration while it does to some extent relate the rate of infiltration to the pavement jointing and the number of joints [46] present in the pavement. Including a parameter such as  $K_p$  in the expression appears to be rather redundant since its value for concrete slab would be exceedingly small and likely negligible aside from being difficult to measure under field conditions.

Certainly noting that  $N_c$  being equal to number of lanes plus one and that  $W_p$  could be assumed to equal to  $W_c$  allows for simplification of the bracketed portion of this expression but considering for instance a unit length longitudinally of a 12 foot wide, 15 foot jointed pavement that includes a single transverse joint, closer examination reveals:

1. Equation (4-1) apparently assumes the longitudinal joint infiltrates 2.5 times more water than the transverse joint given the same joint opening and pressure head for each joint.
2. This assumption is likely the reason that the ratio of  $\frac{q_i}{I_c}$  from equation (4-1) is 3 times the same ratio determined from equating the volume of water infiltrated spatially (based on  $q_i$ ) and the volume of water infiltrated along the joints (based on  $I_c$ ). However, when the pavement section includes only a single longitudinal and transverse joint, the equation (4-1) is accurate.
3. The form of equation (4-1) (i.e.  $q_i$  a function of  $I_c$ ) does however, serve to facilitate a convenient and practical comparison between the calculated infiltration rate and the expected intensity-duration frequency rate.

Few would disagree that the longitudinal joint infiltrates a greater amount of water than the transverse joints but the Ridgeway equation seems to have a set difference based on the geometry configuration of the joints. These comparisons would therefore vary depending on joint geometry, pavement configuration, and flow conditions but it appears some adjustments in the value of  $I_c$  would be in order to affect improvement of the estimate of the infiltration rate using Equation (4-1). Nonetheless, this equation has been used in the current version of the Federal Highway Administration's (FHWA) DRIP program [43].

Given that the Ridgeway formula is more appropriate for spatially distributed infiltration rather than infiltration through partially sealed joints in concrete pavements, it appears that a different approach is in order to model infiltration especially if predicted

infiltration rates are calibrated based on field measurements of joint infiltration. An improved expression for joint infiltration based on flow over a sharp-crested weir [72] is suggested as:

$$q_i = \frac{2}{3} C_d \sqrt{2g} (\sqrt{H})^3 \quad (4-2)$$

where

$q_i$	=	Infiltration rate per unit area, ft <sup>3</sup> /s/ft
$C_d$	=	Calibrated drag or infiltration coefficient redefined as:
	=	$\frac{q_{im}}{\frac{2}{3} \sqrt{2g} H_{avg}^{3/2}}$
$g$	=	Acceleration due to gravity, (ft/s <sup>2</sup> )
$H$	=	Pressure head over the joint, (ft)
$q_{im}$	=	Measured infiltration rate per unit area, ft <sup>3</sup> /s/ft

One could also consider the applicability of the orifice rather than the sharp-crested weir expression but because of the greater dependence on the pressure head (as suggested by the calibration of the infiltration coefficient  $C_d$ ) the sharp-crested weir was considered more appropriate. Nonetheless, the calibrated  $C_d$  coefficient allowed for the flow computation to be adjusted for joint opening as well as pressure head but one factor that needed to be addressed was the joint sealants effectiveness in retarding infiltration into a joint. Properly sealed joints can result in significantly decreased infiltration. Therefore equation (4-2) was adjusted as:

$$q_i = \frac{2}{3} F_c C_d \sqrt{2g} \sqrt[3]{H} (86400) \quad (4-3)$$

where

$F_c$	=	Condition coefficient (function of joint sealant effectiveness)
-------	---	---

The condition coefficient, as subsequently explained, will be a function of the quality of a sealants installation as well as sealant damage due to debonding. The infiltration coefficient ranges between zero to 1.0, where zero represents the situation in which sealants are installed perfectly with perfect bond along the joint and no infiltration can occur and one represents an unsealed condition. The flow associated with a unsealed joint condition ( $F= 1.0$ ) is represented by equation (4-2).

#### **4.5 Infiltration Coefficient Testing**

Results from infiltration testing were used in order to calibrate the infiltration coefficient  $C_d$  with respect to inflow, debonding, and installation quality. These tests were all performed at the Riverside campus of Texas A&M University (74). The subbase layer for all these tests was an open graded granular subbase (Figure 33). The permeability of the subbase material was such as to not greatly affect the results of the infiltration tests. The permeability was sufficiently open graded to allow passage of water through the joint uninhibited. Hence these tests allowed a focus on the joint infiltration itself and the sealants effectiveness and avoid the effect of subbase permeability on the test results.



**Figure 33** Open Graded Granular Subbase Used for Test Program.

Keeping in mind the factors affecting the infiltration rate, the measured flow data previously discussed was used to back calculate vales of  $C_d$  and fit the following model to the test data using the Table Curve regression analysis software (75):

$$C_d = \frac{q_{im}}{\frac{2}{3}\sqrt{2g}H_{avg}^{3/2}} = a + b\frac{w}{H} + c\ln(Fr) + d\left(\frac{w}{H}\right)^2 + e\left(\ln(Fr)\right)^2 + f\frac{w}{H}\ln(Fr) \quad (4-4)$$

where

- $w$  = joint opening, (ft)
- $Fr$  = Froude Number =  $\frac{v^2}{gL}$
- $v$  = Velocity of flow, (ft/s)
- $g$  = Acceleration due to gravity – 32.174 ft/s<sup>2</sup>
- $L$  = Characteristic length, i.e.  $H$  (ft)
- $a, b, c, d, e, f$  = Model coefficients (see Table 10)

This allows for the calculation of infiltration into a joint as a function of the factors noted above particularly the head or the depth of sheet flow ( $H$ ) moving over a joint. Given the rainfall intensity ( $L^3/t/L^2$ ), the following variation of Manning's Equation (assuming the hydraulic radius of sheet flow ( $R_h \approx H$ )) can be used to estimate the depth of flow and any point along a joint:

$$H = \left( \frac{q_r n}{1.486 \sqrt{s}} \cdot \frac{1}{\sqrt{s}} \right)^{\frac{3}{5}} \quad (4-5)$$

where

- $q_r$  = Volume of runoff per unit length (ft<sup>3</sup>/s/ft)
- $n$  = Manning's  $n$  (s/ft<sup>1/3</sup>).
- $s$  = Slope of the drainage surface

**Table 10**  $C_d$  Model Coefficients.

<b>Sealant Type/<math>r^2</math></b>	<b>Model Coefficients</b>					
	<b>a</b>	<b>b</b>	<b>c</b>	<b>d</b>	<b>e</b>	<b>f</b>
Silicone/0.98	0.004507	-0.002870	0.020632	0.000110	-0.006370	0.002706
Hot Pour/0.99	0.008233	-0.002224	-0.002044	9.66E-05	0.001221	0.000408
Preformed/0.98	0.073478	-0.003986	-1.65E-05	5.20E-05	0.001193	0.000488

Using the rational method (73)  $q_f$  can be conveniently assigned the value of the rainfall intensity as determined, for instance, from an applicable intensity-duration frequency (IDF) curve.

The infiltration coefficient was configured to range between zero to 100, in percent, where zero represents the situation in which sealants are installed perfectly with perfect bond along the joint and no infiltration occurs. 100% represents a no-sealed condition or when sealant is significantly damaged and ineffective. The infiltration coefficient consists of two factors; flow factor and installation factor. Flow factor pertains to sealant bond to the joint wall while installation factor pertains to installation quality prior to application of the sealants.

The test program consisted of two sets which were carried out in order to address the infiltration coefficient: sealant damage tests (in order to define a flow factor) and sealant installation tests (in order to define an installation factor). Details of pavement test sections and test procedure were discussed previously.

#### **4.5.1 Sealant Damage Test and Flow Factor**

Sealants were carefully damaged along the joints prior to the tests in different levels.

100%, 75%, 50% and 25% damage. 100% damage represents the condition in which the

sealant is not bonded to the joint as one side of the sealant was carefully cut along the joint. Figure 34 shows the 50 percent damaged sealant.

Joint opening was changed using the movable joint system as previously explained. This was done in order to simulate the effects of season changing that changes the joint opening width. Infiltration tests were performed for each damaged level in different joint opening width. The original joint width was 3/8 inches. Table 11 and Figure 35 show the results for these infiltration tests.

As it is shown sealants with higher damage percent are more sensitive to joint openings. Sealant with hundred percent damage are totally deboned and not capable of preventing the water. As sealants are less damaged they are more effective. The rate of infiltration for different damage level was compared to the one for hundred percent damaged seal rate for each opening width. Results are shown in Figure 36.

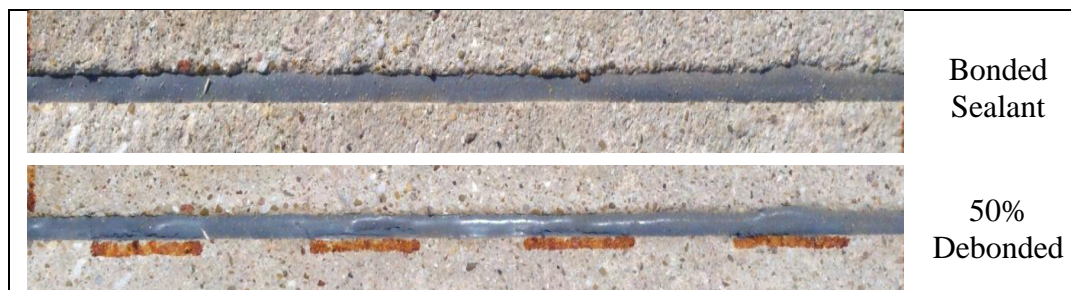


**Figure 34** Fifty Percent Damaged Sealant.

**Table 11** Infiltration Test Results on Damaged Sealants.

Joint opening width (inch)	Joint opening width (mm)	Flow rate (gallon/min./ft)			
		100% damaged	75% damaged	50% damaged	25% damaged
0.002	0.05	0.000	0.000	0.000	0.000

Joint opening width (inch)	Joint opening width (mm)	Flow rate (gallon/min./ft)			
		100% damaged	75% damaged	50% damaged	25% damaged
0.008	0.20	0.002	0.000	0.000	0.000
0.016	0.40	0.349	0.075	0.000	0.019
0.024	0.60	1.107	0.324	0.089	0.079
0.031	0.80	2.076	0.775	0.246	0.270
0.039	1.00	3.125	1.435	0.579	0.432
0.047	1.20	4.196	2.113	1.024	0.668
0.055	1.40	5.357	2.791	1.463	0.901
0.063	1.60	6.522	3.550	1.923	1.186
0.071	1.80	7.407	4.348	2.381	1.415
0.079	2.00	8.738	5.202	2.821	1.744
0.087	2.20	9.836	6.061	3.429	1.961
0.094	2.40	10.909	6.452	3.774	2.128
0.102	2.60	11.765	7.317	4.167	2.419
0.110	2.80	13.043	8.696	4.800	2.679
0.118	3.00		9.836	5.357	3.030



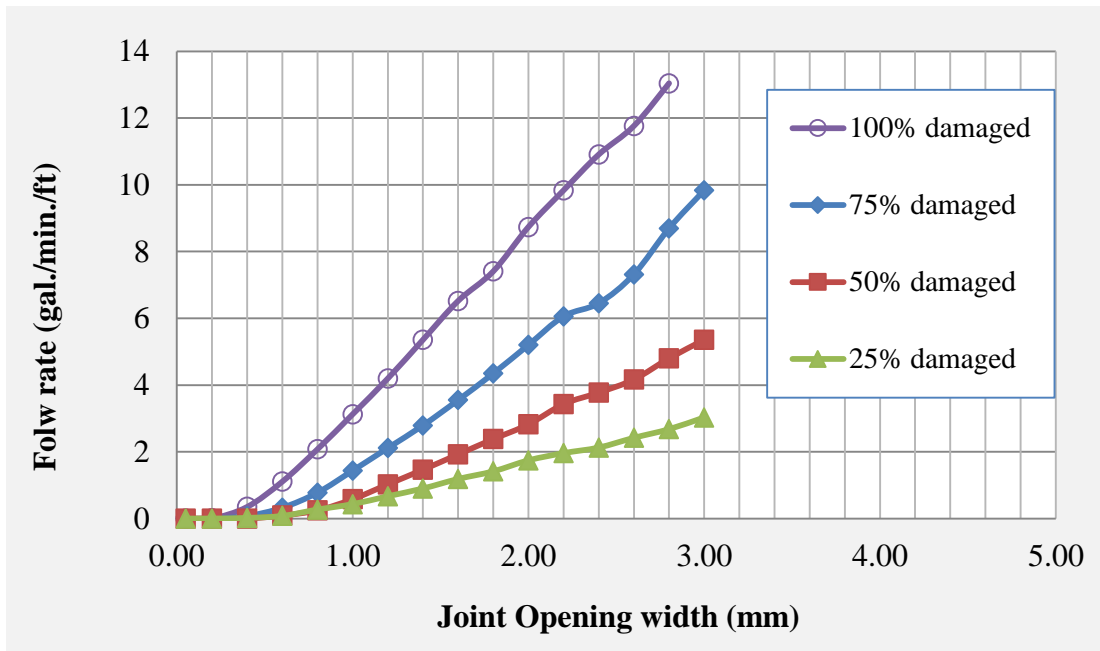


**Figure 35** Infiltration Test Results on Damaged Sealants.

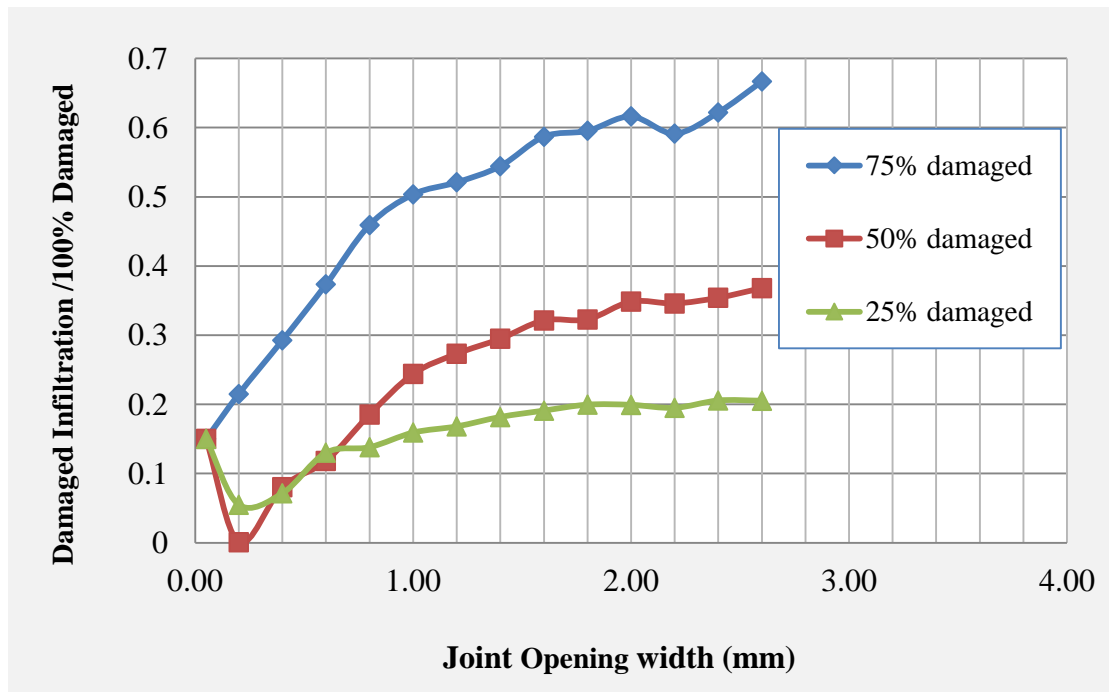


**Figure 36** Infiltrations for Different Damage Levels Compared to 100% Damaged.

The weight average of this analysis can be used in order to assign a flow factor for sealants. Sealants bond condition can be classified from very poor to good condition. Very poor rating is given to the sealant that is fully debonded, ineffective and 100% damaged. Poor rating is given to sealants with 75% damage; fair condition represents sealants with around 50% damage and good ratings are given to sealants that have less than 25% damage. Table 12 shows the flow factor for different sealant conditions. The better the sealant condition the lesser the rate of infiltration through the joint.

**Table 12** Condition/Infiltration Coefficient ( $F_c$ ) for Different Sealant Conditions.

Sealant Condition	Good	Fair	Poor	Very Poor
Calculated Condition Coefficient	21.7%	29.4%	51.6%	100.0%
Flow Factor (Rounded Values)	20%	30%	50%	100%

#### 4.5.2 Sealant Installation Test and Installation Factor

The testing program also addressed the importance of installation quality associated with joint sealing. As previously mentioned, tests were conducted using slurry of saw dust to make three different concentration levels. Results were then analyzed with respect to dirtiness or the degree of contamination and sealant performance. The results are shown in Figure 37 that shows a significant difference when the dirtiness level is zero (clean joint walls).

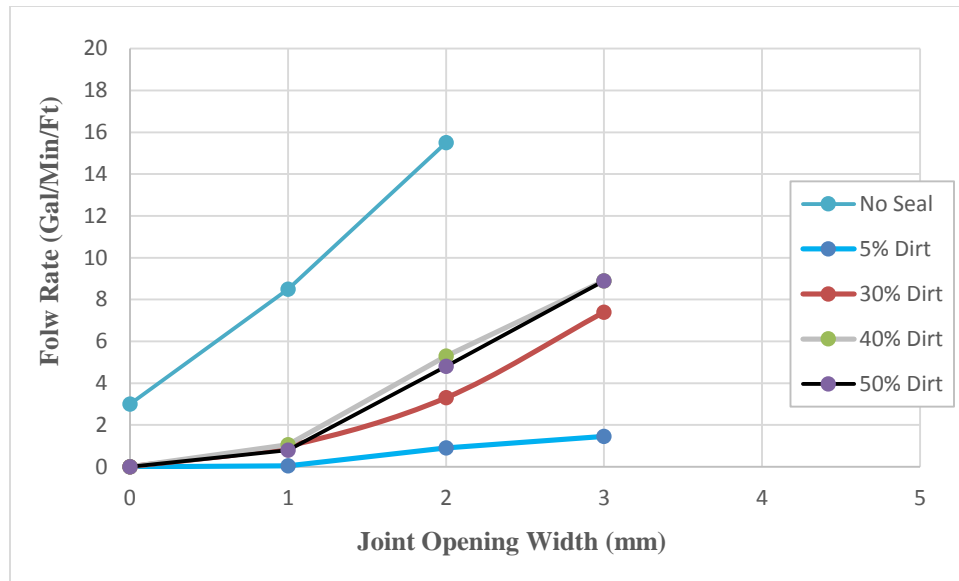


**Figure 37** Water Infiltration Rates for Different Joint Dirtiness Levels.

Same as for damaged sealants the weighted average of these results for different installation qualities and different joint openings was used to assign an installation factor for sealants. Sealants installation quality can be classified from very poor to very good. Very poor rating is given to the sealant installation that leads to debonding sometimes within a few days of installation. Fifty percent dirtiness, the highest level of dirtiness in the test program, represents the same situation where one side of the joint is totally contaminated and debonded. Figure 38 shows the average infiltration rate for different dirtiness levels. Table 13 shows the installation quality factor for different installation qualities; dirtiness levels were scaled to 0-100 range and each dirtiness level assigned to an installation quality rating. The value of the installation factor for clean joints with absolutely no dirtiness defined as 100% and other sealant installation factors were calculated in percent as the given infiltration rate compared to infiltration rate of clean

joints. A greater installation factor means greater potential for sealant bond and lower infiltration through the joint. Table 14 shows installation factors for each installation quality.

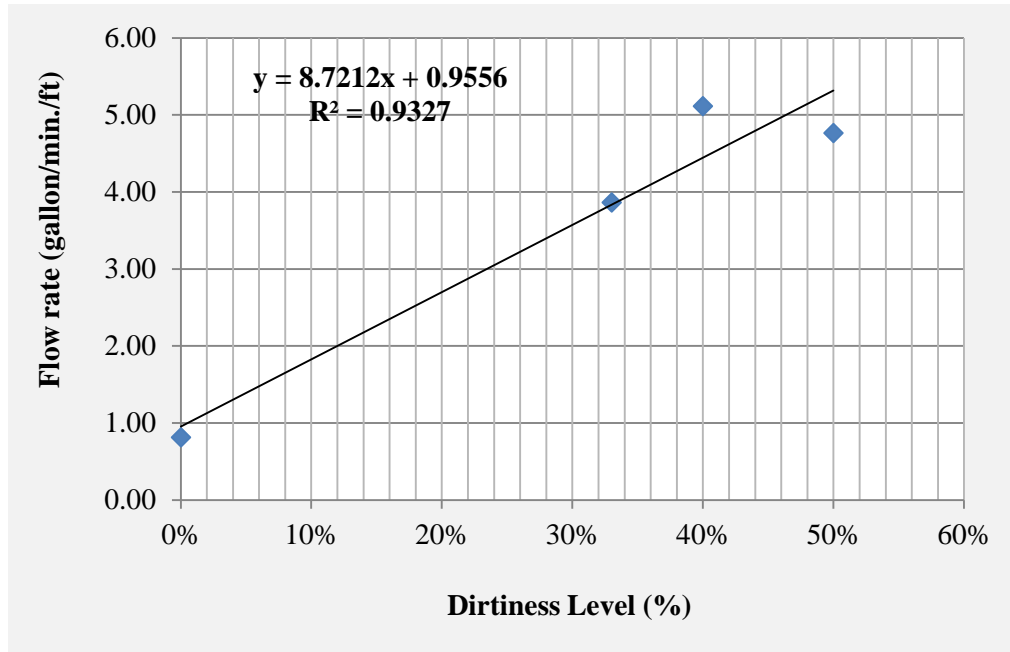


**Figure 38** Average Infiltration Rates for Different Dirtiness Levels.

**Table 13** Dirtiness levels, Installation Qualities and Calculated Installation Factor.

Installation Quality	Dirtiness levels in the test (%)	Scaled Dirtiness in 0-100 Range	Inflow Rate (gallon/min./ft)	Installation Factor
Very Good	0	0	0.956	100.00
Good	15	30	2.264	70.00
Fair	30	60	3.572	40.00
Poor	40	80	4.444	20.00
Very Poor	50	100	5.316	0.00

**Table 14** Installation Factor ( $F_I$ ) for Different Installation Qualities.

Sealant Installation Quality	Very Good	Good	Fair	Poor	Very Poor
Installation Factor	100%	70%	40%	20%	0%

#### 4.5.3 Model for Condition/Infiltration Coefficient

Given the results from extensive test program on sealants, the variation of the condition/infiltration coefficient,  $F_c$ , that was added to the infiltration equation as a function of the installation factor ( $F_I$ ) can be illustrated in Figure 39 and expressed in the following form:

$$F_c = -2.5 * F_I^3 + 7.0 * F_I^2 - 6.6 * F_I + 2.1 \quad (4-6)$$

Based on the data summarized in Table 12 and Table 14. The installation factor has a reverse impact on  $F_c$  i.e. as  $F_I$  increases,  $F_c$  decreases. Since the infiltration tests on damaged seals were

performed on fair installation quality (installation factor of 40%), that level of infiltration coefficient must be equal to flow

factor of 0.40. If the installation is done

carefully at a good or very good quality level, the bond strength of the sealant will be

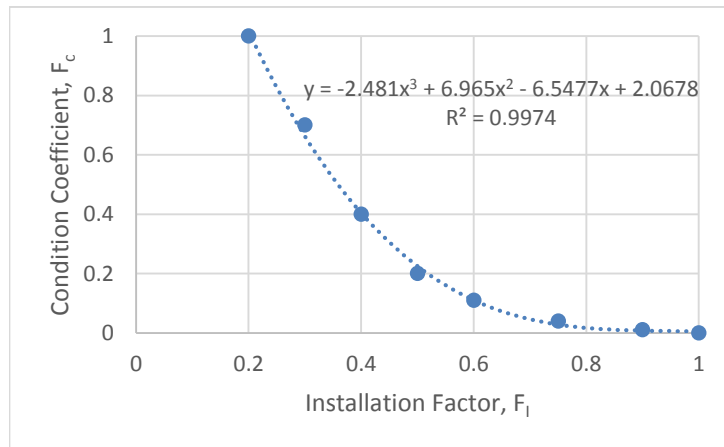


**Figure 39** Variation of the flow factor ( $F_c$ ) with the installation factor ( $F_I$ ).

higher causing the infiltration coefficient to be lower. If the installation is done carelessly resulting in a poor or very poor quality level, the bond strength of the sealant will be weakened and the infiltration will be greater. It should be noted that infiltration coefficient has a maximum value of 100% which corresponds to a value of zero to  $F_c$ . Furthermore, in design, the value of  $F_I$  is clearly a user defined input that presently represents the degree of failure a joint seal may have undergone as a result of the installation process. This parameter can also be made to represent the incremental change in the degree of failure that would take place with a sealant originally bonded to the joint walls (i.e. hot pour or silicone, typically) over the life of the joint seal as it may occur due to aging effects; a factor that future research should address to expand the utility of this being included into the infiltration equation.

#### **4.5.3.1 Permeability based Condition/Infiltration Coefficient**

The product of the parameters  $F_c$  and  $C_d$  in equation 4-3 can be expressed in terms of a ratio of the measured permeability of a given joint as  $k_{joint}$  (with the sealant removed) to the permeability of the joint with the sealant in place (referred to as  $k_{sealant}$ ) as long as the condition coefficient is defined according to Figure 39. Rewriting equation 4-3

$$q_i = \frac{2}{3} \frac{k_{sealant}}{k_{joint}} \sqrt{2g} \sqrt[3]{H} \quad (4-7)$$

Accordingly, the permeability test described in Chapter 3 can be used to assess both the  $C_d$  parameter as well as the  $\frac{k_{sealant}}{k_{joint}}$  ratio as a means to evaluate installation quality and the effective crack opening.

#### 4.5.3.2 $C_d$ Validation Testing

Additional testing was carried out at the Riverside Campus site to investigate the utility of the new approach outlined in this paper. The testing was carried out in two stages on joints spaced at 10 foot intervals both unsealed and sealed with silicone. The first stage of testing involved infiltration testing of the sealed joints in the original condition (as placed) and then with the seal cut away from one face of the joint wall. Using equation (4) it was possible to match the measured  $C_d$  coefficient and determine the effective joint opening based on the measured flow results. The  $C_d$  coefficient was back calculated (shown in Table 14) and then used to calculate infiltration flows using equation (2) for an appropriate value of  $F_c$ . Through the matching process, an effective joint opening was determined (listed in Table 4). The effective joint opening represents the opening representative of the infiltration allowed by the joint seal. This parameter could potentially be used to evaluate joint seal effectiveness. The  $\Delta H_{init}$  parameter is the change in head during the test.

For the flood testing, the effective joint opening was determined in a similar manner using equation (4) and finally equation (2) for the calculated flows again shown in Table 15. The results show a reasonable match between the measured and calculated infiltration flows for both the infiltration and flooded testing. The results also show comparability between the  $C_d$  values from the falling head and the flooded slab testing. The calculated effective crack widths indicate the pavement section was likely under compression and the joints tightly closed. The flooded testing for joint #3 was on an unsealed joint and was assigned an  $F_c$  of 1.00.

**Table 15** Effective  $w$  based on New Infiltration Model.

$\Delta H_{init}$ (in)	$Q_m$ (ft <sup>3</sup> /m/ft)	%Bonded	$F_c/C_d$	Effective $w$ (mm)/ $Q_m$ (ft <sup>3</sup> /m/ft)
<i>Infiltration – Joint #1 (25.4 mm width, sealed)</i>				
2.0	0.013	90	0.05/3.03e-03	0.12/0.010
3.0	0.535	50	0.50/2.67e-02	5.27/0.522
<i>Flooding – Joint #1 (25.4 mm)</i>				
5.0	0.36	50	0.50/7.94e-03	0.15/0.34
<i>Infiltration – Joint #2 (25.4 mm width, sealed)</i>				
0.5	0.003	99	0.05/1.63e-03	0.06/0.004
3.0	0.327	50	0.50/1.05e-02	2.30/0.341
<i>Flooding – Joint #2 (25.4 mm)</i>				
3.0	0.109	50	0.50/5.14e-03	0.08/0.103
<i>Flooding – Joint #3 (9.53 mm width, unsealed)</i>				
3.0	0.054	0	1.00/1.20e-03	0.07/0.048

#### 4.6 Water Movement in the Subbase

The movement of water in the sublayer is mainly due to the gravity. This movement obeys Darcy's law of flow [38] [49];

$$v = ki \quad (4-8)$$

$$Q = kiA \quad (4-9)$$

In which  $v$  is the discharge velocity (L/t),  $i$  is the hydraulic gradient,  $k$  is the coefficient of permeability,  $A$  is the total cross sectional area normal to the direction of flow and  $Q$  is the seepage quantity. Hydraulic gradient is the head loss between two points divided by the distance between them. The hydraulic conductivity of soils depends on several factors:

- Fluid viscosity
- Pore size distribution
- Grain size distribution
- Void ratio



- Degree of soil saturation

K can be determined in the field or in the lab. K is determined in the lab using two methods: Constant-Head Test and Falling-Head Test. The constant head test is used primarily for coarse-grained soils. This test applies a constant head of water to each end of a soil in a “permeameter” (ASTMD2434). The falling head test is used for both coarse-grained soils as well as fine-grained soils in which initial and final head is recorded. Pumping test are used in the field in order to measure the permeability. The average hydraulic conductivity of a soil deposit in the direction of flow can be determined by performing pumping tests from wells.

Darcy’s law can be used in conjunction with the continuity equation to form the differential equation governing ground water flow. A convenient and practical way to solve the equation is by drawing the flow nets, as illustrated by Cederghren, 1977 [36]. In simple applications Darcy’s law can be applied directly in order to define amount and timing of seepage. In a more precise way Darcy’s law could be applied in order to solve Laplace equations of water flow nets. In case of water flow from the joints in to the subbase, flow nets are more accurate and practical as the water flow under the slab is not only in one direction.

A flow net is a graphical representation of two-dimensional steady-state groundwater flow through aquifers. To develop the Laplace equations for flow underneath a slab, the following assumptions are used:

1. The soil/base is homogeneous
2. The voids are completely filled with water

3. The soil and water are incompressible

The two dimensional form of the Laplace equation for water flow is as follows:

$$\frac{\partial^2 h}{\partial x^2} + \frac{\partial^2 h}{\partial z^2} = 0 \quad (4-10)$$

In which  $h$  is the water head and  $x$  and  $z$  are Cartesian coordinates. The equation can be represented by two families of curves that intersect at right angles to form a pattern of square figures know as flow net [36]. One set of lines is called the streamline or flow lines and the other that are perpendicular to flow are called equipotentials. The flow lines represent paths along which water can flow through a cross section. The equipotentials lines are lines of equal energy level or head. Figure 40 shows a sample flow net and flow and equipotential lines. Flow nets must meet certain requirements as follows:

1. Flow lines and equipotential lines must intersect at right angles to form areas that are basically squares,
2. Certain entrance and exit requirements must be met,
3. A basic deflection rule must be followed in passing from a soil of one permeability to a soil with different permeability,
4. Adjacent equipotentials have equal head loses, and
5. The same quantity of seepage flows between adjacent pair of flows.

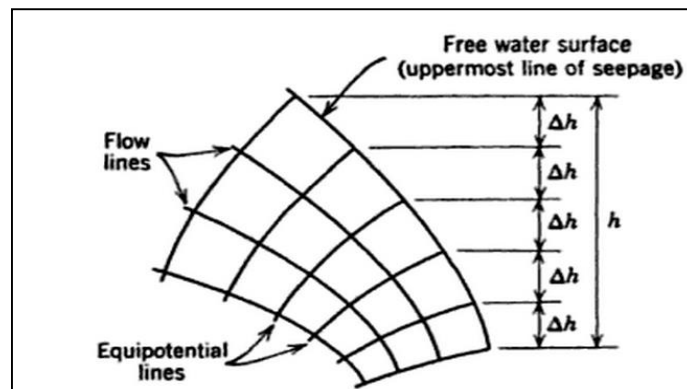


**Figure 40** Sample Flow Net And Flow and Equipotential Lines [36].

Cedergren stated that for a given section flow net drawing provides an accurate solution [36]. From equations 4-6 to 4-8 basic equation for computation of seepage quantities from flow nets can be derived as follows [36];

$$Q = kh \frac{N_f}{N_d} \quad (4-11)$$

Where  $k$  is the coefficient of permeability,  $Q$  is the seepage quantity,  $N_f$  is the number of flow channels and  $N_d$  is the number of equipotential drops. The flow net for the case of concrete pavement joint was drawn carefully. Figure 41 shows flow net for water seepage from the concrete joints into the subbase. The water head is equal to the slab thickness. Therefore for the case of water flow underneath the slab, the equation 4-9 can be written as follows in which  $h_c$  is the slab thickness.

$$Q = kh_c \frac{N_f}{N_d} \quad (4-12)$$

The flow net was drawn in scale for different base thicknesses. As the base layer becomes thicker the number of equipotential lines increases that means thicker subbases have lower  $N_f/N_d$  ratios and so the lower seepage quantity according to equation 4-10. As the base layer becomes thicker water tends to spread more diagonally into the layer that makes the seepage quantity lower. Table 16 shows the number of flow lines and equipotential lines for different base layer thicknesses. Incomplete equipotential lines were measured carefully as a portion of a full channel. It should be noticed that the  $N_f/N_d$  ratio does not depend on slab thickness.

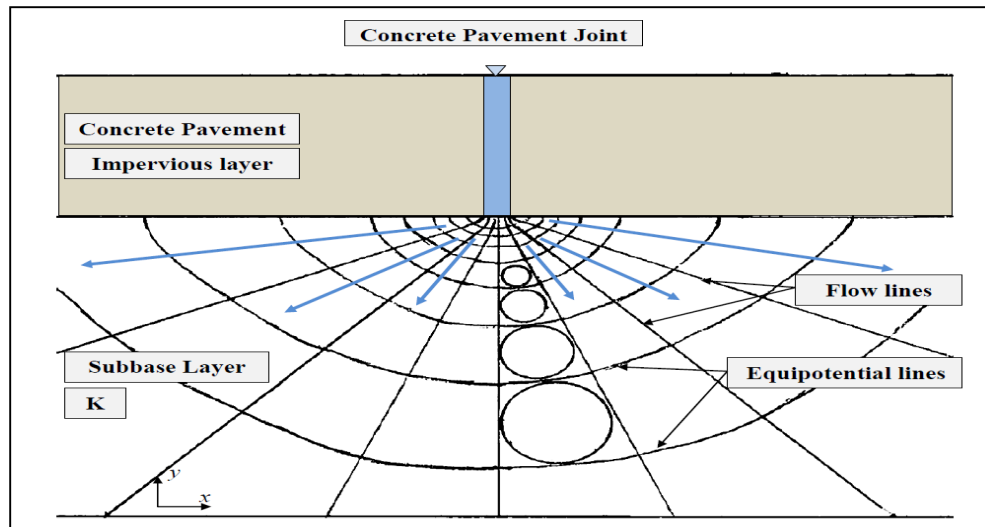


**Figure 41** Flow Net for Water Seepage from the Concrete Joints into the Subbase.

**Table 16** Number of Flow Lines and Equipotential Lines for Different Base Thicknesses.

Base Thickness (inch)	Nf	Nd	Nf/Nd
1	8.00	4.00	2.000
2	8.00	5.70	1.404
3	8.00	6.65	1.203
4	8.00	7.41	1.080
5	8.00	8.00	1.000
6	8.00	8.41	0.951
7	8.00	8.85	0.904
8	8.00	9.61	0.832

Figure 42 shows a regression model to fit the ratio of flow and equipotential lines to base thickness. The R square value is equal to 0.99 and the fit is highly acceptable.

Therefore for a particular case of water flow from the joints into the subbase for concrete pavements equation 4-12 can be written as follows;

$$Q = kh_c * 1.92 h_b^{-0.403}$$

(4-13)

Where Q is the seepage quantity,  $k$  is subbase coefficient of permeability,  $h_c$  and  $h_b$  are slab and base thicknesses and base thickness is in units of inches.

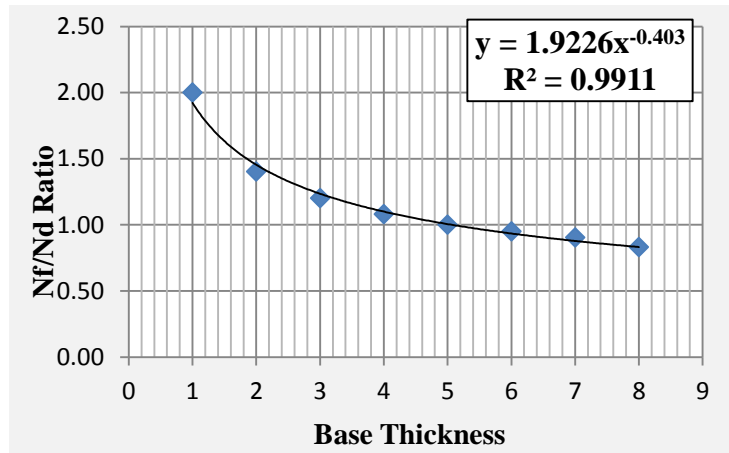


**Figure 42** Regression to Fit the Ratio of Flow Net Lines to Base Thickness.

#### 4.7 Calculation of Number of Wet Days

Number of wet days has been used as a climatic factor in damaged modeling of jointed concrete pavements and in design procedures. As mentioned the latest definition of number of wet days refers to the mechanistic-empirical pavement design guide, in which number of wet days defined as number of days with rainfalls greater than 0.1 inch in a year [41].

But this definition is somewhat nondescript. The definition does not take in to consideration the effects of surface drainage, joint sealants effects or different base materials drainage capacities. Surface drainage can decreases the amount of rain that

gets into the joint by up to 50 percent therefore surface inflow cannot be ignored. Also subbase permeability and seepage rate is a critical factor that can change the actual number of days that moisture exists underneath the slab.

Number of the wet days is calculated herein considering climatic factor, surface inflow, joint and sealant effects and subbase drainage capacity. Number of wet days,  $N_w$ , initially is modeled as a probability function of the total number of days in a year;

$$N_w = P\% * 365 \quad (4-14)$$

Considering the steps of water transmission stated earlier and the importance of surface drainage, joint inflow, sealants and base seepage this probability should break down in to three parts;

$$P\% = p_1 * p_2 * p_3 \quad (4-15)$$

where

$P =$	Percent of wet days
$p_1 =$	Probability of the rain,
$p_2 =$	Probability of infiltration in to the joint
$p_3 =$	Probability of wet subbase

All these probability values are between zero and one ( $0 < p_i < 1$ ). Figure 43 shows an algorithm to calculate the number of wet days.

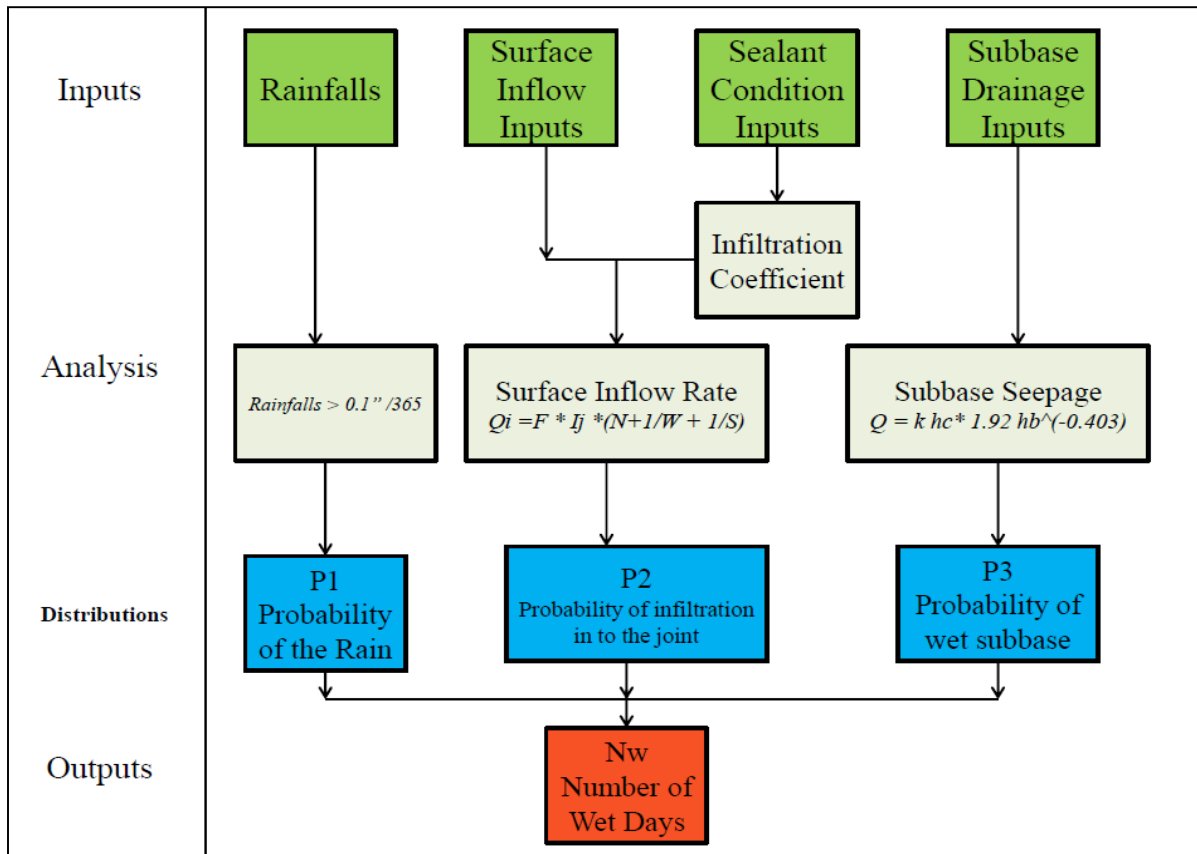


**Figure 43** Algorithm to Calculate the Number of Wet Days.

This algorithm along with all the related equations is used to make a spreadsheet that is capable to analyze the probability functions noted above, create distribution graphs and calculate the number of wet days.

$P_1$  defines as climatic probability function. That is simply the number of rainy days greater than 0.1 inch (2.5 mm) divided by the total number of days in a year. In order to calculate the  $P_2$ , equation 4-3 equation is applied. A beta distribution function is used in order to formulate the probability of infiltration into the joint. The beta distribution can be used to model events which are constrained to take place within an

interval defined by minimum and maximum values. Shorthand computations are widely used to estimate the mean and standard deviation of the beta distribution [50].

$$\sigma = \frac{(b-a)}{6} \quad (4-16)$$

$$\mu = \frac{1}{6}(a + 4 * m + b) \quad (4-17)$$

where

- $\sigma$  = Standard deviation
- $\mu$  = Expected Value (Mean)
- $a$  = Minimum value (Estimation)
- $b$  = Maximum value (Estimation)
- $m$  = Average value (Estimation)

The above estimate for the mean is known as the PERT three-point estimation. This case makes the distribution symmetric and non-skewed that is very similar to the normal distribution. A Taylor series expansion of the Beta distribution probability density function shows that the Beta distribution can be approximated by a Normal distribution when skewness is equal to zero and the range is sufficiently great which is the case here.

Minimum and maximum values of joint infiltration obtained using extremum reasonable values of the variables (optimistic and pessimistic values). The distribution for  $P_2$  was then plotted.

Equation 4-11,  $Q = kh_c * 1.92 h_b^{-0.403}$ , was applied in order to calculate  $P_3$ . A similar approach was applied to estimate extremum values for seepage and to formulate the distribution. Since the equation is for water seepage into the subbase layer, the output of this cumulative distribution is the probability of seepage,  $P_{sb}$ , which is the probability of the water passes through the subbase. Probability of wet subbase,  $P_3$ , is equal to  $1-P_{sb}$  since the water that exists in the sublayer is of the interest rather than the



water that passes through (Figure 44). Figure 45 shows an example of a relatively permeable subbase. Since the permeability is high the seepage quantity and the probability of subbase seepage,  $P_{sb}$ , is high (the colored area under the curve) while the probability of wet subbase,  $P_3$ , is low (the uncolored area under the curve).

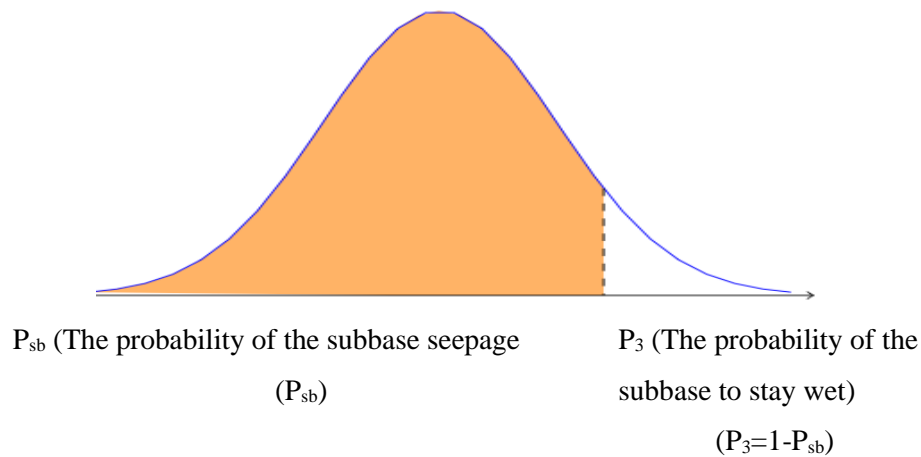


**Figure 44** Example of Subbase Seepage Distribution.

In order to better understand the step by step procedure, the analysis is illustrated in an example. Table 17 shows the input values for the example pavement.

**Table 17** Input Values for the Example Pavement.

Analysis Step	Parameter	Sign	Value
Calculations of $P_1$	Number of Days with Min 0.1" Rain	NA	210.0
Calculations of $P_2$	Number of Lanes in Pavement	N	2.0
	Joint Spacing (ft)	S	15.0
	Slab Width (ft)	W	12.0

Analysis Step	Parameter	Sign	Value
	Flow Factor = $\frac{K_{sealant}}{K_{joint}}$ $K_{sealant} = 125 \text{ ft/day}; K_{joint} = 250 \text{ ft.day}$	i	50.0%
	Installation Factor	d	40.0%
Calculations of $P_3$	Subbase Permeability, ft/day	k	7.00E-01
	Concrete Slab Thickness, inch	$h_c$	8.0
	Subbase Thickness, inch	$h_b$	5.0

Figure 45 shows the main sheet of the computer spreadsheet program that calculates the number of wet days for this example. These calculations can be done without the spreadsheet using equations that were explained but the spreadsheet makes the analysis faster. It also provides graphs and distributions.

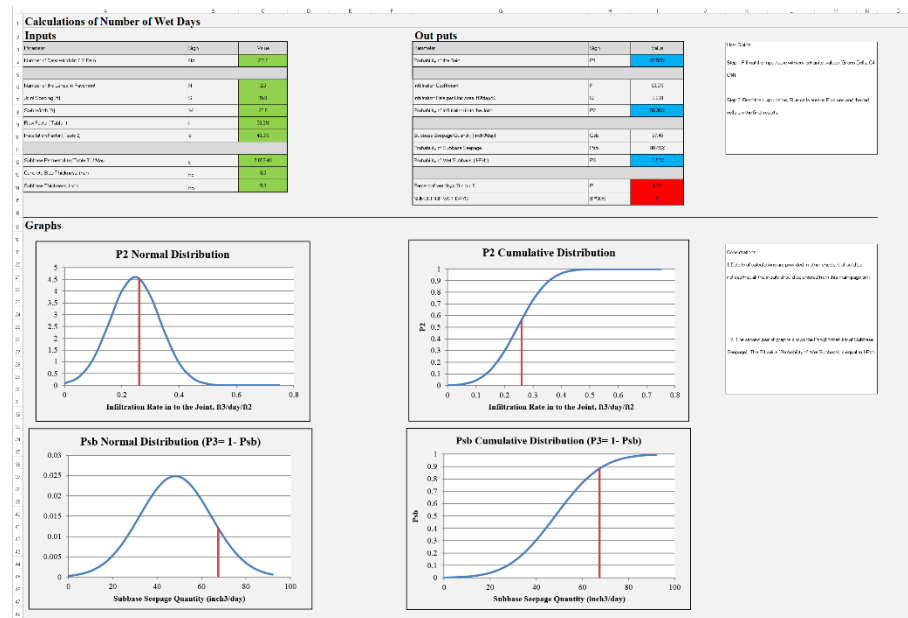


**Figure 45** Computer Spreadsheet Program that Calculates the Number of Wet Days.

The  $P_1$  is simply calculated as  $210/365 = 57.53\%$ . Infiltration rate per unit area in to the joint calculated and its equal to  $Q_i = 0.38 \text{ ft}^3/\text{day}/\text{ft}^2$ . From there  $P_2$  is calculated using

the Beta distribution.  $P_2 = 56.36\%$  means that a bit more than half portion of the water would get into the joint and the rest would drain by surface drainage, cross slopes, etc. the last step is to consider the effects of subbase seepage. The subbase, unless it is very permeable, will hold the water increasing the total number of the wet days. Table 18 shows the output values of the example analysis. Figures 46 and 47 show the distributions for  $P_2$  for these example calculations and Figure 48 and 49 show the distributions for  $P_{sb}$ .

**Table 18** Output Values for the Example Pavement.

Parameter	Sign	Value
Probability of the Rain	$P_1$	57.53%
Probability of Infiltration in to the Joint	$P_2$	56.36%
Probability of Subbase Seepage	$P_{sb}$	88.51%
Probability of Wet Subbase, $(1-P_{sb})$	$P_3$	11.49%
Percent of wet days $(0 < p < 1)$	$P$	3.73%
Number Of Wet Days $(P*365)$	Nw	14

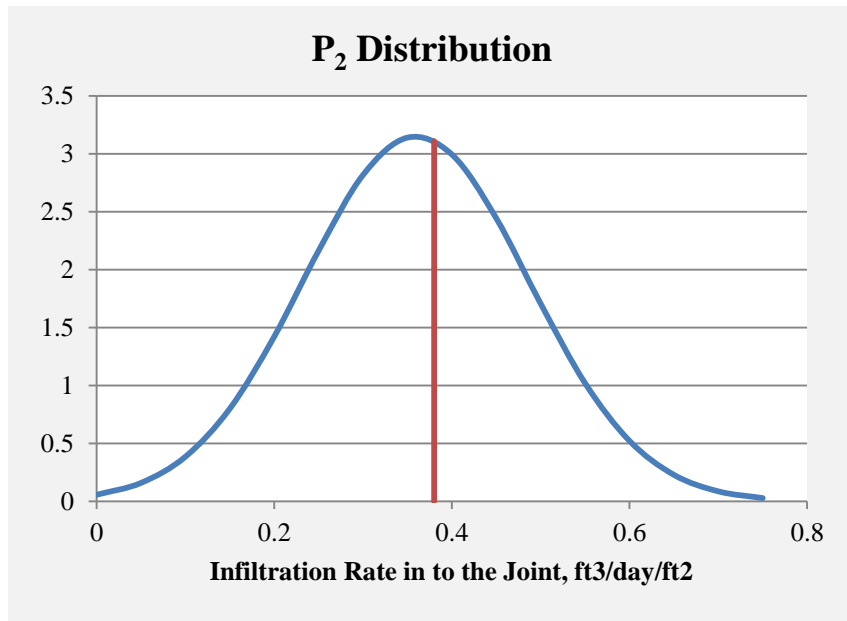


**Figure 46** P<sub>2</sub> Distribution for the Example Analysis.

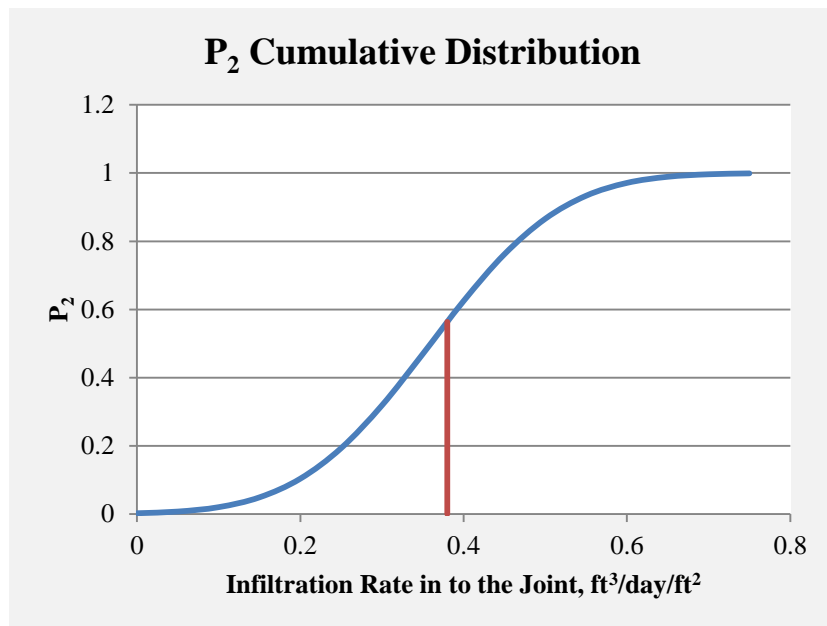


**Figure 47** P<sub>2</sub> Cumulative Distribution for the Example Analysis.

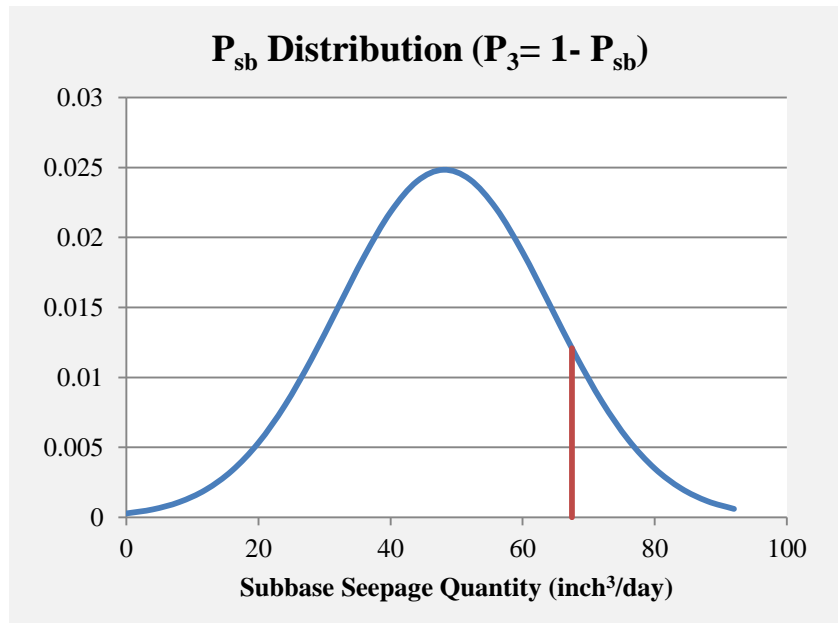


**Figure 48**  $P_{sb}$  Distribution for the Example Analysis.

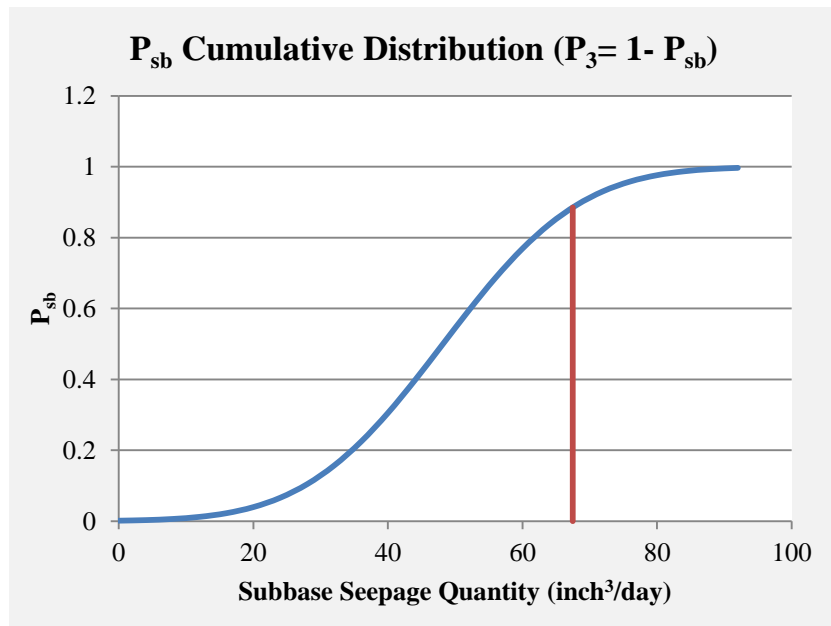


**Figure 49**  $P_{sb}$  Cumulative Distribution for the Example Analysis.

## **5. FAULTING PREDICTION MODEL FOR DESIGN OF CONCRETE PAVEMENT STRUCTURES**

### **5.1 Introduction**

Prior to presenting the design process, the mechanism of faulting is elaborated with respect to the three main elements that cause erosion. A part of the discussion is the description of the erosion model in a step by step format. Key details of the erosion model are presented keeping the focus on analysis results and outcomes and the comparison of them to performance data from pavement sections under service. The erosion process is employed in a concrete pavement computer program. Sensitivity analysis of the design results is also discussed.

### **5.2 Faulting, a Major Distress Type in Concrete Pavements**

According to field observations, faulting is typically a major performance issue for jointed concrete pavements [51]. Faulting, when it occurs, also affects drivers safety and decreases the smoothness of the ride [52]. Faulting is costly to repair and difficult to manage often requiring extensive grinding or in some cases full depth repair involving lane closures impacting public delays etc [53-55]. Faulting is addressed as a main performance indicator in the Mechanistic-Empirical Pavement Design Guide, MEPDG [41]. Therefore faulting could be considered as a dominant distress type when designing a jointed concrete pavement.

Subbase erosion is a key to understanding the process of joint faulting which involves factors such as passing traffic, existence of water along the subbase/slab

interface, and erodibility of the base material [10] (Figure 50). When slab support layers are saturated, vertical slab movement due to loading propels the water back and forth under the slab across the joint creating a pumping action. This action creates voids under the departure slab and leads to a building up of fine particles under the approach slab resulting in faulting. Erosion of slab support can often lead to high deflections and possibly other types of distress such as spalling of the joint, as well as acceleration of the loss of load transfer and bond between the slab and the base layer shortening the life of the pavement [1, 10].

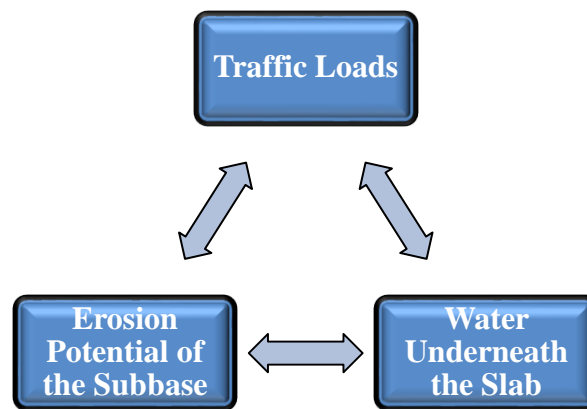


**Figure 50** Three Main Elements Contributing in Subbase Erosion and PCC Faulting.

### 5.2.1 Traffic Loads and Pavement Strength

Heavy trucks continually loading a pavement structure tend to break down the bond between the slab and the subbase. This bond depends upon the shear strength of the supporting layers which over time can affect the overall quality of the performance. If the slab is thin or if the subbase consists of low shear strength, the interfacial shear stress imposed by the applied loading may exceed the strength of the subbase or subgrade layer

and cause erosion damage. Stiffening the pavement at the joints may help to lower the shear stresses. This can be done simply by improving the strength of the subbase material (i.e. stabilization of subbase layer) or by using dowel bars at the joints. Design models with the appropriate sensitivity to shear strength and stress are key advantages in considering the integral effects of loading, subbase strength, and the number of wet days.

### **5.2.2 Existence of Water underneath the Slab**

It is well accepted that the presence of moisture in a pavement structure is a contributor to a variety of governing distress types related to erosion of the support that eventually deteriorates the pavement structure and decreases the pavement service life.

Accumulation of water along the slab/subbase interface in the vicinity of the joint combined with passing traffic can often initiate pumping at the interface transporting eroded material leading to faulting of the joint. Pumping, involves the transportation of abraded interfacial material from beneath slab typically voiding the slab support in the vicinity of a joint [10, 42]. To give consideration to all factors that can affect the performance of the pavement, climatic conditions that may cause the subgrade or subbase to become wetter over time, such as surface water infiltration, and most importantly rainfall should be determined. Possible trapped water directly beneath the slab greatly increases the potential for erosion. Condition of the drainage system and joint seals considerably affects the existence of moisture underneath the slab [56].

Improving joint seal effectiveness may provide opportunities to optimize the design of the pavement structure. Effectiveness of joint sealants and drainage system directly affect the number of wet days for design purposes.



### **5.2.3 Erosion Potential of the Subbase**

A variety erosion tests were developed starting in late 1970s using various testing devices, but few of those tests have been successfully used to develop a model or a framework for design. Most of the laboratory tests in this regard involve the application of loads on the material and define erosion related to weight loss, a parameter not particularly amenable to mechanistic design analysis. One method known as the “brush test” takes too long to run for practical purposes and the rotational shear device or jetting device tends to overestimate the loss of aggregate-sized particles. The rolling wheel erosion test device tends to create an erosion mechanism not like the voiding that occurs under an actual concrete slab [42, 57].

Jung and Zollinger developed a new test procedure that represents concrete pavement joint behavior to overcome these limitations and incorporates a parameter that can be transferred from lab to conditions in the field. This new laboratory test protocol involves measuring the erodibility of subbase materials using the Hamburg wheel-tracking device (HWTB) [42, 58]. The test consists of two component layers, one being a concrete cap on top and the other the material of interest which is placed immediately under the concrete cap. A wheel passes on top of the two layers and the sensors record the deflection versus passes. HWTB testing is mainly conducted under wet conditions in which erosion occurs due to mechanical and hydraulic shearing on the subbase layer generated by slab movement under an applied load [59, 60]. Therefore HWTB can simulate the erosion that occurs underneath the slab due to the shear stress coming from the load in presence of water.

A wide range of subgrade soil materials from seven locations in four states were tested and analyzed in order to evaluate the erosion potential of different subbase materials and the capability of them to perform as a sublayer. The selected samples cover different soil categories; non-plastic pure sands, combination of silt and sand, combination of sand and clay, and clays with high and low plasticity. Results were then plotted as number of load passes versus deflection measured in millimeters. Erosion resistance (ER) is defined as the amount of erosion (in mm) at 1,000,000 load applications under HWTD erosion testing [42]. The greater ER indicates that a subbase or subgrade material has less resistance against erosion. This parameter serves to differentiate different subgrade and base types with respect to erodibility. Details of Hamburg test method, collected sample specifications and erosion test results are discussed in the last chapter of this document.

### **5.3 Faulting/Erosion Model**

The faulting/erosion model explained in this chapter is a new ME (Mechanistic-Empirical) approach that formulates the faulting/erosion as a function of number of load repetitions in respect to wet days and the erosion resistance of the subbase.

#### **5.3.1 General Form of the Model**

The erosion model follows Gumbel cumulative probability function that pertains to structural damage due to aging and loading over time or traffic.

$$\%E = \frac{f_i}{f_{ult}} = e^{-\left(\frac{p}{D_i}\right)^\alpha} \quad (5-1)$$

$$D_i = \Sigma \frac{N_i}{N_f} \quad (5-2)$$

where

$\%E$	= Percent of erosion
$f_i$	= Level of faulting per load cycle $i$
$f_{ult}$	= Ultimate faulting
$D_i$	= Damage ratio per load cycle $i$
$\alpha$	= Erosion rate factor
$\rho$	= Erosion shape factor
$N_i$	= Designed ESAL <sub><math>i</math></sub> per load cycle $i$
$N_f$	= Ultimate ESALs to failure

The model calculates erosion in percentage ( $\%E$ ) that is equal to the ratio between the current faulting to the ultimate amount of faulting. There are two calibration factors associated with the erosion model illustrated in Figure 51; Erosion rate factor, Alpha ( $\alpha$ ) and erosion shape factor, Rho ( $\rho$ ) are calibration factors that change the rate of the damage. Figure 51 demonstrates how changing the value of the  $\alpha$  or the  $\rho$  parameters affects the distribution.

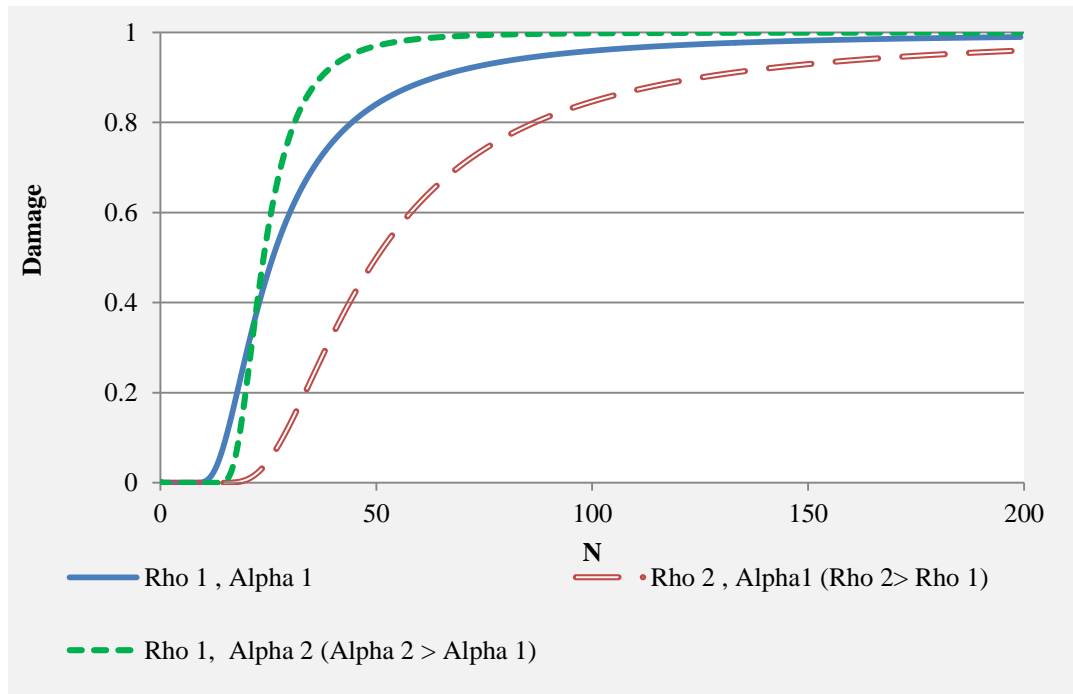


**Figure 51** Sample Gumbel S-Shaped Distribution.

These factors are direct function of erosion resistance (ER) determined for different subgrade categories using extensive lab data on different subgrades and base materials. As previously noted, a useful parameter derived from Hamburg testing is the erosion resistance (ER) of the material. The pavement designer can use this factor to differentiate one material from another with respect to its erodibility. The factor applies to either the subgrade or the subbase. As was previously mentioned erodibility, traffic loading and existence of water underneath the slab are three main factors affecting the potential for erosion. Two of these factors are taken in to consideration during the calculation of damage. Damage,  $D_i$ , is determined with respect to an equivalent traffic level (i.e. an erosion-based ESAL previously elaborated) and the allowable loads to failure  $N_f$  (i.e.  $D_i = N_i/N_f$ ).

### **5.3.2 Calculations for Equivalent Traffic Level**

In order to convert the daily traffic to an erosion-based equivalency, a traffic model was incorporated into this analysis process. The equivalency determination, expressed in terms of an equivalent single axle load (ESAL) in this chapter is based on an erosive mode of failure using the deformation energy (DE) concept assuming the slab corner to be the critical location. The model, given in equation 5-3 incorporates several parameters such as lane distribution factor (LDF), equivalent load factor (ELF), an equivalent axle factor (EAF), and an equivalent wander factor (EWF). LDF estimates the number of trucks in the design lane; *ELF* converts the different load group to the design single axle load; *EAF* adjusts tandem or tridem axle configurations to a single axle configuration. The equivalent ESAL can be obtained by equation 5-4 using the

equivalent wander factor, *EFW* which accounts for the traffic distributed laterally in the lane.

$$ESAL_i = \frac{ADT}{2} * GF * LDF * \sum_{j=1}^3 [(\% a_{i+1,j} - \% a_{i,j}) A_j * ELF_j] * EAF_i \quad (5-3)$$

$$ESAL_d = EWF * \sum ESAL_i \quad (5-4)$$

where

ESAL <sub>i</sub>	= ESAL converted from all load groups and axle types (daily)
ESAL <sub>d</sub>	= Equivalent ESAL as a result of traffic wandering consideration
%a <sub>kj</sub>	=Percent of loaded radius within a load group
ADT	= Average daily traffic
GF	= Growth Factor
LDF	= Lane distribution factor
i	= Per load group
j	= Per axle configuration (axle type)
A <sub>j</sub>	= Load group, (%)
ELF <sub>j</sub>	= Equivalent load factor
EAF <sub>i</sub>	= Equivalent axle factor
EFW	= Equivalent wander factor

### 5.3.3 Calculations for Effective ESALs, N<sub>i</sub>

The design ESAL is adjusted for the expected pavement drainage conditions. This is accomplished through consideration of the joint sealant condition, drainage characteristics and the potential of rainfall:

$$N_i = ESAL_i * P (\%) * 365 \quad (5-5)$$

where

P =	Percent wet days, [ $P = p_1 * p_2 * (p_3)$ ]
p <sub>1</sub> =	Probability of the rain,
p <sub>2</sub> =	Probability of infiltration in to the joint
p <sub>3</sub> =	Probability of wet subbase

As noted above, the design traffic is moderated by the value of three different factors.

The use of these factors basically delineates the portion of traffic distribution to that which is applied to the pavement only when moisture exists underneath the pavement.

Probability of rain,  $P_1$ , is simply a climatic factor defined as the number of days with rainfalls greater than 0.1 inch [42]. One important aspect in this model is the consideration of sealant quality,  $P_2$ . The sealant quality affects the infiltration of moisture into the slab/subbase interface. Sealants installed correctly are assumed to have the capability of keeping water from penetrating the joint into the subbase. Sealants potentially should decrease the number of wet days in order to be an effective component of the pavement.  $P_3$  shows the effect of subbase drainage capacity. This factor considers the effectiveness of drainage system in terms of conducting the moisture out of pavement with respect to the permeability of the supporting layers. The P values were discussed thoroughly in Chapter four.

#### 5.3.4 Ultimate Load and Shear Strength, $N_f$

As discussed, damage ratio is the ratio between the adjusted traffic load (effective ESALs) and Ultimate loads to failure ( $D_i = N_i/N_f$ ). Ultimate load is a function of shear strength of the pavement structure.

$$N_f = 10^{k_1 + k_2 r_i} \quad (5-6)$$

$$r_i = \frac{\tau_i}{f_\tau} \quad (5-7)$$

where:

- $N_f$  = Ultimate loads to failure
- $k_i$  = Erosion damage coefficients (determined from calibration)
- $\tau_i$  = Interfacial Shear Stress ( $FL^{-2}$ )
- $f_\tau$  = Shear Strength ( $FL^{-2}$ )

The resistance of the slab/subbase interface can perhaps be broken down into two segments one relating to interfacial adhesive bond (as may be represented by the

cohesive strength of the subbase material) and the other related to interfacial sliding resistance. In this regard, two basic premises are stated:

1. The adhesive bond strength across the slab/subbase interface can be defined by the cohesive shear strength of the subbase layer ( $f_c$ ) which is determinable from laboratory tri-axial testing (Figure 52).
2. The coefficient of sliding friction ( $f_F$ ) can be defined by the tangent of the  $\phi$  angle as again would be determined from tri-axial laboratory testing data (Figure 50).

Characterization of the interfacial adhesive bond between the slab and the subbase layer in this manner is considered to be a manifestation of the shear capacity of the subbase layer. Under field conditions, once the adhesive shear strength of the interface has been exceeded, the sliding frictional resistance is in force and represented by the angle of friction ( $\tan \phi$ ).

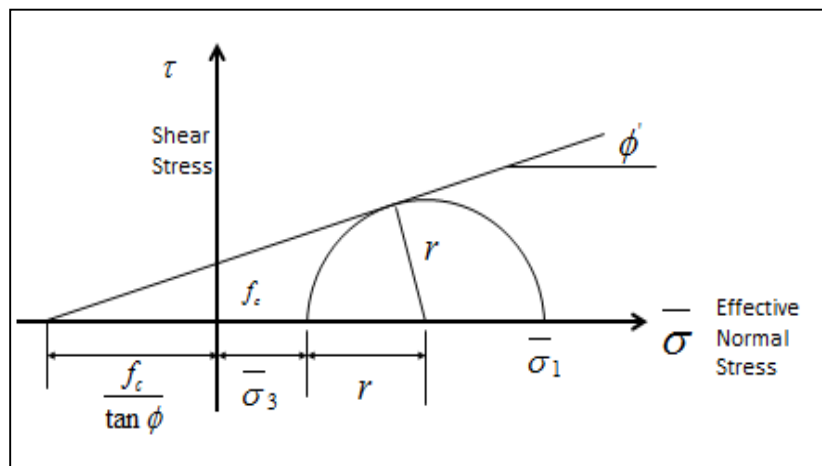


**Figure 52** Shear Strength and Angle of Friction Determinations.

$k_1$  and  $k_2$  are erosion damage coefficients that are determined using the calibration on field data. Interfacial shear stress can be determined as follows:

$$\tau_i = (1 - x_b) \frac{\partial \delta_{L_i}}{\partial X} \frac{E_{sb}}{2(1+\nu)} \quad (5-8)$$

where

$x_b$	= Degree of bond between slab and subbase
$\delta_{L_i}$	= Deflection from the load (Function of design load, modulus of subgrade reaction ( $k$ ) and radius of relative stiffness ( $l$ ))
$X$	= Distance from the point of loading along the diagonal from the corner or from the edge of the slab
$E_{sb}$	= Subbase modulus
$\nu$	= Subbase Poisson's ratio

The equation clearly shows that interfacial shear stress is a function of load level  $P$ , subgrade  $k$ -value, slab thickness (as affected by load transfer efficiency). Load transfer efficiency (LTE) is a factor included in the model through its effect on deflection and in the calculation of the shear stress which ultimately affects the amount of accumulated damage. It's well known that aggregate interlock and the use of dowels can significantly affect the capability of concrete slabs to resist erosion damage under load. Field observations have shown that slabs with dowels develop less faulting than those without dowels[42, 52]. Data from more than 100 LTPP jointed concrete pavement sections indicated that dowel bar use significantly reduced joint faulting for all pavement age categories [51].

#### 5.4 Demonstration Spreadsheet

A spreadsheet was developed to demonstrate the erosion model explained previously and to illustrate the analysis of the effect of joint sealant factors with respect to predicted erosion and faulting related performance. The spreadsheet considers key distress types



that occur in concrete pavement systems and may eventually be used for design purposes. Although the spreadsheet is still only in preliminary stages development, a sensitivity analysis and field verification of the erosion model is provided and subsequently discussed. Even though one of the main advantages of this spreadsheet is that it can be calibrated with the local performance data, the results subsequently discussed are not to be interpreted with respect to any aspect of pavement design. The spreadsheet consists of input data, calibration, and analysis. The output includes the faulting prediction as a function of load transfer efficiency and interfacial shear stress.

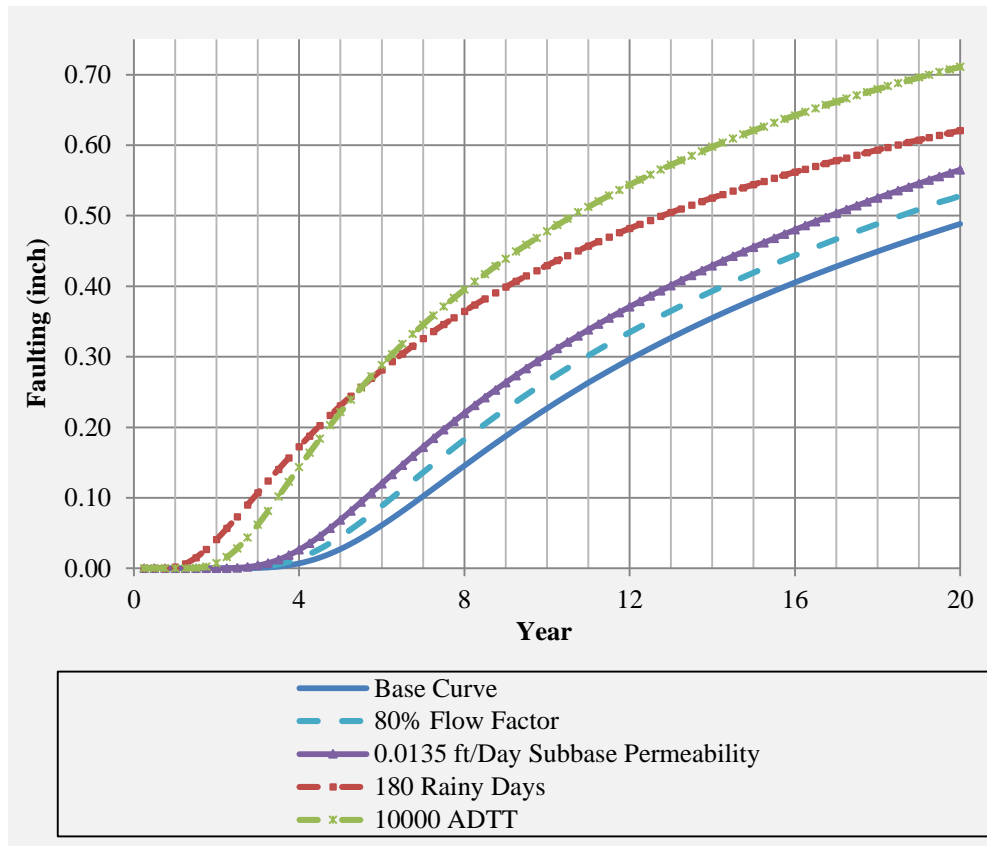
### **5.5 Sensitivity Analysis**

Figure 51 summarizes a sensitivity analysis for the erosion model with respect to components that affect number of wet days including sealants effectiveness. The base curve in Figure 51 is faulting prediction for a 10 inch concrete slab, on top of 10 inches of granular subbase (AB-subbase permeability equal to 13.5 ft/day) with 15 ft joint spacing. The ADTT is equal to 5000 trucks with annual growth rate of 3%. Number of rainy days with rainfall greater than 0.1" is 120 days in a year. Joints are sealed and the installation and seal quality is in a poor condition (the flow factor equal to 0.50). Factors were all changed in such a manner to increase the amount of erosion damage; this way the comparison of each factor would be more prevalent. Figure 51 shows that slight increase in sealant flow factor, which means having a greater amount of seal damage, directly increases the amount of faulting in the pavement section. Figure 51 also shows the effects of subbase permeability on number of wet days and its effect on erosion damage at the interface. Changing the granular subbase to an impervious clayey subbase

lowers the pavement drainage quality, the rate of erosion, and increases the number of wet days at the slab subbase interface increasing the potential for erosion. Furthermore, Figure 53 shows the effects of higher traffic level (twice than the traffic in the base curve) and increasing the number of rainy days from 120 days to 180 days in a year. Table 19 shows how variables for sensitivity study were defined.

**Table 19** Input Parameters for the Base Analysis.

Pavement Type	JPCP
Analysis Period	15 Years
Slab Thickness	10"
ADTT	5000
Base Layer	AB
Joint Spacing	15'
Lane Width	12'
Shoulder	No
Dowel Bar	No
Subgrade K value	150 pci
Wet Days	120
Coarse Aggregate	Limestone



**Figure 53** Sensitivity Analysis on Base Curve.

Although, not included in the above variations, Figure 54 shows how changes in load transfer efficiency with and without doweled joints. When load transfer is only a function of aggregate interlock it is susceptible to the magnitude of the joint opening.

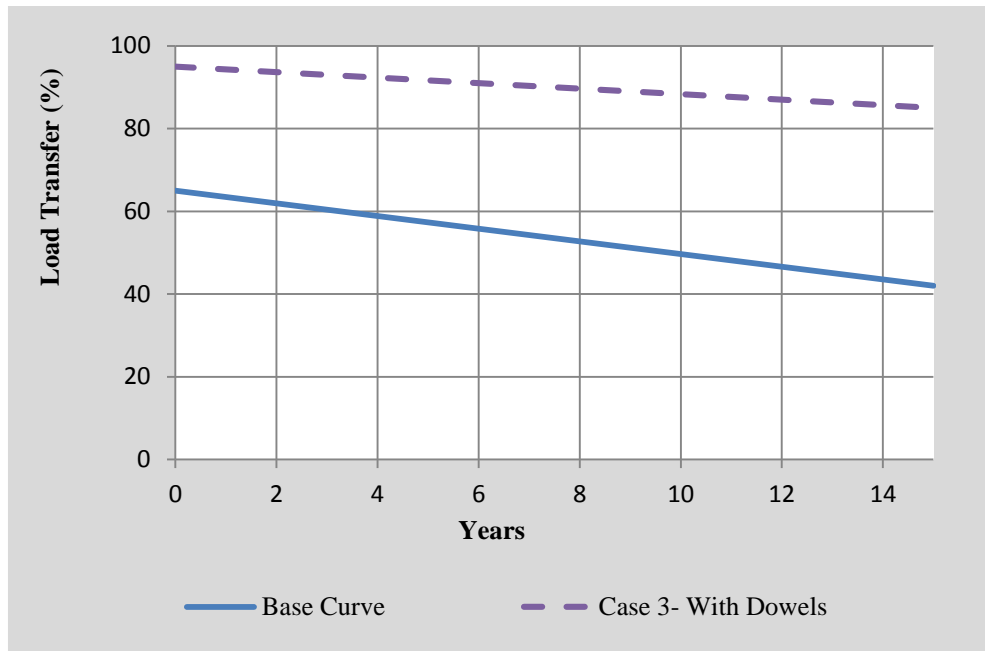


**Figure 54** Changes of Load Transfer Efficiency with and Without Dowel Bars.

### 5.6 Validation Using LTPP Data

Data from the Long-Term Pavement Performance database (LTPP) were used to validate the model's results [61]. Table 20 shows construction and traffic information of the selected LTPP pavement sections included in this analysis. All sections are located in Texas. The subbase layers are all treated except for the one denoted by "G" that indicates granular base or subbase.

Figure 55 shows the fit to the model using LTPP section 48-4143 (Texas data). As a result of this fitting, values of  $k_1$  and  $k_2$  (the coefficients in the erosion damage equation) were found.

**Table 20** Construction Information on LTPP Sections.

SHRP ID	Slab Thickness (in)	Base Thickness (in)	Subbase Thickness (in)	AADT Truck*
4143	10.4	4.5	5.5	279
3003	9.3	3.5	7	915
3699	10.2	6.2	6.1	1895
4152	11.4	6.4	6.6	312
B420	10	4.3	5.5	347
D410	11.4	6.4	6.6	341
E420	9.6	7.6	4(G)**	450

\*Annual Average Daily Number of Trucks in the LTPP lane

\*\*Granular (Non-Treated) Layer

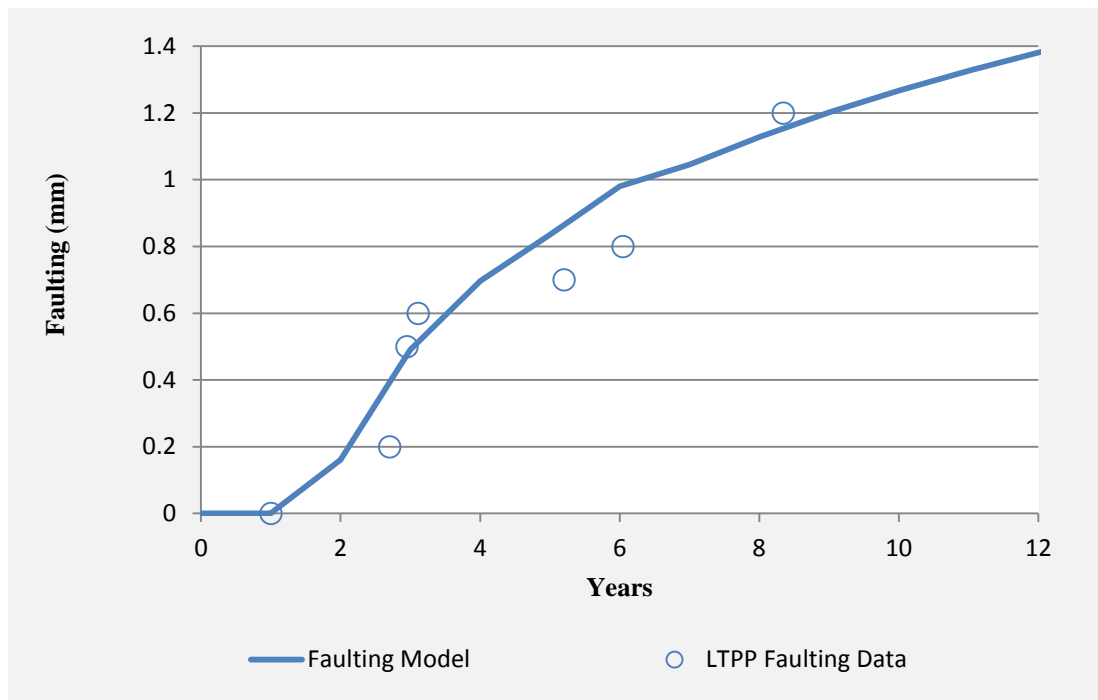


**Figure 55** Calibration of the Model Using the Field Data.

The model was then checked accordingly to analyze pavement sections with known performance histories to compare to observed field performance. The correlation between observed and model-fitted faulting is presented in Figure 56 (section 4143 that was used for calibration is excluded). The R square value is 84%, which represents a very good fit to the data. It should be noticed that each section provides several data points that were collected during the service time. Table 21 shows the T-Test results for the data analysis. The null hypothesis of zero mean difference is accepted at a 95% confidence level as the P Value is much larger than 0.05.

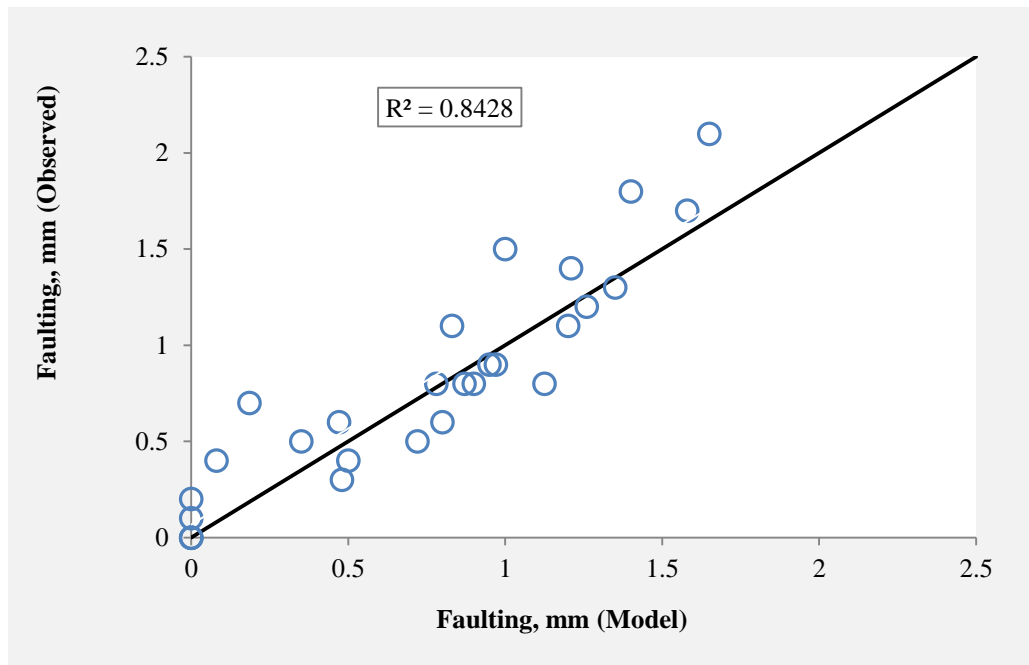


**Figure 56** Modeled versus Measured Faulting of LTPP Data.

**Table 21** Statistical Analysis for Sampled LTPP Faulting Data.

Statistical Quantity	Observed	Model
Mean	0.804	0.738
Variance	0.317	0.268
Observations	28	28
P Value	0.651	

### 5.7 Conclusions and Discussion

Faulting directly affects the serviceability of the pavement. It indirectly contributes to other major distress types that affect the performance of jointed concrete pavement. The mechanistic empirical model presented in this chapter can effectively analyze the faulting and erosion in JPCP's. The erosion resistance of materials were precisely defined and considered in this model. The model is capable of calibration for local conditions as a distinct advantage over other faulting models. The model was successfully implemented and calibrated into a spreadsheet format. Comparison of the model analysis versus the field data shows a good fit as noted in Figure 56.

## **6. CONCLUSIONS AND DISCUSSIONS**

As background, joint and sealant practices were reviewed. Different sealant types were discussed and compared. A brief review on sealant failure mechanism was provided and review of previous studies and observations on the subject were presented.

An experimental program on sealant effectiveness as represented by varying degrees of damage in regards to water infiltration was performed. Several important conclusions can be drawn from this test program which lead to the collection of valuable data during the field testing of joint sealant effectiveness. The experimental results showed that if joint seals are properly installed, they can be very effective in preventing moisture infiltration. Unsealed joints have significantly higher flow rates compared to joints with damaged sealants. Without regard to recommended extension limits, results showed that different joint seals start to infiltrate greater and greater amounts of water at different threshold widths under 100% debonded conditions. Preformed sealants have a higher threshold before infiltration commences (at 100% debonding) however hot pour and silicone sealants are capable of allowing infiltration at reduced levels corresponding to debonding amounts less than 100% debonding. The test results in this study have also demonstrated the effect of proper sealant installation on performance. The water infiltration rates for dirty joints were as high as the amount of water that was infiltrated for the joints with 50% debonding. In comparison to a clean joint with a 3mm joint opening, the infiltration rate was more than 5 times the infiltration rate of that allowed for dirty joints. The sensitivity of the sealants to poor installation is more dramatic when



debonded joint openings are wider as may occur in cases where climatic conditions experience a wide range of temperature change.

Analysis of the field data collected in Illinois and Arizona demonstrated the viability of using GPR to ascertain the relative amount and presence of moisture in a joint. Although more data is needed to establish threshold values of the volumetric concentration of moisture, the use and analysis of GPR data serves as a rapid method to provide the data needed to ascertain the number of wet days a pavement section experiences. The data collected clearly demonstrates that base permeability does play a role in the number of wet days and appears to offset the lack of joint sealing – at least in drier climates.

Actual number of wet days was redefined and analyzed. Most definitions relate the number of wet days only to climatic factors such as rainfalls. But the actual number of days that water exists underneath the slab is not only a factor of rainfall. Several other factors such as surface and subsurface drainage, joint sealants or subbase permeability must be taken into consideration when defining the actual number of wet days. As an example for a certain pavement section in a high rainfall zone a clay subbase can hold water but a granular subbase drains the water. Therefore number of wet days for the pavement with clay subgrade is greater even though they are both in a same climatic condition. Number of wet days was analyzed and formulated in order to be used for design purposes the  $F_c$  factor serves as a measure of failure based on initial conditions but can be extended to include the effect of aging over time.

An intensive erosion test program was performed on different subbase materials. Several important conclusions can be drawn from this test program those are summarized as follows:

- Water is a critical factor in the process of erosion underneath the slab. Subgrade materials when exposed to water show considerably less resistance against erosion compared to a dry condition. Existence of water significantly decreases the shear strength at the slab/subbase interface therefore it greatly increases the potential of erosion in subbase material. The wet erosion rate was found to be on the average 20 times greater than the dry erosion rate for subgrade samples.
- All the subbase samples showed acceptable performance in the absence of water. Even though erosion occurred in dry tests, the rate of dry erosion was low for all samples.
- Cohesiveness increases the soil shear strength and as a result increases the resistance against erosion in a subbase. Sands were found to be highly erodible, particularly when the clay content is lower. Sandy soils are not as cohesive which causes the sand to be very weak against erosion. Clays on the other hand found to be more resistant to erosion.
- While dried clays are very resistant against erosion, clays are extremely weak when they become completely saturated. It should be noted that complete saturation of the whole clay layer rarely occurs unless pavement is in an extremely rainy climate with unsealed joints and poor drainage system.

- These results suggest that clays could be used as a subgrade in a dry condition for minor roads or parking lots but using clays should be avoided in places with heavy rain and unsealed joints. Another problem with clays in the moist condition is an increase in the volume and swelling that causes damage on concrete slab.
- Stabilization significantly improved the resistance of the samples against erosion. Seven percent added cement caused a decrease in erodibility index by 14 times in the fat clay. Stabilization also improved the resistance of sand against erosion.
- Cement stabilization showed better erodibility resistance as compared to lime stabilization. Also stabilization has greater impact on clay as compared to sands mainly because of faster and stronger chemical reactions of clay particles.

Faulting directly affects the serviceability of the pavement. It indirectly contributes to other major distress types that affect the performance of jointed concrete pavement. A faulting prediction model was developed and presented. The presence of water on the interface along with the effect of traffic and erodibility are the three main elements of the erosion/faulting process. Traffic, the erosion resistance of materials, and number of wet days were precisely defined and considered in this model. The mechanistic empirical model presented in this dissertation can effectively analyze the faulting and erosion in JPCP's. The model is capable of being calibrated for local conditions which is a distinct advantage over other faulting models. The model was successfully implemented and calibrated into a spreadsheet format. Results show that the model fits well with the field data and can be implemented for design and maintenance management purposes.

By using the model the effectiveness of sealant in pavement sustainability can be determined. The most valuable outcome of this study is the demonstration mechanistically of the role of joint sealing at varying degrees of failure on service life of jointed concrete pavements. Sealants, by limiting water infiltration into the pavement sublayers, can improve concrete pavement performance.

## REFERENCES

1. K. T. Hall, J.A.C., T. E. Hoerner, K. D. Smith, A. M. Ioannides, and J. Armaghani, *Effectiveness of Sealing Transverse Contraction Joints in Concrete Pavements – Final Report*, 2008, U.S. Department of Transportation ,Federal Highway Administration.
2. Teller, L. and E. Sutherland, *The Structural Design of Concrete Pavements: Part 4A, Study of the Structural Design of Several Types of Transverse and Longitudinal Joint Designs*. Public Roads, 1936. **17**(7): p. 143-149.
3. Ioannides, A.M., A.R. Long, and I.A. Minkarah, *Joint sealant and structural performance at the Ohio route 50 test pavement*. Transportation Research Record: Journal of the Transportation Research Board, 2004. **1866**(-1): p. 28-35.
4. Morian, D.A. and S. Stoffels, *Joint seal practices in the United States: Observations and considerations*. Transportation Research Record: Journal of the Transportation Research Board, 1998. **1627**(-1): p. 7-12.
5. Olson, R.C., et al., *Edge-Joint Sealing as a Preventive Maintenance Practice*. 2003: Minnesota Dept. of Transportation, Office of Research Services.
6. Lynch, L., et al., *Joint-and Crack-Sealing Challenges*. Transportation in the New Millennium, 2000.
7. *ASTM D5078*, in *Standard Specification for Crack Filler, Hot-Applied, for Asphalt Concrete and Portland Cement Concrete Pavements*, 2011, American society for testing and materials.
8. *ASTM D5893*, in *Standard Specification for Cold Applied, Single Component, Chemically Curing Silicone Joint Sealant for Portland Cement Concrete Pavements*, 2010, American society for testing and materials.
9. *ASTM D2628*, in *Standard Specification for Preformed Polychloroprene Elastomeric Joint Seals for Concrete Pavements*, 2011, American Society for Testing and Materials.
10. Neshvadian Bakhsh, K., D.G. Zollinger, and Y.-S. Jung, *Evaluation of Joint Sealant Effectiveness on Moisture Infiltration and Erosion Potential in Concrete Pavement*, in *Transportation Research Board 92nd Annual Meeting* 2013.
11. Smith, K. and A. Romine, *LTPP Pavement Maintenance Materials: SHRP Crack Treatment Experiment*, 1999, Report No. FHWA-RD-99-143, Federal Highway Administration, Washington, DC.
12. Caltrans, *Caltrans / Industry Joint Sealing Field Review*, 2012, California Department of Transportation.
13. Brown, H.E., *Joint Sealant Materials for Concrete Pavement Repairs*, 1991, Virginia Transportation Research Council.
14. Lynch, L.N., J.G. Chehovits, and D.G. Luders, *Ten-Year Field Performance Evaluation of Joint Resealing Project*. Transportation Research Record: Journal of the Transportation Research Board, 2002. **1795**(-1): p. 40-48.
15. ARA, *Arizona SPS-2 PCC Joint Seal Performance* 2013, Applied Research Associates.

16. Eacker, M.J. and A.R. Bennett, *Evaluation of various concrete pavement joint sealants*, 2000.
17. Lynch, L.N., et al., *Joint Resealing Project at Fairchild Air Force Base, Washington*. Transportation Research Record: Journal of the Transportation Research Board, 2013. **2361**(1): p. 98-105.
18. Scofield, L., *Relative Cost of Concrete Highway Features: Final Report 12-27-10*, 2010, American Concrete Pavement Association: Rosemont, IL.
19. Shober, S.F., *The Great Unsealing: A Perspective on Portland Cement Concrete Joint Sealing*. Transportation Research Record: Journal of the Transportation Research Board, 1997. **1597**(-1): p. 22-33.
20. Li, Q., *Development of testing system for analysis of transverse contraction joints in Portland cement concrete pavement*. 2012: University of Florida.
21. Gurjar, A.H., T. Tang, and D.G. Zollinger, *Evaluation of Joint Sealants of Concrete Pavements*. NASA, 1997(19990008235).
22. Gurjar, A., D.G. Zollinger, and T. Tang, *Strain and age effects on behavior of a concrete pavement joint sealant material*. Transportation Research Record: Journal of the Transportation Research Board, 1996. **1529**(-1): p. 95-100.
23. Gurjar, A., et al., *Laboratory investigation of factors affecting bond strength in joint sealants*. Transportation Research Record: Journal of the Transportation Research Board, 1998. **1627**(-1): p. 13-21.
24. Hawkins, B.K., A.M. Ioannides, and I.A. Minkarah, *To seal or not to seal? A field experiment to resolve an age-old dilemma*. Transportation Research Record: Journal of the Transportation Research Board, 2001. **1749**(-1): p. 38-45.
25. Cho, Y.K., *Advanced Cleaning Device to Remove Debris and Chemicals for Crack/Joint Sealing in Pavement*, 2013.
26. Cook, J. and I. Minkarah, *PAVEMENT DESIGN FEATURES AND THEIR EFFECT ON JOINT-SEAL PERFORMANCE (ABRIDGEMENT)*. Transportation Research Record, 1980(752).
27. Morian, D.A., N. Suthahar, and S. Stoffels, *Evaluation of rigid pavement joint seal movement*. Transportation Research Record: Journal of the Transportation Research Board, 1999. **1684**(-1): p. 25-34.
28. Weisgerber, F.E. and C.P. Wang, *Stress Distributions in Highway Joint Seals*. Science and technology of building seals, sealants, glazing, and waterproofing, second volume, 1992: p. 213.
29. Woo Lee, S. and S.M. Stoffels, *Analysis of in situ horizontal joint movements in rigid pavements*. Transportation Research Record: Journal of the Transportation Research Board, 2001. **1778**(-1): p. 9-16.
30. Tons, E., *Factors in Joint Seal Design*. Highway Research Record, 1965(80).
31. Ray, G.K., *Effect of Defective Joint Seals on Pavement Performance*. Transportation Research Record, 1980.
32. Dunn, K.H., *The Effect of Sealed vs. Unsealed Joints on the Performance of Jointed PCC Pavement*, 1987, Wisconsin Department of Transportation.
33. Burke Jr, M.P. and J.W. Bugler, *The Long-Term Performance of Unsealed Jointed Concrete Pavements*. 2002.

34. Hall, K.T. and J.A. Crovetto, *LTPP data analysis: Relative performance of jointed plain concrete pavement with sealed and unsealed joints*. 2000: Transportation Research Board, National Research Council.
35. Curt Dunn, B. and K.E. Fuchs, *Practice of Unsealed Joints in New Portland Cement Concrete Pavements*, 2009, North Dakota Department of Transportation.
36. Cedergren, H.R., *Seepage, drainage, and flow nets*. Vol. 16. 1997: John Wiley & Sons.
37. Forsyth, R.A., G.K. Wells, and J.H. Woodstrom, *Economic impact of pavement subsurface drainage*. 1987.
38. Huang, Y.H., *Pavement analysis and design*. 1993.
39. Geo-Hydro. <http://geohydro.com/>. Comany Webpage 2014.
40. AASHTO, G., *Guide for Design of Pavement Structures*. American Association of State Highway and Transportation Officials, Washington, DC, 1998.
41. NCHRP, *Mechanistic-Empirical Pavement Design Guide*, 2004, National Cooperative Highway Research Program: Champaign, Illinois.
42. Jung, Y.S. and D.G. Zollinger, *New Laboratory-Based Mechanistic-Empirical Model for Faulting in Jointed Concrete Pavement*. Transportation Research Record: Journal of the Transportation Research Board, 2011. **2226**(-1): p. 60-70.
43. DRIP, *Drainage requirements in pavements Version 2.0*. Federal Highway Administration, US Department of Transportation, Washington, DC, 2002.
44. Marek, M., *Roadway Design Manual*. TxDOT Online Manuals, Texas Department of Transportation, Austin, Texas, USA, 2010.
45. Cedergren, H.R., J.A. Arman, and K.H. O'Brien, *Development Of Guideline For The Design Of Subsurface Drainage Systems For Highway Pavement Structural Sections*, 1973.
46. Reddi, L.N., *Seepage in soils: principles and applications*. 2003: John Wiley & Sons, Inc.
47. Ridgeway, H., *Infiltration Of Water Through The Pavement Surface (Abridgement)*. Transportation research record, 1976(616).
48. Ridgeway, H.H., *Pavement subsurface drainage systems*. NCHRP Synthesis of Highway Practice, 1982(96).
49. Munson, B.R., D.F. Young, and T.H. Okiishi, *Fundamentals of fluid mechanics*. 1990: New York.
50. Keefer, D.L. and S.E. Bodily, *Three-point approximations for continuous random variables*. Management Science, 1983. **29**(5): p. 595-609.
51. Selezneva, O., J. Jiang, and S.D. Tayabji, *Preliminary Evaluation And Analysis Of LTPP Faulting Data-Final Report*, 2000.
52. Byrum, C.R. and R.W. Perera, *The Effect of Faulting on IRI Values for Jointed Concrete Pavements*, 2005.
53. Jung, Y.S., D.G. Zollinger, and T.J. Freeman, *Evaluation and Decision Strategies for the Routine Maintenance of Concrete Pavement*. 2009.
54. Freeman, T.J. and D.G. Zollinger, *Guidelines for Routine Maintenance of Concrete Pavement*, 2008.

55. Neshvadian Bakhsh, K., *Evaluation of Bond Strength between Overlay and Substrate in Concrete Repairs*. 2010.
56. ACI, *Guide for Design of Jointed Concrete Pavements for Streets and Local Roads*, in ACI 325-12R-022002, American Concrete Institute: Farmington Hills, Michigan, USA.
57. De Beer, M., *Aspects of Erodibility Lightly Cementitious Materials*. South African Council for Scientific Industrial Research. . 1989: Flexible Pavement Programme.
58. TxDoT, *Tex-242-F*, in *HAMBURG WHEEL-TRACKING TEST*2009, Texas Department of Transportation.
59. Jung, Y.S., D.G. Zollinger, and A.J. Wimsatt, *Test Method and Model Development of Subbase Erosion for Concrete Pavement Design*. Transportation Research Record: Journal of the Transportation Research Board, 2010. **2154**(-1): p. 22-31.
60. Zollinger, D.G., et al., *Subbase and Subgrade Performance Investigation and Design Guidelines for Concrete Pavement*, 2012.
61. LTPP. *Long-Term Pavement Performance program*. 2013; Available from: <http://www.ltp-projects.com/>.
62. Neshvadian Bakhsh, K., D.G. Zollinger, and Y.-S. Jung. *Evaluation of Joint Sealant Effectiveness on Moisture Infiltration and Erosion Potential in Concrete Pavement*. in *Transportation Research Board 92nd Annual Meeting*. 2013.
63. "USDA/The COMET Program". [Web] 2012 [cited 2012 10 September ]; Basic Hydrologic Science Course, Runoff Processes,Section Four: Soil Properties].
64. ASTM D6913, in *Standard Test Methods for Particle-Size Distribution (Gradation) of Soils Using Sieve Analysis*2009, American society for testing and materials.
65. ASTM D4318, in *Standard Test Methods for Liquid Limit, Plastic Limit, and Plasticity Index of Soils*2010, American Society for Testing and Materials.
66. ASTM D2487, in *Standard Practice for Classification of Soils for Engineering Purposes (Unified Soil Classification System)*2011, American Society for Testing and Materials.
67. ASTM D698, in *Standard Test Methods for Laboratory Compaction Characteristics of Soil Using Standard Effort (12 400 ft-lbf/ft<sup>3</sup> (600 kN-m/m<sup>3</sup>))*2007, American Society for Testing and Materials.
68. ASTM D1557, in *Standard Test Methods for Laboratory Compaction Characteristics of Soil Using Modified Effort (56,000 ft-lbf/ft<sup>3</sup>(2,700 kN-m/m<sup>3</sup>))*2009, American Society for Testing and Materials.
69. ASTM D2216, in *Standard Test Methods for Laboratory Determination of Water (Moisture) Content of Soil and Rock by Mass*2010, American Society for Testing and Materials.
70. Kawamura, M. and S. Diamond, *Stabilization of clay soils against erosion loss*, 1975.
71. *Tex-121-E*, in *SOIL-LIME TESTING*2002, Texas Department of Transportation.



- 72. Henderson, F.M., *Open Channel Flow*, Macmillan Publishing Co., New York, 1996.
- 73. Wurbs, R.A, and W.P. James, *Water Resources Engineering*, Prentice Hall, N.J. 2002.
- 74. Neshvadian Bakhsh, K., *Evaluation Of Joint Sealant Effectiveness On Jointed Concrete Pavement Sustainability*. Ph.D Disseration 2014, Texas A&M University, College Station, Tx.
- 75. TableCurve 3D v4 for Windows User's Manual, 2002 Systat Software Inc

## Appendix A

### Layer Moisture and Density

An important output from ground coupled radar data is the dielectric constant; an interesting aspect of dielectric data is its representation of the composite nature of the material being. A composite view of a soil material is ideally scanned shown in Figure A-1 where the soil material is divided into three components of solid, air, and water. Each of these components has distinctively different dielectric values particularly when comparing the dielectric of air ( $\epsilon_a$ ) and water ( $\epsilon_w$ ) to the dielectric of other materials. This feature allows for the separation of one component from the other, volumetrically speaking, based on the measurement of the composite dielectric value ( $\epsilon_m$ ) to extract both the dry density and moisture content among other features of interest in the floor structure.

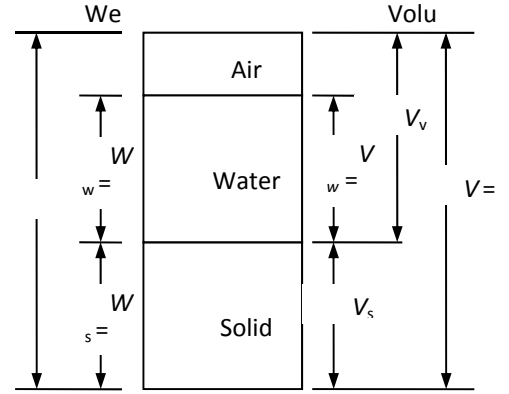


**Figure A.1** Soil Mixture with volume of soil solids equal to 1.

Elaborating further, the weight relationship between the moisture content and the unit weight is:

$$w = \frac{W_w}{W_s} \quad (\text{A.1})$$

$$\gamma = \frac{W}{V} \quad (\text{A.2})$$

where

- $w$  = gravimetric moisture content (%)
- $\gamma$  = unit weight ( $\text{g/cm}^3$ )
- $W$  = total weight of mixture (g)
- $V$  = volume of the sample ( $\text{cm}^3$ )
- $W_w$  = weight of water (g)
- $W_s$  = weight of solids (g)

To determine the gravimetric moisture content, the volume of water can be:

$$V_w = \frac{W_w}{\gamma_w} = wG_s \quad (\text{A.3})$$

where

- $\gamma_w$  = unit weight of water ( $\text{g/cm}^3$ )
- $G_s$  = specific gravity of solids

and the dry density of soil can be written as:

$$\gamma_d = \frac{W_s}{V} \quad (\text{A.4})$$

where

- $\gamma_d$  = dry unit weight of soil (or soil dry density,  $\text{g/cm}^3$ )

Thus, the gravimetric moisture content can be expressed in terms of the unit weight of water and solid and volumetric moisture content from equations above:

$$w = \frac{V_w}{V} \frac{\gamma_w}{\gamma_d} = \theta \frac{\gamma_w}{\gamma_d} \quad (\text{A.5})$$

where

$\theta$  = volumetric moisture content (%)

Equation 5 is needed to convert soil moisture from a volume to weight basis.

Based on what is known as the Bruggeman formula<sup>1</sup>:

$$\frac{\gamma_d}{G_s \gamma_w} \cdot \frac{\alpha_1 - \varepsilon_m}{\alpha_1 + 2\varepsilon_m} + \theta \cdot \frac{\alpha_2 - \varepsilon_m}{\alpha_2 + 2\varepsilon_m} + \left( 1 - \frac{\gamma_d}{G_s \gamma_w} - \theta \right) \frac{\alpha_3 - \varepsilon_m}{\alpha_3 + 2\varepsilon_m} = 0 \quad (\text{A.6})$$

where

$\gamma_d$  = dry density of soil, g/cm<sup>3</sup>,

$G_s$  = specific gravity of soil,

$\gamma_w$  = density of water, 1 g/cm<sup>3</sup>,

$\alpha_1$  = dielectric constant of the sand solid,

$\alpha_2$  = dielectric constant of water (= 80),

$\alpha_3$  = dielectric constant of air (= 1),

$\varepsilon_m$  = dielectric constant of the soil mixture determined from the radar scan, and

$\theta$  = ratio of water fraction (= 0 for dry sand)

This expression can be used for the calculation of volumetric water content and dry density based on established values of  $\alpha_1$ ,  $\alpha_2$ ,  $\alpha_3$ , and  $G_s$ . The soils characteristics  $\alpha_1$  and  $G_s$  are found from calibration using samples of the subgrade materials. From that, all calculations of  $\gamma_d$  and  $\theta$  can be determined at any other positions in the layer.

[1] D.A.G. Bruggeman, Berechnung verschiedener physikalischer Konstanten von heterogenen Substanzen. I. Dielektrizitätskonstanten und Leitfähigkeiten der Mischkörper aus isotropen Substanzen, Annalen der Physik, 416 (1935) 636-664

## Appendix B

### Assessment of Effective Slab Thickness and % Erosion

Even though most design procedures for concrete pavements are framed around the assumption that the subbase is unbonded from the slab, analysis of performance tends to suggest otherwise. Subbase requirements in pavement design are typically limited to thickness and material stiffness considerations which have been compatible with the unbonded assumption. These parameters have allowed for the calculation of load stress according to the composite nature of the slab/subbase system. However, the preponderance of performance and calibration studies of concrete pavement seem to require a fully bonded section, at least for part of the design period, in order to avoid under prediction of pavement life. But certainly such an assumption necessitates the consideration of the potential for wear-out to occur along with frictional and other related effects in a broader context particularly as it may pertain to erosive action and eventual damage of the support interface along edges and corners of loaded concrete slabs.

Imperceptible as it may be, a certain amount of slip may occur between layers of a pavement structure under load that is capable of generating considerable shear stress sufficient to create a failure plane along or even through one of the layers adjoining the interface. A more complete assessment of subbase behavior and the requirements for design would consider in greater detail the effects of interlayer adhesion and friction as well as subbase thickness and stiffness effects on performance. Such considerations would expand the capability of design methodology and better address and predict the complexities of slab/subbase interaction. Ignoring this aspect of pavement behavior has had its consequences with regard to the capability to adequately predict performance. This paper addresses the important subject of modeling interlayer frictional resistance to advance to a more complete framework for the design of subbase layers under concrete pavements than design methodology presently considers.

#### Model for Interlayer Bond

The resistance of the slab/subbase interface can perhaps be broken down into two segments one relating to interfacial adhesive bond (as may be represented by the cohesive or shear strength of the subbase material) and the other related to interfacial sliding resistance  $f_F$ . In this regard, two basic premises are stated:

1. The adhesive bond strength across the slab/subbase interface can be defined by the cohesive shear strength of the subbase layer  $f_c$  which is easily determined from laboratory tri-axial testing data (Figure B.1).
2. The coefficient of sliding friction typically defined by the tangent of the  $\phi$  angle as determined from tri-axial laboratory testing data (Figure B.1) is likely a composite of the layers comprising the interface.

Characterization of the interfacial adhesive bond between the slab and the subbase layer in this manner is considered to be a manifestation of the shear capacity of the subbase layer. Under field conditions, once the adhesive shear strength of the interface has been exceeded, the sliding frictional resistance dominates and is represented by the angle of friction  $\tan \phi$ . It has often been observed that the failure plane in a friction sliding test rarely occurs at the interface of the two materials used in the test but occurs in the layer having the lowest shear strength which has cast doubt on the validity of the test results.

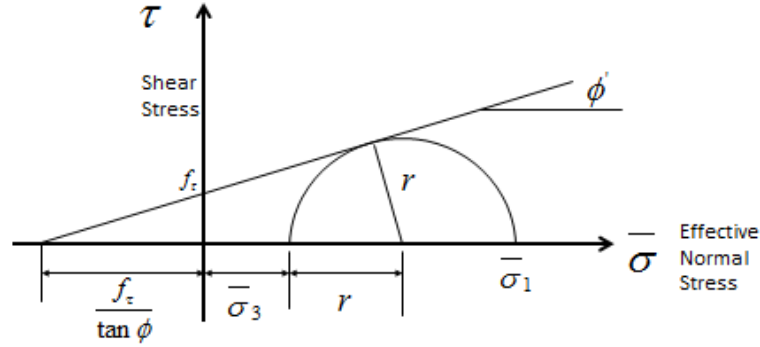


**Figure B.1** Shear Strength and Angle of Friction Determinations.

A ‘yield’ strength type model (as depicted in Figure B.2 – friction is not mobilized until the interface adhesion has yielded) for the effective interfacial resistance or strength is formulated with respect to the interfacial shear strength and the sliding friction as follows:

$$f_e = (1 - \%E) \left[ (1 - P(\sigma_n > 0)) f_c + f_F \right] \quad (B.1)$$

where,

$f_e$  = effective interfacial frictional resistance or bond strength

=  $\sigma_v \mu_e$

$\sigma_v$  = normal stress

=  $k_{eff} \Delta$

$k_{eff}$  = effective modulus of subgrade reaction

$\Delta$  = loaded deflection

$\mu_e$  = effective coefficient of friction

$\%E$  = % contamination or probability of erosion

$P(\sigma_n > 0)$  = probability of adhesive bond failure as a function of curling and warping behavior

$\sigma_n$  = net stress =  $(\sigma_0 - f_t)$

$\sigma_0$  = interfacial separation stress

$$\begin{aligned}
f_t &= \text{tensile strength of the weakest layer adjoining the interface} = \frac{f_\tau}{\tan \varphi} \\
f_\tau &= \text{cohesive shear strength of the weakest layer adjoining the interface} \\
&= \sigma_v \mu_c \\
\mu_\tau &= \text{cohesive coefficient of friction} \\
f_F &= \text{frictional interfacial shear strength} \\
&= \sigma_v \cdot \tan \varphi = \sigma_v \mu_F \\
\mu_F &= \text{interfacial coefficient of sliding friction} (= \tan \varphi)
\end{aligned}$$

After substituting the expressions for  $f_c$ ,  $f_\tau$ , and  $f_F$  in equation (B.1), an expression for effective coefficient of friction can be obtained as follows:

$$\mu_e = (1 - \%E) \left[ (1 - P(\sigma_n > 0)) \mu_\tau + \mu_F \right] \quad (\text{B.2})$$

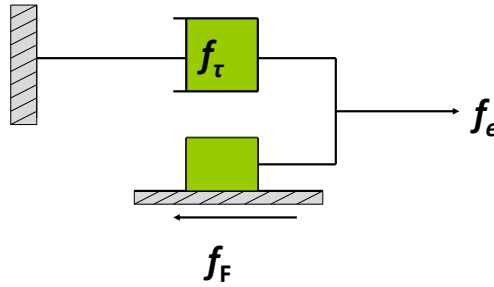


**Figure B.2** Resistance Model for Slab/Subbase Interface of Concrete Pavement.

The parameter  $f_e$  in equation (B.1) is considered to be an effective shear strength since it represents a composite of the interfacial adhesive and sliding friction components. Each component contributes to the interfacial frictional resistance. The cohesive component is dependent upon the amount of slab lift off due to slab curling and warping that has taken place (subsequently discussed) and the sliding friction component is dependent upon the extent of contamination on the interface. This contamination is created by erosion of the slab/subbase interface – at least in the areas of the slab where the adhesive bond nears a yielding condition. It should be noted that erosion effects are obviously minimal for initial interfacial strengths immediately after construction where adhesion and friction component are likely to be present. The mechanism of wear-out of the frictional resistance is at the heart of the erosion process where erosion related wear-out is a function of traffic, wet days, and the shear strength of the subbase layer (Jung and Zollinger 2011). Sliding and shearing movements become active when the load-induced shear stress  $\tau$  exceeds the effective frictional interfacial shear strength of the subbase generating a layer of loosen material as part of the sliding action that takes place (i.e. the sliding action initiates the erosion of the interface).

This model is based on the concept that the change in subbase friction over the service life of a pavement is in part generated by the built up of an erosive layer of loosen subbase material that reduces the ‘bond’ or the adhesion of the subbase to the slab and thus creates a wearing out or variation of the overall frictional resistance of the interface. It is also worth noting that the parameter  $f_t$  will also vary as a function of slab lift off which will be important in defining the level of frictional resistance along slab edges and corners which can vary significantly from that in the center regions of the panel. The normal stress component, which affects the magnitude of the shear resistance, is a direct reflection of the subgrade and subbase stiffness (as represented by an effective k value  $k_{eff}$  and the load-induced deflection  $\Delta$ ). A certain amount of cohesion howbeit affected by slab lift-off may always be present on any sliding surface.

### Erosion Damage

The incidence of erosion is thought to affect both the capability of the interfacial resistance to develop a mechanical interlock and an adhesive strength component between the layers that comprise the interface. As noted in the model for  $\mu_e$  (see equation (B.2)), the effect on the frictional resistance is directly proportional to the amount of erosion damage that can be formulated based on a modification of a model originally proposed by Jung and Zollinger. Interested readers can obtain further information regarding the erosion model elsewhere (Jung et al. 2010, Jung and Zollinger 2011, Jung, Y., et al., 2012.).

$$\% E = \frac{f_i}{f_0} = e^{-\left(\frac{\rho}{D_i}\right)^\alpha} \quad (B.3)$$

where,

$\%E$  = percent of erosion

$f_i$  = level of faulting

$f_0$  = ultimate faulting

$D_i$  = Erosion damage =  $\sum \frac{N_i}{N_f}$

$\rho, \alpha$  = calibration factors (based on laboratory erosion testing)

The accumulated damage along the interface is due to load induced shearing action between the layers. The damage  $D$  along the interface can be defined as follows:

$$Damage, D_i = \sum \frac{N_i}{N_f} \times (\% \text{ Wet Days}) \quad (B.4)$$

where,

$N_f$	= Ultimate loads to failure = $10^{k_1 + k_2 r_i}$
$k_i$	= Erosion fatigue damage calibration coefficients
$r_i$	= $\frac{\tau_i}{f_e}$
$\tau_i$	= interfacial shear stress
$f_e$	= effective interfacial frictional resistance or bond strength

Interfacial shear stress can be further broken down as follows:

$$\tau_i = (1 - x_b) \frac{\partial \delta_{L_i}}{\partial X} \frac{E_{sb}}{2(1 + \nu)} \left( \frac{1}{\psi} \right) \quad (B.5a)$$

$$\frac{\partial \delta_{L_i}}{\partial X} = \frac{\partial \delta_{L_i}^*}{\partial x} \frac{P}{L^* k \ell^2} \quad (B.5b)$$

$$\frac{\partial \delta_{L_i}^*}{\partial x} = b + 2dx + fy \quad (B.5c)$$

where,

$x_b$	= degree of bond (subsequently discussed)
$\delta_{L_i}$	= loaded deflection = $\frac{\delta_{L_i}^* P}{k \ell^2}$
$\delta_{L_i}^*$	= dimensionless deflection
$P$	= load
$\ell$	= radius of relative stiffness
$k$	= modulus of subgrade reaction
$X$	= distance from the point of loading along the diagonal from the corner or from the edge of the slab
$E_{sb}$	= subbase modulus
$\nu$	= subbase Poisson's ratio
$\psi$	= load transfer factor = $a_i (LTE) + 1$
$a_i$	= 0.03 for edge loading; 0.07 for corner loading
$LTE$	= load transfer efficiency (%)
$x$	= $\frac{X}{L^*}$
$L^*$	= $\frac{W}{2}$ (for slab edge); = $\frac{W}{\sqrt{2}}$ (for slab corner)
$W$	= slab width



b, d, f = edge or corner coefficients

$$y = \frac{h}{\ell}$$

h = slab thickness

The fatigue coefficients (i.e.  $k_1$  and  $k_2$ ) in the expression for  $N_f$  could be determined experimentally from erosion tests of the candidate subbase material or from field performance data. The expression for shear stress in equation (B.5) clearly shows that interfacial stress is a function of load level P, LTE, k-value, and slab thickness.

### Composite Slab Behavior: Relating Interfacial Bond to Effective Friction Coefficient

Composite slab behavior considering the degree of bond between concrete and subbase layers can be represented by the effective thickness of the slab  $h_{e-i}$ . The following equations apply in defining  $h_{e-i}$ .

Effective thickness for fully bonded layers  $h_{e-b}$  is defined as (Ioannides et al. 1992):

$$h_{e-b} = \left\{ h_1^3 + \frac{E_2}{E_1} h_2^3 + 12 \left[ \left( x_{na} - \frac{h_1}{2} \right)^2 h_1 + \frac{E_2}{E_1} \left( h_1 - x_{na} + \frac{h_2}{2} \right)^2 h_2 \right] \right\}^{1/3} \quad (B.6)$$

Effective thickness for unbonded layers  $h_{e-u}$  can be defined as (Ioannides et al. 1992):

$$h_{e-u} = \left[ \left( h_1^3 + \frac{E_2}{E_1} h_2^3 \right) \right]^{1/3} \quad (B.7)$$

Depending on the bonding situation between layers, the effective radius of relative stiffness (RRS or  $\ell$ ) of the slab is defined as:

$$\ell_{e-i} = \sqrt[4]{\frac{E_c h_{e-i}^3}{12(1-\nu^2)k}} \quad (B.8)$$

where,

- $h_{e-b}$  = Effective thickness of the bonded PCC layers
- $h_{e-u}$  = Effective thickness of the unbonded PCC layers
- $h_{e-p}$  = Effective thickness of partially bonded PCC layers
- $h_{e-i}$  =  $h_{e-b}$ ,  $h_{e-u}$ ,  $h_{e-p}$  as the case may be
- $E_1$  or  $E_2$  = Elastic modulus for layer 1 or 2
- $h_1$  or  $h_2$  = Thickness for layer 1 or 2

$x_{na}$  = Neutral axis distance from top of layer 1

$$= \frac{E_1 h_1 \frac{h_1}{2} + E_2 h_2 \left( h_1 + \frac{h_2}{2} \right)}{E_1 h_1 + E_2 h_2}$$

$\ell_{e-i}$  = Radius of relative stiffness corresponding to  $h_{e-i}$

$E_c$  = Elastic modulus of the PCC layer

$\nu$  = Poisson's ratio

$k$  = Modulus of Subgrade Reaction

$i$  = u, b, or p

The above expressions for effective thickness are involved in the determination of the effective slab thickness for partially bonded conditions  $h_{e-p}$  between the slab and the stabilized layer assuming that the frictional slippage between these layers under load represents the interlayer structural restraint. Whether the restraint or the variation of it between the layers is due to friction or chemical cohesion, its determination is also referred to in this paper as the degree of bonding denoted as “ $x_b$ ” (which ranges between 0 and 1) and is incorporated in the formulation of  $h_{e-p}$  as (Zollinger et. al 2005):

$$h_{e-p} = (1 - x_b) h_{e-u} + (x_b) h_{e-b} \quad (B.9)$$

From rearrangement of equation (24), the degree of bonding  $x_b$  can be assessed as:

$$x_b = \frac{h_{e-p} - h_{e-u}}{h_{e-b} - h_{e-u}} \quad (B.10)$$

In pavement design and evaluation, the degree of partial bonding parameter is important to address the evaluation of partially bonded behavior is perhaps most conveniently done via the analysis of FWD testing data at certain locations on a slab. The relationship for stresses between the partially bonded and unbounded cases can be obtained as depicted in Figure B.3; using simple proportioning, the effective partially bonded stress  $\sigma_{e-p}$  can be found as:

$$\sigma_{e-p} = \sigma_e \left[ \frac{2h_{e-u}}{h_{e-p}} - 1 \right] \quad (B.11)$$

where,

$\sigma_e$  = effective bending stress

$$= \frac{s_{e-i} P}{h_{e-i}^2}$$

$s_{e-i}$  = dimensionless stress

$$= a + b\ell_{e-i} + c\ell_{e-i}^2$$

$P$  = applied FWD load in lb.

$a, b, c$  = 0.0006, 0.0403, and -0.0002

Note that the coefficients  $a$ ,  $b$ , and  $c$  were derived from finite element analysis using ISLAB2000 for FWD plate loading.

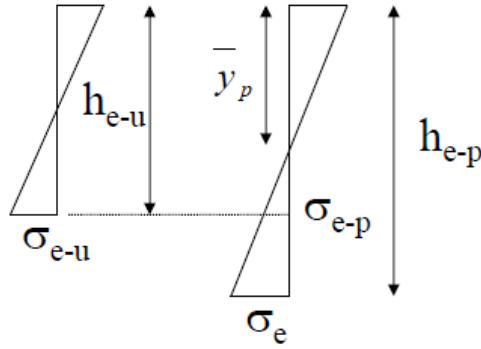


**Figure B.3** Unbonded and Partially-Bonded Transformed Section of a Concrete Slab (Zollinger et.al. 2005).

In order to formulate a relationship to the effective interlayer friction coefficient  $\mu_e$ ,  $\sigma_{e-p}$  is equated to the difference between the unbonded stress  $\sigma_{e-u}$  and the effective frictional stress  $\tau_e$  at the bottom of the slab as:

$$\sigma_{e-p} = \sigma_{e-u} - \tau_e \quad (\text{B.12})$$

The effective frictional stress can be further expressed as:

$$\tau_e = \mu_e \left[ \frac{h_c}{12} + \sigma_v \right] \quad (\text{B.13})$$

where,

$h_c$  = insitu concrete slab thickness

$\sigma_v$  = load induced vertical pressure at the partially-bonded interface

Equations (B.11), (B.12), and (B.13) can be rearranged to develop an expression for  $\mu_e$  as:

$$\mu_e = \frac{\sigma_{e-u} - \sigma_e \left[ \frac{2h_{e-u} - 1}{h_{e-p}} \right]}{\frac{h_c}{12} + \sigma_v} \quad (\text{B.14})$$

The above expression relating  $h_{e-p}$  to  $\mu_e$ , one of the parameter of equation (B.2), further develops the determination of  $h_{e-p}$  relative to its use in design methodology.

Using FWD measurements, it is possible to back calculate  $x_b$  as well as  $\mu_e$  for each location of testing. As an example, results of these back calculations are shown in Figure B.4 for several FWD test locations made at the Bush International Airport in Houston, Texas. The results suggested that  $x_b$  can be related to  $\mu_e$  and to that end, the relationship between  $x_b$  and  $\mu_e$  is proposed according to Equation (B.15).

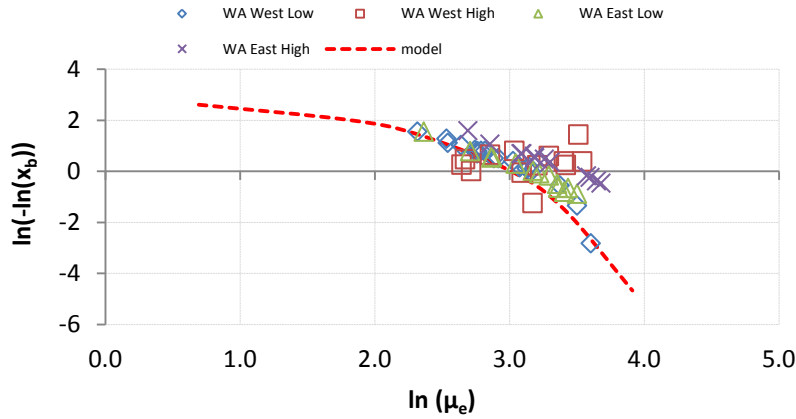


**Figure B.4** Relationship between  $\mu_e$  and  $x_b$  Back-calculated from FWD Test Data.

$$x_b = e^{-\left(\frac{A}{\mu_e}\right)^B} \quad (\text{B.15})$$

After performing logarithm transformation, equation (B.15) can be written as follows. This linearization facilitates the analysis of  $\mu_e$  and  $x_b$  as shown in Figure B.4.

$$\ln(-\ln(x_b)) = B(\ln(A) - \ln(\mu_e)) \quad (\text{B.16})$$

where,

$$A = e^{\left(\frac{3.0 - 0.2\mu_e}{B}\right)}$$

$$B = -0.039 \{ \ln(\mu_e) \}^2$$

The evaluation of the effective coefficient of friction based on back-calculation of the collected FWD data certainly carries certain advantages and clearly includes an adhesive component. Furthermore, equation (B.15) can serve as an integral component in relating the coefficient of friction to the degree of bond and the interlayer structural restraint between the concrete layers for design purposes

### **In Situ Assessment of Erosion-Related Parameters**

FWD data were used to determine the following quantities:

- Area of the deflected basin (BA) (L)
- Radius of relative stiffness (RRS also referred to as  $\ell$  value) (L)
- Effective slab thickness ( $h_e$ ) (L)
- Dynamic foundation modulus (k value) ( $FL^{-2}/L$ )
- Joint load transfer efficiency (LTE) (%)
- Values for  $\mu_\tau$  and  $\mu_F$ ,
- Percent of erosion (%E), and
- Degree of partial bonding ( $x_b$ ) and effective slab thickness ( $h_e$ ).

The BA is determined directly from the sensor deflection data recorded for the FWD:

$$BA = \frac{SS}{2 * D_0} \left[ D_0 + 2(D_1 + D_2 + \dots + D_{j-1}) + D_j \right]$$

where

SS = sensor spacing  
 $D_i$  = sensor deflection ( $i = 0$  to  $j$ )

The determination of RRS is directly dependant upon the basin area but relies on a theoretical relationship developed from finite element (FE) analysis. The FE model used for this relationship is described in the next section this analysis resulted in a relationship illustrated in Figure B.5 which was used to determine the insitu RRS at each position where center of slab measurements were made. The basin area can also be determined in a dimensionless form by dividing it by the RRS. From the following relationship for RRS, the effective slab thickness was determined as:

$$h_e^3 = \frac{12(1-\nu^2)k}{E_c} \ell_e^4$$

This parameter is very useful since the comparison of its value to the measured in place thicknesses can represents the how structurally thick the pavement system is. The RRS along with the center plate deflections is also useful to determine the foundation modulus of the subgrade. Since the deflection data is associated with a rather high frequency loading cycle, the resulting calculation is assumed to result in a dynamic foundation modulus ( $k_{dyn}$ ) as:

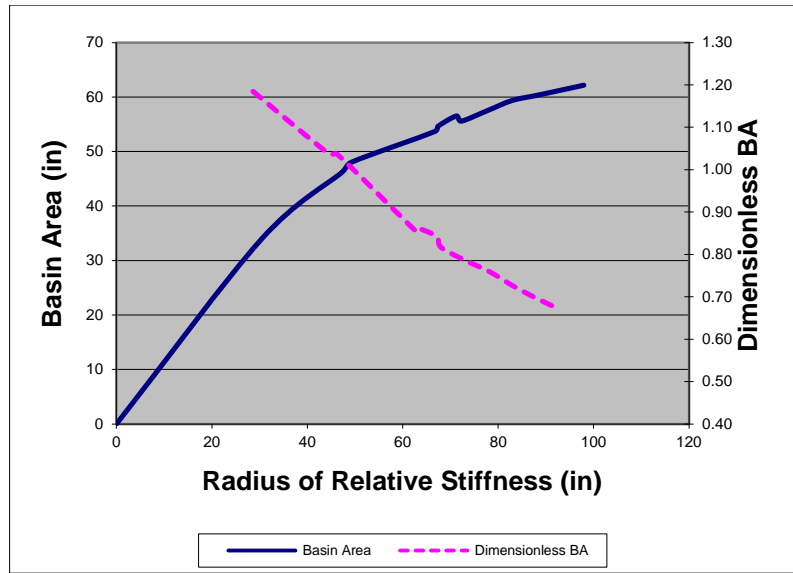


**Figure B.5** Basin Area – RRS Relationship.

$$k = \frac{w_0^* P}{w_0 \ell^2}$$

where

$P$  = wheel load (F)

$w_0$  = center plate deflection (L)

$$w_0^* = \frac{1}{8} \left[ 1 + \left( \frac{1}{2\pi} \right) \left( \ln \left( \frac{a}{2\ell} \right) + \gamma - 1.25 \right) \left( \frac{a}{\ell} \right)^2 \right] \text{ (center of slab loading)}$$

The parameters  $h_e$ ,  $\mu_e$ , and %E were determined for three different slab positions - interior, edge, and corner was analyzed. Using equation (B.14), the effective friction coefficient values were calculated for each tested slab position. The difference in calculated friction coefficient values between the edge and corner confirms the assertion that lower amount of erosion takes place at the edge versus the corner.

The effective friction coefficient data is used to back-calculate the values of %E,  $\mu_\tau$  and  $\mu_F$  for these sites using equation (B.2). In this process, the amount that the cohesive affects  $\mu_e$  is determined relative to the probability of debonding  $P(\sigma_n > 0)$ . Expressing equation (2) in terms of FWD load positions - J1 (slab center), J2 (slab corner), and J3 (slab edge) yields the following set of expressions:

$$\text{for J1: } \mu_e = (1 - \%E)_{J1} \left[ (1 - P(\sigma_n > 0))_{J1} \mu_\tau + \mu_F \right] \quad (\text{B.17a})$$

$$\text{for } J2: \mu_e = (1 - \%E)_{J2} \left[ (1 - P(\sigma_n > 0))_{J2} \mu_\tau + \mu_F \right] \quad (\text{B.17b})$$

$$\text{for } J3: \mu_e = (1 - \%E)_{J3} \left[ (1 - P(\sigma_n > 0))_{J3} \mu_\tau + \mu_F \right] \quad (\text{B.17c})$$

For slab center, it is reasonable to assume that both %E and  $P(\sigma_n > 0)$  are zero and therefore. Hence, equation (B.17a) can be rewritten as follows:

$$\text{for } J1: \mu_e = \mu_\tau + \mu_F \quad (\text{B.18})$$

The System Identification (SID) (Natke 1982) method is an iterative solution scheme that can be used to minimize the error between the system output and the model output based on the same input signal by adjustment of the variable unknowns. The output of the model is changed systematically using a search technique (Lytton 1989) until the model output is close to the system output. In this paper, the SID is used to fit the equation for  $\mu_{e-i}$  at positions J1, J2, and J3 by iteration until  $\Delta X_i^n$  (the difference in the unknown parameter from iteration to iteration) equals zero by satisfying the following expression for each test position as:

$$\sum_i^3 \sum_m^5 \left( \frac{\partial \mu_{e-i}}{\partial X_m} \frac{X_m}{\mu_i} \right) \left( \frac{\Delta X_m}{X_m} \right)_n = \left( \frac{\Delta \mu_{e-i}}{\mu_{e-i}} \right)_n \quad (\text{B.19})$$

where,

- m = number of  $X_i^n$  which are determined for each  $\mu_{e-i}$  (in this case = 5)
- $X_m$  = %E<sub>i</sub>,  $\mu_\tau$ , and  $\mu_F$
- i = FWD test position/drop count (3 positions: J1, J2, and J3)
- $\Delta X_m$  =  $X_m^{n+1} - X_m^n$
- n = iteration count
- $\Delta \mu_{e-i}$  =  $\mu_{e-ic} - \mu_{e-im}$
- $\mu_{e-ic}$  = calculated value based on the current values of  $X_m$  using equation
- $\mu_{e-im}$  = based on FWD measurements

For each of the unknowns above ( $X_m$ ), matrix analysis can be utilized to solve the set of resulting equations for each FWD test position/drop as:

$$[F] \{ \beta \} = [r] \quad (\text{B.20})$$

where,

$$[F] = \text{matrix of } \frac{\partial \mu_{e-i}}{\partial X_m} \frac{X_m}{\mu_i} \text{ elements (sensitivity matrix)}$$

$$\{\beta\} = \text{matrix of } \frac{\Delta X_m}{X_m} \text{ elements (unknown gradient matrix)}$$

$$[r] = \text{matrix of } \frac{\Delta \mu_{e-i}}{\mu_{e-i}} \text{ elements (residual matrix)}$$

The number of recorded data points from the FWD drops determines the number of rows in matrices  $[F]$  and  $[r]$ , while the number of columns in matrix  $[F]$  and the number of rows in matrix  $[\beta]$  are the same as the number of unknown parameters to be calculated. The matrix equation can be solved as:

$$\{\beta\} = [F^T F]^{-1} [F^T] [r] \quad (\text{B.21})$$

By minimizing the residual matrix  $\{\beta\}$ , solutions for  $X_m$  (i.e. %E<sub>J1</sub>, %E<sub>J2</sub>, %E<sub>J3</sub>,  $\mu_t$ , and  $\mu_F$ ) are found. The minimization of error contained within the residual matrix  $[r]$  is analogous to the minimization or reduction of error employed least squared error analysis. In this approach, when each element of the matrix  $\{\beta\}$  is less than 0.01 by using the iteration process, then it was considered that the parameters were found.

This process also involves the determination of P ( $\sigma_n > 0$ ) as described previously but additional solution criteria can be derived from the available strength relationships. Ideally, the interfacial shear strength would be determined from triaxial shear tests of the subbase material, but since such data was unavailable for these sites, the interfacial shear strength ( $f_\tau$ ) was estimated from the calculated compressive strength ( $f'_c$ ) for base materials. Lim et al (2003) suggested the following for  $f'_c$  as:

$$f'_c = \left[ \frac{E_b}{4.38 \times uw^{1.5}} \right]^{\frac{1}{0.75}} \quad (\text{B.22})$$

where,

$E_b$  = modulus of the base in psi

$uw$  = unit weight in lb/cf

Using  $f'_c$ , an estimate of the shear strength ( $f_\tau$ ) can be obtained for each subbase type by taking 50% of  $7.5\sqrt{f'_c}$ , i.e.

$$f_\tau = 0.5 \times 7.5\sqrt{f'_c} \quad (\text{B.23})$$




From the choice of angle  $\varphi$  associated with  $\mu_F$ , it is assumed the slab interfacial tensile strength is approximately equivalent to the material cohesive strength as  $f_t = \frac{f_r}{\tan\varphi}$ . Once the interfacial tensile strength are known,  $P(\sigma_n > 0)$  can be estimated.

Clearly, the effective pavement thicknesses depend upon the interlayer degree of partial bond and the representation of the degree of partial bond is important in order to model properly the fatigue damage at pavement edge and the faulting at pavement corner or at transverse joint. A rational approach, as such outlined herein, is needed to mechanistically represent the progression of wear out and the degree of bond between the base and the slab over time. Furthermore, these calculations indicate the dominant role that cohesion has on the interfacial resistance and preserving the adhesion across the interface can serve as a good measure against delaying or preventing erosion damage.

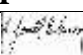
## References

- Bari, M. E. "Modeling the Effect of Curing on Early-age Distress Potential of Concrete Slab". Dissertation, Texas A&M University, 2014.
- Bazant, Z. P., and L. Panula. Practical Prediction of Time-Dependent Deformation of Concrete. Part 3: Drying Creep. Part 4: Temperature Effect on Basic Creep. *Materiaux et Constructions*, Vol. 11, No. 66, 1978, pp. 415–434.
- Ioannides, A.M., L. Khazanovich, and J. L. Becque. Structural Evaluation of Base Layers in Concrete Pavement Systems. Transportation Research Record 1370, Transportation Research Board, Washington, D.C., 1992, pp. 20-28.
- Jeong, J., and D. Zollinger. Environmental Effects on the Behavior of Jointed Plain Concrete Pavements." *Journal of Transportation Engineering*, 131(2), 2005, pp. 140-148.
- Jung, Y., D. G. Zollinger, B. H. Cho, M. Won, and A. J. Wimsatt. Subbase and Subgrade Performance Investigation and Design Guidelines for Concrete Pavement. FHWA/TX-12/0-6037-2, 2010, Texas Transportation Institute, The Texas A&M University System, College Station, Texas 77843-3135.
- Jung, Youn, and Dan Zollinger. New Laboratory-Based Mechanistic-Empirical Model For Faulting in Jointed Concrete Pavement. Transportation Research Record (2226), 2011, pp. 60-70.
- Jung, Y., Zollinger, Dan G., and Bari, Ehsanul "Improved Mechanistic Empirical CRC Pavement Design Approach using a Modified Punchout Model" 91<sup>st</sup> Meeting of the Transportation Research Board, Washington, D.C., 2012.

- Lim, Seungwook, and Dan G. Zollinger, Characterization of Crushed Concrete Materials for Paving and Non-Paving Applications, Research Report 4954-1, Texas Transportation Institute, The Texas A&M University System, College Station, Texas, January 2003.
- Lytton, R.L., Backcalculation of Pavement Layer Properties, Nondestructive Testing of Pavements and Backcalculation of Moduli. ASTM 1026. A.J. Bush III and G.Y. Baladi, Editors, American Society of Testing Materials. Philadelphia, pp.7-38, 1989
- Mohamed, A. R., and W. Hansen. Effects of Nonlinear Temperature Gradient on Curling Stress in Concrete Pavements. In *Transportation Research Record 1568*, TRB, National Research Council, Washington, D.C., 1997, pp. 65–71.
- Natke, H.G., Identification of Vibrating Structures, Springer-Verlag, New York, 1982.
- Wimsatt, A.W., McCullough, F.B., and Burns, N.H. (1987). Methods of Analyzing and Factors Influencing Frictional *Effects of Subbases*, Report 459-2F, Center For Transportation Research, Austin, TX.
- Zollinger, Corey, Dan G. Zollinger, Dallas Little, and Adel Godiwalla, Innovative Approach to Pavement Rehabilitation Analysis and Design of Runway 15L-33R at George Bush Intercontinental Airport in Houston, Tx,” Proceedings, Eighth International Conference on Concrete Pavements, August 14-18<sup>th</sup>, 2005, Vol. 3, pp. 1101-1119, Colorado Springs, Colorado.

 <b>400 FM Experimental Lab Report Form</b>	Document Title: Materials Engineering Manual
	Revision Number <u>1</u>

Report No. C-15-002R1  
Project No. 1.1

<b>Material: P/N 34902</b>			
<b>Evaluation of 20yr. Old I-10 Silicone Joint Sealant</b>			
<b>Sampled By: Texas A&amp;M University</b>	<b>Date: 12/10/14</b>	<b>Source: CrafcO</b>	
<b>Requested By: DGZ</b>	<b>Date: 12/10/14</b>	<b>Tested By: GH</b>	<b>Date: 12/17/14</b>
<b>Written By: JEB</b>	<b>Date: 01/28/15</b>	<b>Reviewed By:</b> 	<b>Date: 1/28/15</b>

### **PURPOSE AND BACKGROUND:**

Samples of 20 year old silicone joint sealant were removed from I-10 ADOT test sections on December 10, 2014 by Texas A&M University engineers. Tensile elongation testing was requested and conducted by CrafcO, Inc. on December 17, 2014.

### **SAMPLE PREPARATION AND TESTING:**

The samples were generally irregular in shape and contained imbedded dirt. Some samples had concrete attached. A few samples had pieces of wire, presumably from tires, driven through their cross section. Samples were cleaned for inspection by scrubbing with Dawn dish detergent followed by rinsing in running tap water and air dried. Each sample was inspected for its suitability to cut uniform specimens for tensile and elongation testing. A number of the samples were deemed unsuitable because of the non-uniform shape, imbedded dirt, tears and stress concentration points.

Test specimens were pressed from the samples using a lab press and a razor die with a 0.25 inch spacing between the blades. All specimens had an irregularly shaped cross section. The cross sectional area needed to determine stress values was determined by tracing an outline of each specimen's cross section, photo enlarging the tracing and subdividing the tracing into squares and rectangles. The area of the squares and rectangles were determined and summed for the cross sectional area of each specimen.

Tensile elongation tests were conducted at 20 inches per minute using an ATS Model 1601 Universal Test Machine with elastomer grips. A Sharpie marker was used to place one inch gauge marks on each specimen. The gauge mark separation was followed using a tape measure during the test and the elongation at break was recorded. The load and crosshead displacement was recorded continuously during the test.

### **RESULTS:**

Tensile elongation data are shown in Table 1 with the silicone sealant specification requirement. Figures 1 through 4 show the tensile test set up and an example of an untestable sample. Figure 5 is an example of the stress vs. crosshead displacement curve. Load, stress and displacement data are recorded in I10-Tensile Test Data.xlsx.

Table 1: Tensile Elongation		
Specimen	Stress at Break, psi	Elongation at Break, %
Sealant Specification	---	800 minimum
I10-40223PSN2	247	250
I10-40223PSN3	157	112
I10-40221	232	250
I10-40262	219	275
I10-40219	166	225

Figure 1 – Tensile Test Set-Up



Figure 2 – Before Tensile Test



Figure 3 – After Tensile Test



Figure 4 – Example of Untestable Sample

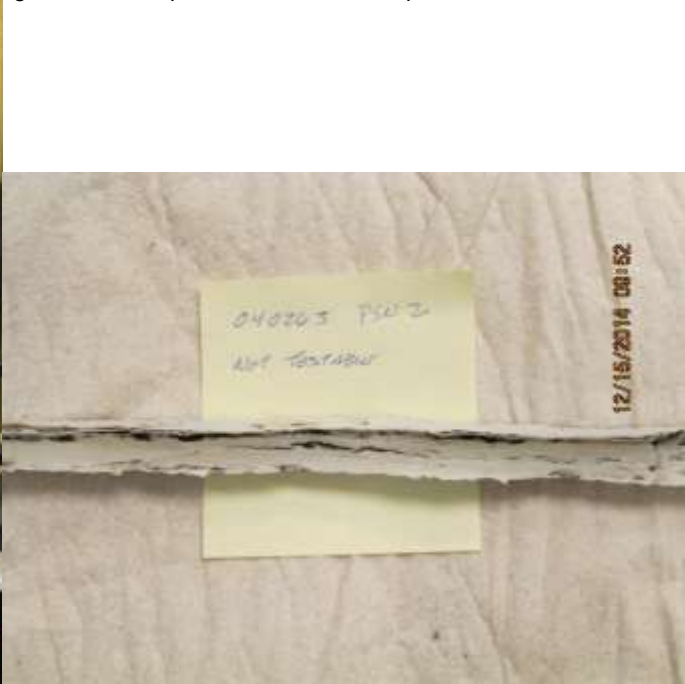
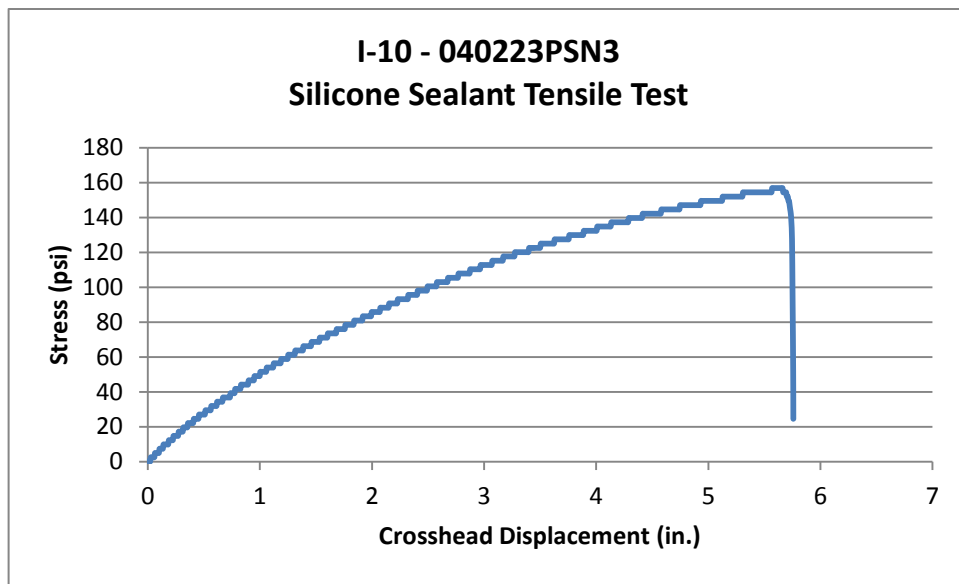


Figure 5 – Example of Stress vs. Displacement Curve



## Appendix D

### Analysis of HWDT Data

The erosion test incorporates the use of the HWTD which allows for water to transport material that has been abraded due to mechanical wear (and to some extent hydraulic shear action) generated by slab movement under an applied load along the interface between the slab and the surface of the base layer. The configuration of the test device is the same as normally used with the HWTD except for the multi-layering of the test sample shown in Figure D.1. The test configuration consists of a 1 inch thick subbase material placed on a neoprene material below a 1 inch thick jointed concrete cap (modification of the HWTD sample mold may allow for thicker subbase layers). The test configuration is such that it allows for testing either a laboratory compacted specimen or a core sample obtained from the field. A 158-lb wheel load is applied to the test sample at a load frequency of 60 rpm up to 10,000 load repetitions under selected moisture conditions typically at a temperature of 70°F. Measurements consist of the depth of erosion at 11 locations versus number of wheel load passes. In most cases, maximum deflection occurs at measuring points # 5, 6, or 7. Shear stress for the HWTD configuration can be calculated using:

$$\tau_{e-p} = \chi \tau_b + (1 - \chi) \tau_u$$

and using beam theory:

$$\tau_i = \frac{V_s \left\{ 1 - \left[ \frac{2(h_c - x_{na})}{h_i} \right]^2 \right\}}{h_i b \frac{E_{base}}{E_c}} \quad (D.1)$$

where:  $\tau_i$  = partially (*p*), bonded (*b*) or unbonded (*u*) shear stress, (psi)  
 $\chi$  = degree of partial bonding (as a function of the coefficient of friction ( $\mu$ ) where 0 = unbonded and 1 = fully bonded)  
 $V_s$  = shear load (158 lbs)  
 $h_c$  = thickness of the concrete cap  
 $h_i$  = effective unbonded (*u*) or bonded (*b*) thickness  
 $x_{na}$  = distance to the neutral axis  
 $E_i$  = elastic modulus of concrete cap (*c*) or subbase (*base*) layer, (psi)

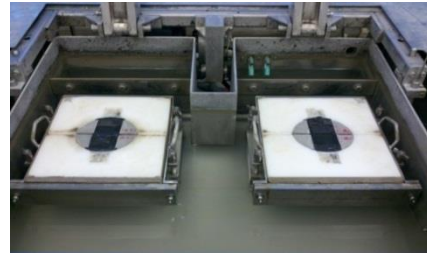
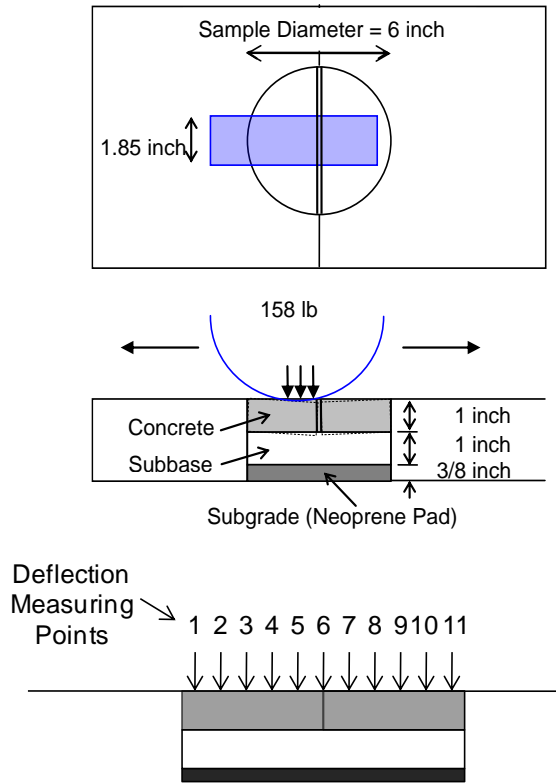


**Figure D.1** Erosion Test Using Hamburg Wheel-Tracking Device.

The data used for calibration in this instance is generated from the Hamburg Wheel Tracking Device (HWT) from tests on a subbase or subgrade material. HWT data is shown in Figure D.2 for an unbound aggregate base material.

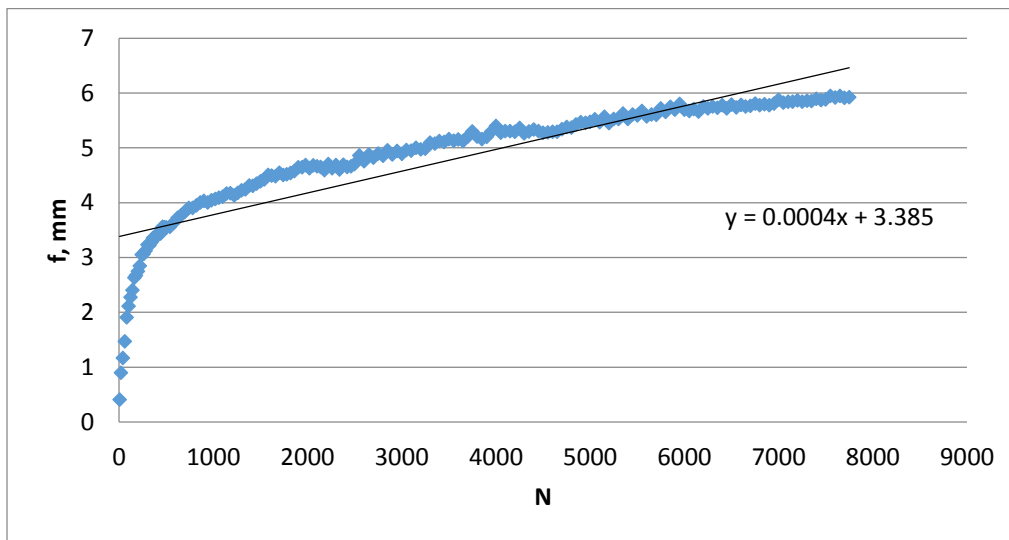


**Figure D.2** Plot of Faulting and Load Application HWT Data.

The analysis of this data is carried out using the following transformation of the HWTd data to determine the regression parameters  $\beta_e$  and  $\rho_e$ :

$$\frac{N}{N_\infty} = e^{-\left(\frac{\rho_e}{f}\right)^{\beta_e}}$$

$$\ln(N) - \ln(N_\infty) = -\left(\frac{\rho_e}{f}\right)^{\beta_e}$$

$$\frac{\partial \ln(N)}{\partial f} - \frac{\partial \ln(N_\infty)}{\partial f} = \frac{\partial \ln\left(-\left(\frac{\rho_e}{f}\right)^{\beta_e}\right)}{\partial f}$$

$$\frac{1}{N} \frac{\partial N}{\partial f} = \beta_e \left(\frac{\rho_e}{f}\right)^{\beta_e - 1} \frac{\rho_e}{f^2} = \beta_e \left(\frac{\rho_e}{f}\right)^{\beta_e} \frac{1}{f}$$

$$\frac{f}{N} \frac{\partial N}{\partial f} = \beta_e \left(\frac{\rho_e}{f}\right)^{\beta_e}$$

$$\ln\left\{\frac{f_i}{N_i} \frac{\partial N}{\partial f}\right\} = \ln(\beta_e) + \beta_e \ln(\rho_e) - \beta_e \ln(f_i) \quad (8)$$

$$\ln(y) = b + mx$$

$$\ln(y_i) = \ln\left\{\frac{f_i}{N_i} \frac{\partial N}{\partial f}\right\}$$

$$x_i = \ln(f_i)$$

$$b = \ln(\beta_e) + \beta_e \ln(\rho_e) = \ln(\beta_e \rho_e^{\beta_e})$$

$$m = -\beta_e$$

A plot of the transformed data shown in Figure 5 where the slope  $\frac{\partial N}{\partial f}$  was estimated based on the regression shown in Figure D.3. Results of the regression analysis are shown in Table D.1.

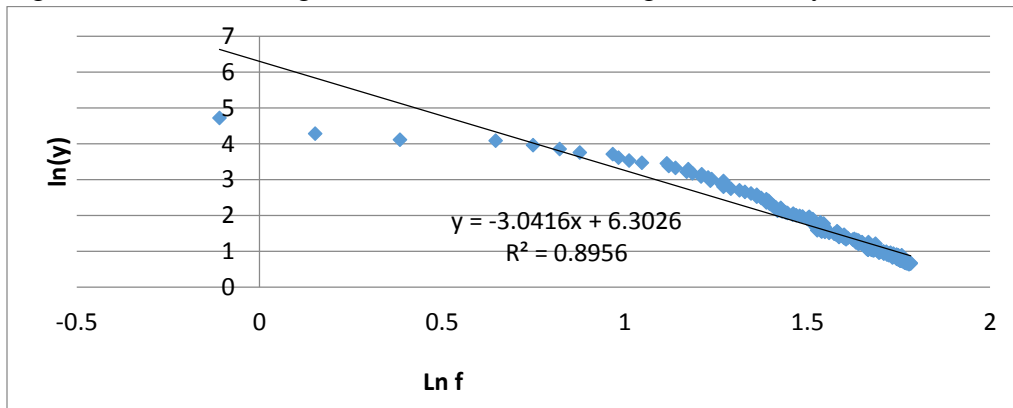


**Figure D.3** Plot of Transformed HWTd data.



**Table D.2** Regression Parameters for Transformed HWDT Data.

<b>m</b>	<b>b</b>	<b>β<sub>e</sub></b>	<b>ρ<sub>e</sub></b>
-3.042	6.3026	3.042	378.750

Given the β<sub>e</sub> and ρ<sub>e</sub> parameters, the following expression is used to estimate the ultimate faulting:

$$f_{\infty} = \rho_e \left( \frac{\beta_e}{\beta_e + 1} \right)^{\frac{1}{\beta_e}}$$

Which was determined to 727.8 mm which is quite large; obviously, this material appears to be highly erodible but this high value of the ultimate faulting is likely due to the effect of bulk stresses within the layer rather than erosive damage causing the initially high level of voiding seen in Figure D.2 (approximate 60 to 70% of the total measured faulting). It seems that this effect helps to explain the high values of %E found from field testing of the SR-59 section. In order to determine N<sub>∞</sub> it is necessary to invert equation (8) and use the following form:

$$\frac{N_{ei}}{f_i} \frac{\partial f}{\partial N} = \left( -\beta \text{Ln} \left( \frac{N_{ei}}{N_{\infty}} \right) \right)^{-1} = a + b^* N + c \text{Ln}(N_{\infty})^2 \text{Ln}(N_{\infty})$$

setting

$$A = e^{\frac{a+b^*N}{B}}; B = c \text{Ln}(N_{\infty})^2$$

$$\frac{N_{ei}}{f_i} \frac{\partial f}{\partial N} = B \text{Ln}(A) + B \text{Ln}(N)$$

or

$$\left( -\beta \text{Ln} \left( \frac{N_{ei}}{N_{\infty}} \right) \right)^{-1} = B \text{Ln}(A \cdot N_{ei})$$

where:

$$N_{\infty} = e^{\frac{1}{\beta B \text{Ln}(A \cdot N_{ei}) + \text{Ln}(N_{ei})}}$$

The value of N<sub>∞</sub> = 4.18e04. Similar analysis can be carried out on a partially stabilized sample of the same base material to find other set of values of N<sub>∞</sub> and f<sub>∞</sub> allowing the next step in the calibration process is to determine the k<sub>1</sub> and the k<sub>2</sub> parameters in the expression for the loads to

failure for erosion using  $N_{\infty} = 10^{k_1 + k_2 r}$  where  $r = \frac{\tau_{lab}}{f_{\tau}}$ ; and equation D.1.

However, before α<sub>e</sub> and β<sub>e</sub> (damage related) can be determined, values of k<sub>1</sub> and k<sub>2</sub> must be found which requires 2 sets of results from the HWTD testing of the same material (provided by the user) but for different shear strengths (one stabilized and one un-stabilized). Use the two values of N<sub>f<sub>e</sub></sub> and the following:

$$\text{Log}(N_{\infty}) = k_1 + k_2 r$$

Additionally, these parameters can be found from with field or the lab erosion data but  $\tau$  is found from the expression for the HWTD; since the applied load in the Hamburg device cannot be changed, the strength of the material is changed in order to generate two values of  $r$  and  $N_\infty$  - a set at a low erosion strength and a set at a high erosion strength. Thus

$$k_1 = \text{Log}(N_{f_{e-hs}}) - k_2 r_{e-hs} = \text{Log}(N_{f_{e-ls}}) - \left( \frac{\text{Log}(N_{f_{e-ls}}) - \text{Log}(N_{f_{e-hs}})}{r_{e-ls} + r_{e-hs}} \right) r_{e-hs}$$

$$k_2 r_{e-ls} = \text{Log}(N_{f_{e-ls}}) - \text{Log}(N_{f_{e-hs}}) - k_2 r_{e-hs}$$

$$k_2 = \frac{\text{Log}(N_{f_{e-ls}}) - \text{Log}(N_{f_{e-hs}})}{r_{e-ls} + r_{e-hs}}$$

The results of the analysis of the HWTD data is given in Table D.3 where key calibration parameters are determined and found. The shear strength ( $f\tau$ ) of the tested materials were estimated for the purposes of this calculation which shows the potential of using the testing data for calibration purposes.

**Table D.3** Determination of the Erosion Damage Coefficients.

$N_\infty$	$f_\infty$ (mm)	$\tau$	$f\tau$	$r$	Log (N)	$k_1$	$k_2$
4.18e04	727.8	120.46	35.00	3.44	4.62		